

2.08 Matter Transport in Fast Reactor Fuels[☆]

Michael J Welland¹, Canadian Nuclear Laboratories, Chalk River, ON, Canada

© 2020 Elsevier Ltd. All rights reserved.

2.08.1	Transport Phenomena	203
2.08.1.1	The Theory of Irreversible Processes	203
2.08.1.2	Solid State Mass Transport	205
2.08.1.2.1	Mass transport	205
2.08.1.2.2	Mass and heat transport	207
2.08.1.2.3	Single component vacancy/interstitial diffusion	209
2.08.1.2.4	Origin of the heat of transport	210
2.08.1.2.5	Other thermodynamic driving forces	211
2.08.1.2.5.1	Stress induced diffusion	211
2.08.1.2.5.2	Phase change	211
2.08.1.2.5.3	Curvature	211
2.08.1.3	Vapor Phase Transport	211
2.08.1.3.1	Factors affecting equilibrium vapor pressure	212
2.08.1.3.1.1	Temperature	212
2.08.1.3.1.2	Composition of the condensed phase	212
2.08.1.3.1.3	Surface curvature	212
2.08.1.3.2	Temperature driven vapor phase transport	213
2.08.1.3.3	Gradient in vapor pressure	213
2.08.1.3.4	Carrier-gas assisted	213
2.08.2	Microscopic Structures	214
2.08.2.1	Sintering and Grain Growth	214
2.08.2.1.1	Sintering	214
2.08.2.1.2	Grain growth	215
2.08.2.2	Void Migration	215
2.08.2.2.1	Void migration mechanisms	215
2.08.2.2.1.1	Void migration by surface diffusion	216
2.08.2.2.1.2	Void migration by volume diffusion	217
2.08.2.2.1.3	Void migration by vapor phase transport	217
2.08.2.2.2	Void migration forces	218
2.08.2.2.2.1	Migration driven by thermodiffusion	218
2.08.2.2.2.2	Pinning	219
2.08.2.2.3	Comparison of void migration behavior and experimental applications	219
2.08.2.3	Pore Migration	220
2.08.2.3.1	The origin of pores	221
2.08.2.3.2	The shape of migrating pores	221
2.08.2.3.3	Pore migration speed	222
2.08.2.3.4	Redistribution of matrix material	224
2.08.3	Bulk Phenomena	225
2.08.3.1	Cracks	225
2.08.3.2	Porosity Evolution	226
2.08.3.2.1	Columnar grain growth	226
2.08.3.2.2	Central void	226
2.08.3.3	Melting	227
2.08.4	Fuels	227
2.08.4.1	Mixed Oxide Fuels	227
2.08.4.1.1	MOX restructuring	228
2.08.4.1.2	U – Pu redistribution	232

[☆]Change History: July 2015. Michael J. Welland updated the MOX restructuring, and U-Pu redistribution sections, in addition to minor grammatical corrections. July 2019. Michael J. Welland updated the Pore migration, Pore evolution, and Fission product redistribution sections, added a new figure in the introduction illustrating the high burnup structure, made various clarifications, and minor grammatical corrections.

This is an update of Welland, M.J., 2012. Chapter 3.21 – Matter Transport in Fast Reactor Fuels. In: Konings, R.J.M. (Ed.), Comprehensive Nuclear Materials, Elsevier, pp. 629–676.

¹This work was originally written during a stay at the European Commission, Joint Research Centre, P.O. Box 2340, 76125 Karlsruhe, Germany.

2.08.4.1.3	Oxygen redistribution	234
2.08.4.1.4	Fission product redistribution	238
2.08.4.2	U-Pu-C-N	239
2.08.4.3	U-Pu-Zr	240
2.08.4.4	TRISO Particles	242
2.08.5	Summary	244
References		244

Nomenclature

λ	Jump distance	H_i	Energy required to remove atom from the initial site
Γ	Jump frequency	h_k	Partial specific enthalpy of species k
σ	Surface energy	H_m	Migration energy
$\Delta H_{vap,k}$	Enthalpy of vaporization of species k	H_s	Energy required to prepare the saddle point for a migrating atom
γ_k	Activity coefficient of species k	J_k	Flux of species k
μ_k	Chemical potential of species k	J_q	Reduced heat flux
Ω_k	Specific volume of species k	J_u	Energy flux
σ_{stress}	Isostatic stress field in the solid	J_x	Generalized flow of x
∇_T	Gradient taken at constant temperature	k	Boltzmann constant
D_{AB}	Chemical interdiffusion coefficient	k	Index a particular chemical species
\overline{D}_k	Intrinsic diffusion coefficient of species k	K	Thermal conductivity
h_v^f	Enthalpy of formation of vacancies	KMC	Kernel migration coefficient
J_k^o	Mass flux of species k measured with respect to the non-diffusing ends	L_{ab}	Kinetic parameter, either diagonal or cross-term related to mobility
J_k^o	Material flux with respect to laboratory frame of reference	l_{bw}	Characteristic depth of bow wave in front of migrating pore
Q_{AB}^{**}	Process heat of transport for interdiffusion of species A and B	n_k	Concentration of species k
$Q_{k,vap}^*$	Effective heat of transport through carrier-gas mechanism	N_k	Mole fraction of species k
Q_k^{**}	Effective heat of transport of species k	P_{fill}	Pressure of the fill gas
U_k^*	Energy of transport of species k	p_k	Partial pressure of species k
n_k^e	Equilibrium concentration of species k	q	Atomic ratio of $Pu/U + Pu$
s	Entropy production rate	r	Radius
A_{Aitken}	Constant of integration from the Aitken equation	R_v	Source of vacancies
D_k	Self-diffusion coefficient of species k	T	Temperature
$D_{m,surf}$	Surface diffusion coefficient	T_c	Centreline temperature
$D_{v,vol}$	Volume diffusion coefficient	i	Interstitial defect species
f_k	Thermodynamic factor of species k	v	Vacancy defect species
f_o	Diffusion correlation factor	v_k	Velocity of species k
F_x	Conjugate thermodynamic force for flow of x	$v_{lattice}$	Velocity of the solid lattice with respect to the non-diffusing ends/laboratory frame of reference
G	Gibbs energy	V_{Pu}	Valence of plutonium
H_f	Energy required to make space for the atom at the final site	V_U	Valence of uranium
		x	Index of system state variable
		x	Stoichiometry deviation

The fuel of fast neutron spectrum nuclear reactors may be subject to extreme operating conditions. In particular centreline temperatures may regularly exceed 2000K and incur temperature gradients in excess of thousands of degrees per centimeter. Such large temperatures and temperature gradients produce a variety of mass transport phenomena affecting the chemical and physical state of the fuel. The physical evolution of the fuel has consequences on the generation and diffusion of heat, in addition to mechanical behavior and fission product release.

The large temperatures and temperature gradients can directly or indirectly produce driving force acting on the constituents of the fuel, causing their migration. Such driving forces act on all constituents of fuel, be they fission products or the primary constituents of the solid matrix itself. For discussion purposes, we can consider mass transport as resulting in *redistribution* of the chemical species which leaves the general structure of the matrix intact, and *restructuring* of the solid matrix itself.

Restructuring of the solid matrix occurs when, for example, voids migrates through the fuel. In a radial temperature gradient, voids migrate towards higher temperatures and coalesce in the center, resulting in movement of solid towards the outer periphery of the fuel and forming the *central void* an example of which is shown for a mixed oxide [MOX] fuel pellet in Fig. 1. With regards to the thermal

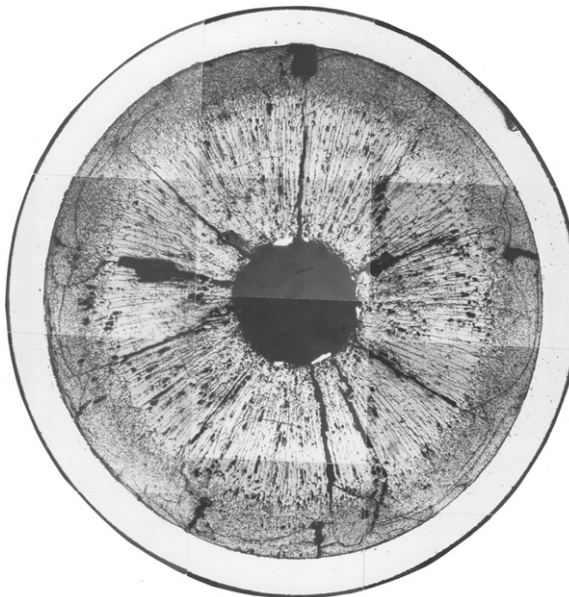


Fig. 1 Microstructure of a fast reactor pelletized MOX fuel showing effects of restructuring due to mass transport. A discussion on the visible zones in this sample is presented in Section 2.08.4.1. © European Communities, reproduced with permission.

performance of the fuel, this relocation of fuel away from the hot center towards the cooler periphery means that heat is generated closer to the heat sink, thus lowering the maximum temperature. Meanwhile, the removal of voids from the fuel matrix changes the heat transport characteristics, and so restructuring can be seen to play a large role in the overall heat transport process.

Redistribution results in demixing of solutions and migration of chemical species such as fission products. For example, in MOX fuels, this phenomenon results in the migration of oxygen through the sample and demixing of U and Pu in addition to other species present in the fuel. Several material properties are dependant on the chemical state of the fuel including thermal conductivity, heat capacity, density and the incipient melting temperature. Redistribution may also lead to safety concerns as, for example, redistribution of Pu up the temperature gradient increases the heat generation at the innermost region. Since avoidance of melting is a key concern for solid fuel operation, this phenomenon may culminate in a penalty of the maximum linear heat rating by as much as 8.2 kW/m, 15% for a liquid metal fast breeder reactor mixed-oxide fuel element compared to the restructured case without plutonium redistribution.^{1,2}

Redistribution of chemical species can also degrade the structural integrity of the fuel cladding by moving reactive species towards the clad where they can attack it. In particular, volatile fission products such as Ce , Cs , Te , Se , Rb and I , may be transported down the temperature gradient through cracks and, depending on the local oxygen concentration, attack the cladding.^{3,4}

In this article, matter transport is discussed as it occurs in a variety of reactor fuels. Due to the higher operating temperatures of some fast reactor fuels, these effects are more pronounced and relevant compared to conventional fuels. However, the key parameters incuring matter transport are usually the temperature and temperature gradient and therefore thermal spectrum reactor fuels also exhibit these effects if operated at high enough temperatures for long enough.

This article is divided into sections describing the mass transport process on different scales of space and time. Restructuring and redistribution are discussed from a common standpoint although the distinction is maintained for discussion purposes. The mechanisms described are common to all materials however the characteristics of each fuel affects the magnitude of each effect, and thus their relative importance.

Firstly, fundamental mass transport processes are described in terms of the atomic transport mechanisms and their thermodynamic driving force. Gradients in temperature, chemical potential and stress may all contribute to matter transport and so are placed on a common footing, the requirement of entropy production. By comprehensively treating all the constituent of the system, including vacancies, phenomena such as the Kirkendall effect, and Darken's equation for interdiffusion are derived. We therefore seek to unite several theories on a common footing based on irreversible thermodynamics in Section 2.08.1.

The collective behavior of particles under the action of these fundamental mechanisms leads to the emergence of microscopic structures which play a large role in fuel restructuring and redistribution. In particular, the behavior of grains and voids significantly affects fuel performance. Different characteristics of voids permit their categorization into bubbles and pores depending on, among other factors, the relative importance of the fundamental mechanisms which depend on the void's size, shape and gas content. Grain growth and void behavior are described in Section 2.08.2.

Evolution of the fuel through fundamental mechanisms and microscopic structures leads to macroscopically observable effects of redistribution and restructuring. The evolution of the fuel porosity, and redistribution by phase changes and interconnected porosity are discussed. The redistribution of chemical constituents as shown to have resulted from the balance of driving forces in the solid matrix, through voids or as a result of restructuring. These large-scale phenomena are discussed in Section 2.08.3.

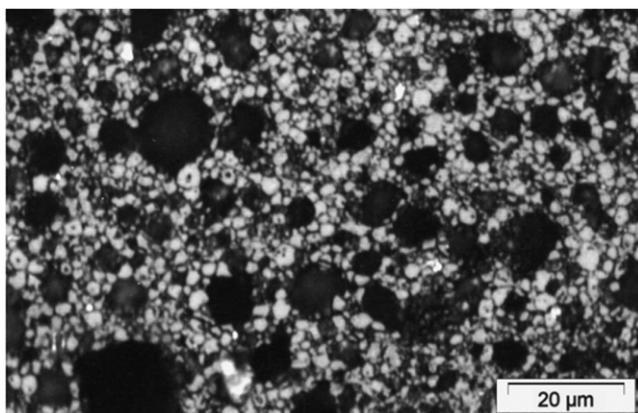


Fig. 2 Optical ceramography with chemical etching of 20% Pu/(U + Pu) fast breeder reactor fuel showing restructuring of the initial $\sim 10 \mu\text{m}$ grains into small grains surrounding large bubbles 17% FLMA. Reproduced from Noirot, J., Desgranges, L., Lamontagne, J., 2008. Detailed characterisations of high burn-up structures in oxide fuels. *J. Nucl. Mater.* 372 (2), 318–339.

Finally, different fuel types are discussed using the developed theoretical framework. Most of the section is dedicated to MOX fuels, as these are the most commonly investigated, which may be used in pelletized, spherepac and vipac forms. Carbide and nitride fuels are also discussed, in addition to *U-Pu-Zr* fuels and finally tristructural isotropic [TRISO] particles. These fuels are discussed in Section 2.08.4.

A few features related to restructuring and redistribution are not addressed in this work but are worthy of mention. High-burnup fuels, both in fast and thermal spectra reactors, have been shown to undergo other changes in structure and phase. Volatile fission products may migrate down the temperature gradient towards the fuel-cladding gap where they can form agglomerations, known as the 'Joint Oxide Gaine' [JOG].⁵ At extended burnups, there is also a reaction layer observed between the cladding and fuel surface.⁶ Also evolved is the so-called 'rim structure' which is characterized by $<1 \mu\text{m}$ diameter grains in a porous recrystallized configuration as shown in Fig. 2.^{7–9} In certain situations, a fraction of the rim structure may evolve into a 'white layer', which is nearly free of voids.⁸ While these phenomena are undoubtedly relevant to fuel operation at longer burnups, this work will focus on behavior at lower burnups.

By approaching this topic through beginning with the fundamentals and advancing through spacial scales, the connection between the different restructuring and redistribution observations in a variety of fuels is elucidated, and the common principles leading to mass transport is highlighted.

2.08.1 Transport Phenomena

This section describes some of the fundamental mechanisms which drive material transport. Nuclear fuel is subject to extreme conditions in both magnitude and gradient of state variables, e.g., both very high temperatures and very large temperature gradients. Usually, fluxes of energy and mass are expressed in terms of gradients in temperature and chemical potential (mole fraction) respectively and separately. In the extreme conditions produced during fuel operation, coupling between the transport of heat and mass becomes an important consideration in correctly predicting fuel behavior. The coupling between mass flux and temperature gradient is known as thermodiffusion, or the Soret effect, and is critical to understanding fuel behavior.

The many interrelated phenomena applicable to restructuring and mass transport is placed on a common base through the Theory of Irreversible Processes [TIP] (The TIP is sometimes referred to as Non-equilibrium Thermodynamics). Within the TIP, all processes which produce entropy, and therefore occur spontaneously, are accounted for in such a way that coupling between phenomena is derived naturally. Mathematical relationships between fluxes and thermodynamic driving forces are derived comprehensively and consistently and naturally includes such concepts as thermodiffusion (Thermomigration is also important to the nuclear industry in the consideration of the formation of zirconium hydride within the fuel sheath¹⁰).

2.08.1.1 The Theory of Irreversible Processes

The TIP relates the evolution of a system, as described by its state variables x , to the change in its thermodynamic state with respect to changing the state variables. The change in a state variable is described by a generalized flow, J_x , where the flow is driven by its conjugate driving force, F_x . The driving force is given as the gradient of a potential function related to state variable x , e.g.: a mass flux (flow) is driven by a chemical potential gradient. The fundamental principle of the TIP is that entropy is produced when this flow proceeds along its driving force:

$$\dot{s}T = \sum_x J_x F_x \geq 0 \quad (1)$$

where \dot{s} is the rate of entropy generation and places certain restrictions on the magnitude of T is the absolute temperature. Flow-driving force pairs include vectorial fluxes such as heat and mass flux driven by gradients in temperature and concentration respectively, and also scalar flows such as chemical reactions and phase changes driven by minimization of free energy (maximization of universal entropy through entropy production). The inequality essentially reflects the second law of thermodynamics and so describes only real, spontaneous processes.

An important concept relevant to discussion about the TIP is that of thermal equilibrium. In cases where transport phenomena is concerned, the system is clearly not in *global* thermodynamic equilibrium as net fluxes are spontaneously generated. A fundamental concept of the TIP is that a system which is not in global equilibrium may be divided into a set of infinitesimally small regions which are considered to be in a state of *local* equilibrium. These small regions must therefore contain enough atoms to define statistical quantities relevant to thermodynamics such as temperature and chemical potential, and be in thermodynamic equilibrium in the sense that such quantities are suitable.¹¹

The inequality of (1) is assured by expressing the flows in terms of the thermodynamic driving forces. The simplest relation is through the linear phenomenological laws, in which the flows are expressed as being proportional to linear combinations of *all* possible thermodynamic forces (In fact, Curie's law states a flow may only be coupled to driving forces of similar tensorial character due to spatial symmetry.¹² e.g.,: chemical reactions, which are scalar flows of tensor rank 0, cannot be driven by a vectorial, rank 1, forces such as the gradient in temperature, although dependence of the direction and kinetics of such a process may be affected by the temperature, rank 0, directly). These linear relationships do not necessarily apply for large deviations from equilibrium, however they have been shown to represent experimental observations well and form the basis of much of current transport phenomena analysis.¹¹

The power and comprehensiveness of the TIP is accompanied by somewhat cumbersome equations. Therefore, the remainder of this discussion will be limited to heat and mass transport as these are most relevant to the topic of this work. For a more complete discussion of this subject, the interested reader is referred to references.^{11,13-15} Eq. (1) will however be referred to again for description of vacancy creation/annihilation and evaporation/condensation. We therefore consider a system described by its temperature and relative concentrations of K chemical constituents, each denoted by k . The mass flux of species k is represented by J_k . Heat transport is described by the *reduced* heat flux: J_q which differs from the flux of energy, J_u , by the local change in energy associated with the flux of a diffusing species:

$$J_q = J_u - \sum_{k=1}^K h_k J_k \quad (2)$$

in which h_k is the partial specific enthalpy of species k . The reduced heat flux therefore describes only heat conduction, and excludes the movement of energy accompanying a change in composition as, for example, the lattice changes to accommodate the change in composition. The choice of using J_q instead of J_u is for better understanding, but J_u may also be used as will be discussed shortly.

The conjugate thermodynamic driving forces for the heat and mass fluxes are the gradients in temperature and chemical potentials respectively. Therefore in (1) we have $F_q = -\nabla T/T$ and $F_k = -\nabla_T \mu_k$, where the choice of using the reduced heat flux has necessitated that the gradient in chemical potential be taken at constant temperature. If the flux of energy, J_u was chosen instead, the force conjugate to the mass flux in (4) would be $\nabla(\mu_k/T)$. The two quantities are related by¹¹:

$$d\left(\frac{\mu_k}{T}\right) = \frac{d\mu_k}{T} + h_k d\left(\frac{1}{T}\right) \quad (3)$$

Using the reduced heat flux, Eq. (1) may be written:

$$-J_q \frac{1}{T} \nabla T - \sum_{k=1}^K J_k \nabla_T \mu_k \geq 0 \quad (4)$$

In the general case, the inequality of (4) may be assured by expressing the heat and mass fluxes as linear combinations of both the temperature and chemical potential gradients:

$$J_q = -L_{qq} \frac{1}{T} \nabla T - \sum_{j=1}^K L_{qj} \nabla_T \mu_j \quad (5a)$$

$$J_k = -L_{kj} \frac{1}{T} \nabla T - \sum_{j=1}^K L_{kj} \nabla_T \mu_j \quad (5b)$$

The L coefficients are kinetic parameters which may be a function of the state variables but are independent of the thermodynamic forces (gradients in state variables) (An alternative expression includes an additional factor of $1/T$ on each term of this system. This choice culminates in different expressions for the L coefficients).¹⁴ In order to satisfy (4) (or more generally Eq. (1)), the mobilities must form the elements of a positive definite matrix.¹⁶ For the current case, this implies that the diagonal elements are positive: $L_{qq}, L_{kk} \geq 0$, and places certain restrictions on the magnitude of the off diagonal elements.

Note that the expression of the matter flux is in line with the Nernst-Einstein equation for matter flux driven by a force (potential gradient):

$$J_k = n_k v = n_k \frac{D_k}{kT} F_k \quad (6)$$

where n_k and D_k are the local concentration and diffusion coefficient of species k respectively.¹³

Through an argument of time-reversal symmetry, it is possible to demonstrate that in the absence of rotation or a magnetic field, the L matrix is symmetric:

$$L_{jj'} = L_{j'j} \quad (7)$$

This relationship is known as the Onsager reciprocal relation, and helps to reduce the number of coefficients required by (5).

The nature of the coefficients may be intuited by considering the role they play in linking a flux with the respective driving force. We may expect the diagonal components L_{qq} and L_{kk} to be related to the thermal conductivity and diffusion coefficient of species k respectively. The off-diagonal terms define cross-effects between fluxes such as L_{kq} relating to mass transport driven by a temperature gradient, thermodiffusion or the Soret effect.¹⁷ The Onsager relation equates $L_{qk} = L_{kq}$, where L_{qk} is related to a heat flux being driven by a chemical potential gradient, a phenomenon known as the Dufour effect.¹⁸ The Soret and Dufour effects are therefore considered reciprocal relations stemming from the same source. Regarding the mass fluxes, the $L_{kk'}$ coefficients are related to correlation coefficients between mass fluxes of different species and will be discussed in more detail below.¹³ Logically $L_{kk'} = L_{k'k}$ as one may expect that the correlation effect of one particle flux on the other applies equally so in vice versa.

We have now used the TIP to obtain expressions for heat and mass fluxes which may occur in nuclear fuel. In the next section this framework is applied to specific cases of matter transport in the solid and vapor phases.

2.08.1.2 Solid State Mass Transport

The following section will discuss the mass transport which occurs in the solid state. The discussion will begin by considering an isothermal system before proceeding to the non-isothermal case.

2.08.1.2.1 Mass transport

In considering mass transport of the K species in an isothermal system, point defects play an important role and may be included as a separate diffusing species which, unlike the chemical constituents of the system, are not conserved but rather created and destroyed locally. Defects are included in (5b) as the $K + 1$ species.

If we consider a system with a constant density of normal lattice sites (The assumption of a constant atomic volume is clearly not always correct and may be lifted by introducing the partial molar volumes¹³), and that diffusion occurs primarily through defect mechanisms, then not all the $K + 1$ mass fluxes are independent. For vacancies diffusing on the same crystal lattice, the flux of vacancies must satisfy $J_v = -\sum_{k=1}^K J_k$. For interstitials, which may occupy a distinct lattice, the sign is reversed and $J_i = \sum_{k=1}^K J_k$. These relations can be exploited to eliminate the defect flux from explicit calculation, but then require a modification to the thermodynamic driving forces as given in (11) to include the chemical potential of the defects. The choice to eliminate the defect flux from explicit calculation is entirely arbitrary and in some cases, such as the diffusion of oxygen in MOX, it is more convenient to eliminate a material flux instead.¹⁴ For the sake of simplicity, only vacancies will be considered for the remainder of the derivation.

The creation and annihilation of vacancies constitutes a *flow* in the sense of (1), where the driving force is expressible as the deviation of the vacancy chemical potential to its equilibrium value. To describe this scalar flow (source), the source of vacancies will be denoted as R_v . The linear phenomenological theory then implies a source/sink of vacancies where creation or annihilation occurs due to local sub or super-saturation:

$$R_v \propto \frac{\partial G}{\partial n_v} \quad (8)$$

$$= L_v \mu_v = L_v kT \frac{n_v^e - n_v}{n_v^e} \quad (9)$$

where L_v is a phenomenological kinetic coefficient akin to the other L coefficients, and n_v^e and n_v are equilibrium and actual defect concentration, respectively. Generally, the L_v coefficient depends on the concentration of vacancy sources and sinks. The chemical potential of the vacancies, μ_v may be positive or negative, but by definition, must be zero if the vacancies are at their equilibrium concentration (This does not imply that the vacancy concentration is constant everywhere, merely that it is equal to the equilibrium concentration value. The equilibrium value may vary with chemical composition and temperature). Thermal equilibrium of the vacancies will frequently be assumed in the ensuing derivations which, for isothermal systems, implies $\mu_v = 0$. Later, non-isothermal systems will be discussed in which case the gradient of μ_v is taken at a constant temperature, and the result will include the enthalpy of vacancy formation, h_v^f ¹⁴.

$$\nabla_T \mu_v = h_v^f \nabla T / T \quad (10)$$

In general, the equilibrium concentration of vacancies is much less than the concentration of a chemical species, $n_v^e \ll n_k$. In this case, the constant concentration of lattice sites implies that $n \approx \sum_K n_k$.

We must now define the frame of reference in which fluxes are expressed which, due to the creation and annihilation of point defects, may differ from the frame in which fluxes are measured. Under the assumption of a constant density of lattice points, the creation of vacancies in some regions of the material and annihilation in other regions, implies that the atomic lattice itself is moving with respect to the fixed (non-diffusing) ends of the sample.¹³ This phenomenon is known as the Kirkendall effect, although first observed by Hartley, and is observed through the use of inert markers placed in the diffusion area.^{19,20} The markers move with the lattice and therefore indicate the velocity of the lattice by their displacement, and the divergence of the lattice velocity by the change in spacing.

The equations derived thus far refer to the moving, lattice frame of reference. If we consider an isothermal system in which two chemical species diffuse, we must then consider the fluxes of three species: A, B and vacancies:

$$J_A = -L_{AA}\nabla_T(\mu_A - \mu_v) - L_{AB}\nabla_T(\mu_B - \mu_v) \quad (11a)$$

$$J_B = -L_{BA}\nabla_T(\mu_A - \mu_v) - L_{BB}\nabla_T(\mu_B - \mu_v) \quad (11b)$$

$$J_v = -J_A - J_B \quad (11c)$$

$$R_v = -L_v\mu_v \quad (11d)$$

where it is noted here that $L_{BA} = L_{AB}$ but are written separately for illustrative purposes.

If we assume that vacancy sources/sinks are numerous and efficient, then n_v will be approximately constant at its equilibrium value and μ_v will then be negligible with respect to $\mu_{A,B}$. Note that this simplification does not exclude a vacancy flux, but rather implies that it will be entirely determined by the difference between J_A and J_B .

The chemical potential may be expressed in terms of the mole fraction of species k , N_k and the activity coefficient, γ_k :

$$\mu_k = \mu_k^0 + kT \ln(\gamma_k N_k) \quad (12)$$

from which we can readily express $\nabla_T \mu_k$ as:

$$\nabla_T \mu_k = \frac{kT}{N_k} \left(1 + \frac{\partial \ln \gamma_k}{\partial \ln N_k} \right) \nabla N_k \quad (13)$$

$$= \frac{kT}{N_k} f_k \nabla N_k \quad (14)$$

where $f_k = \left(1 + \frac{\partial \ln \gamma_k}{\partial \ln N_k} \right)$ is the *thermodynamic factor* which effectively relates the gradient in chemical potential to that of the mole fraction. In accordance with the Gibbs-Duhem equation, the thermodynamic factors for both species are the same, and thus the subscript may be neglected. The system in (11) may then be simplified and compared to Fick's law of diffusion to determine the *intrinsic diffusion coefficients*, \bar{D} :

$$J_A = -kT \left[\frac{L_{AA}}{n_A} - \frac{L_{AB}}{n_B} \right] f \nabla n_A = -\bar{D}_A \nabla n_A \quad (15a)$$

$$J_B = -kT \left[\frac{L_{BB}}{n_B} - \frac{L_{BA}}{n_A} \right] f \nabla n_B = -\bar{D}_B \nabla n_B \quad (15b)$$

where the intrinsic diffusion coefficients are given by:

$$\bar{D}_A = kT \left(\frac{L_{AA}}{n_A} - \frac{L_{AB}}{n_B} \right) f = kT \frac{L_{AA}}{n_A} \left[1 - \frac{L_{AB} n_A}{L_{AA} n_B} \right] f \quad (16a)$$

$$\bar{D}_B = kT \left(\frac{L_{BA}}{n_A} - \frac{L_{BB}}{n_B} \right) f = kT \frac{L_{BB}}{n_B} \left[1 - \frac{L_{BA} n_B}{L_{BB} n_A} \right] f \quad (16b)$$

The intrinsic diffusion coefficients determine how the species will diffuse through the lattice in the moving frame of reference. The coefficients consist of two parts: the first term $kT \frac{L_{AA}}{n_A}$ does not contain any reference to species B and thus represents the self-diffusion coefficient as is discussed for the case of infinite dilution of A in B as discussed later. The second term, $\left[1 - \frac{L_{AB} n_A}{L_{AA} n_B} \right]$, relates to the cross-coupling between the diffusion of species A and B. This is the "vacancy wind" effect as discussed by Manning and relates to the population of vacancies.^{13,21} It also has ramifications when discussing tracer diffusion experiments. Note that (16) reveals that the intrinsic diffusion coefficients need not be equal.

Returning to (11), we consider the flux of vacancies with respect to the assumption of thermal equilibrium in which the concentration of vacancies remains constant, and so the defects must be created and destroyed at different parts of the material leading to the previously mentioned Kirkendall effect. The lattice, with a site concentration n , moves with respect to the laboratory at a speed $v_{lattice}$, which is related to the vacancy flux:

$$J_A + J_B = -J_v = nv_{lattice} \quad (17)$$

which, using Eq. (15) becomes:

$$v_{lattice} = (\bar{D}_A - \bar{D}_B) \nabla n_A \quad (18)$$

We can now perform a coordinate transformation to express the mass fluxes in the laboratory frame of reference in which they are typically measured using $J_A^0 = J_A + n_A v$ ¹³:

$$J_A^0 = -\tilde{D}_{AB} \nabla n_A \quad (19a)$$

$$J_B^0 = -\tilde{D}_{AB} \nabla n_B \quad (19b)$$

where the chemical inter-diffusion coefficient between species A and B, \tilde{D}_{AB} has been defined:

$$\tilde{D}_{AB} = N_A \bar{D}_B + N_B \bar{D}_A \quad (20)$$

The matter fluxes in the laboratory frame of reference, J_A^o and J_B^o , are what is commonly predicted in mass transport calculation and typically observed in experimentation. As one would expect in a system in which the local density does not vary in time, $J_A^o = -J_B^o$. If the velocity of the local lattice is measured with inert markers, the intrinsic diffusion coefficients may be calculated using Eq. (18).

In the limiting case of infinite dilution of A in B, it is clear that $n_A \rightarrow 0$ and $f \rightarrow 1$. Furthermore, it can be shown that whereas $\frac{L_{AA}}{n_A}$ approach may then be simplified and compared to a finite value, $\frac{L_{BA}}{n_B}$ approaches zero. Thus,

$$\lim_{n_A \rightarrow 0} \bar{D}_A = kT \frac{L_{AA}}{n_A} = D_A \quad (21)$$

where D_A is the self diffusion coefficient of A. The same cannot be said about the \bar{D}_B in the infinite dilution of A in B.¹³

A special case of the above theory is to the diffusion of a radioactive tracer, A^* in a matrix of A. In this case the mobility of the diffusing species are equal and mix ideally, implying that the intrinsic diffusion coefficients are equal. From (21) and (16), we have:

$$D_{A^*} = \bar{D}_{A^*} = \bar{D}_A = D_A \left[1 - \frac{L_{AA^*} n_A}{L_{AA} n_{A^*}} \right] \quad (22)$$

$$D_{A^*} = D_A f_0 \quad (23)$$

where f_0 is the correlation factor, related to the probability of a diffusing tracer atom interacting with the vacancy.¹³

The Darken equation is a convenient approximation for the chemical inter-diffusion coefficient calculated from the diffusion of radioactive tracers. The intrinsic diffusion coefficients from (16) are taken and combined with the self-diffusion coefficient expressions in terms of the radioactive tracer experiments from (23). If the correlation factor and the vacancy wind terms are assumed to cancel, then the intrinsic diffusion coefficients are expressed simply in terms of the radioactive tracer diffusion:

$$\bar{D}_A = D_A^* f \quad (24)$$

an expression which is particularly useful in (20) since, as previously mentioned, f is equal for both diffusing species in a binary solution:

$$\tilde{D}_{AB} = (N_A D_B^* + N_B D_A^*) f \quad (25)$$

This equation commonly used in the analysis of the experimental data.^{22,23}

The approximation of neglecting the correlation coefficients in the derivation of Darken's equation was lifted by Manning who determined other relations relating the intrinsic diffusion coefficient to the tracer diffusion including the presence of the correlation factor, in addition to the vacancy wind^{14,21}:

$$\tilde{D}_{AB} = (N_A D_B^* + N_B D_A^*) f \left[1 + \frac{1 - f_0}{f_0} \frac{N_A N_B (D_A^* - D_B^*)^2}{(N_A D_A^* + N_B D_B^*)(N_A D_B^* + N_B D_A^*)} \right] \quad (26)$$

Similarly, there is a factor of f^{-1} on the Kirkendall velocity given in Eq. (18). Allnatt and Lidiard noted that the correction for the vacancy wind, although significant, will never be very large and provide an example of a 30% increase over the Kirkendall velocity calculated with (18).¹⁴

A subject of particular interest to the nuclear community is that of radiation induced diffusion. This is often described as an athermal contribution to the diffusion coefficient of slow-moving species through the solid matrix in which the diffusion coefficient may be described by²⁴:

$$D_k^{rad} \propto \text{fission rate} \quad (27)$$

and may lead to significant enhancement by as much as 10^{10} , especially in the cold regions where thermally activated self-diffusion is slow.²⁴ As described by Matzke, the reason for this is the damage to the lattice structure and the nuclear collision process, as well as local thermal and pressure effects due to the slowing down process. These considerations therefore contribute to an enhancement of kinetic processes or produce a system out of thermodynamic equilibrium.²⁴

The basic equations of mass transport in a binary system have thus been derived, and the relationships between different diffusion coefficients formally established. The equations in (19) reconcile with basic understanding of Fickian mass flux, and experimental observations, such as the movement of inert markers in inter-diffusion experiments has also been justified within the same framework. The precise meaning of the different diffusion coefficients such as \tilde{D} has been rigorously defined and method of determining this value from related experiment such as radioactive tracers has been explained. This is critical in determining the behavior of chemical redistribution in nuclear fuel elements.^{25,26}

2.08.1.2.2 Mass and heat transport

Having discussed mass transport in the previous section, we will now lift the isothermal condition and deduce the ramifications of considering a temperature gradient. As will be discussed, coupling appears between heat transport and mass transport and introduces new considerations into the treatment of each.

Returning to the description of heat transfer described in (5a). If we consider a homogeneous system with no diffusion, then the heat flux is simply Fourier heat flux:

$$J_q = -L_{qq} \frac{1}{T} \nabla T = -K \nabla T \quad (28)$$

and so we conclude that for a non-diffusing system, $L_{qq} = TK$.

We now apply (5) in its entirety for the case of diffusion in a non-isothermal system. Once again, diffusion is considered to occur by the vacancy mechanism, and so we arrive at a set of equations resembling (11) into which the temperature gradient is introduced. In the frame of reference moving with the lattice we have:

$$J_A = -L_{AA}\nabla_T(\mu_A - \mu_v) - L_{AB}\nabla_T(\mu_B - \mu_v) + L_{Aq}\frac{1}{T}\nabla T \quad (29a)$$

$$J_B = -L_{BA}\nabla_T(\mu_A - \mu_v) - L_{BB}\nabla_T(\mu_B - \mu_v) + L_{Bq}\frac{1}{T}\nabla T \quad (29b)$$

$$J_v = -J_A - J_B \quad (29c)$$

$$R_v = -L_v\mu_v \quad (29d)$$

$$J_q = -L_{qA}\nabla_T(\mu_A - \mu_v) - L_{qb}\nabla_T(\mu_B - \mu_v) + L_{qq}\frac{1}{T}\nabla T \quad (29e)$$

The definition of the reduced heat flux presented in (2) must now include the partial specific enthalpy of the vacancies:

$$J_q = J_u - \sum_k^{K+1} h_k J_k = J_u - [(h_A - h_v)J_A + (h_B - h_v)J_B] \quad (30)$$

System (29) may be expressed in a simplified form by two considerations. Firstly, the gradient of the vacancy chemical potential may be expressed in terms of the enthalpy of formation as described in (10). Secondly, we can eliminate the cross terms between heat and mass fluxes by defining the *reduced heat of transport* of species k , Q_k^* , as:

$$L_{kq} = \sum_{i=1}^K L_{ki} Q_i^* \quad (31)$$

The reduced heat of transport is related to the (unreduced) heat of transport via the partial specific enthalpy in a manner similar to Eq. (30).¹⁴

The system in (29) then becomes:

$$J_A = -L_{AA}\nabla_T\mu_A - L_{AB}\nabla_T\mu_B - [L_{AA}(Q_A^* - h_v^f) + L_{AB}(Q_B^* - h_v^f)]\frac{1}{T}\nabla T \quad (32a)$$

$$J_B = -L_{BA}\nabla_T\mu_A - L_{BB}\nabla_T\mu_B - [L_{BA}(Q_A^* - h_v^f) + L_{BB}(Q_B^* - h_v^f)]\frac{1}{T}\nabla T \quad (32b)$$

$$J_v = -J_A - J_B \quad (32c)$$

$$R_v = -L_v\mu_v \quad (32d)$$

$$J_q = Q_A^* J_A + Q_B^* J_B + (L_{qq} - L_{Aq} - L_{Bq})\frac{1}{T}\nabla T \quad (32e)$$

Expression (32e) is revealing about the nature of the heat of transport since, for an isothermal system, this equation shows that Q_k^* relates the heat flux with the flux of species k , in excess of the enthalpy associated with the transported mass. This notion also reconciles with the description of Wirtz for the heat of transport, as discussed below. Allnatt and Lidiard comment that in terms of determining the heat of transport, while (32a) lends itself to experimental determination, (32e) may be used with $\nabla T = 0$ in computational techniques such as molecular dynamics, in which isothermal systems are more tractable.¹⁴

We may continue to simplify (32) by the introduction of the *effective heat of transport*:

$$Q_k^{**} = Q_k^* - h_v^f \quad (33)$$

We see now that if the effective heat of transport is positive, the species will preferentially migrate down the temperature gradient. If it is negative, the species will migrate up the gradient.

We also note that most of the first four lines in (32) is the same as for isothermal binary interdiffusion in (11), and may be treated as such in order to calculate the intrinsic diffusion coefficients. The mass fluxes equivalent to (15) are then:

$$J_A = -\bar{D}_A \nabla n_A - [L_{AA}Q_A^{**} + L_{AB}Q_B^{**}] \frac{\nabla T}{T} \quad (34)$$

$$J_B = -\bar{D}_B \nabla n_B - [L_{BA}Q_A^{**} + L_{BB}Q_B^{**}] \frac{\nabla T}{T} \quad (35)$$

These fluxes are defined relative to the lattice frame of reference, moving at a speed calculated by (17).

Again, we arrive at a cumbersome equation due to the presence of the cross-terms. If the cross-terms (and correlation factor) are dropped as was done in defining Darken's equation, then we arrive at an equation useful in experimental analysis:

$$J_A^o = -n\tilde{D}_{AB}\nabla N_A - \frac{nN_AN_B}{kT_f} [\bar{D}_A Q_A^{**} - \bar{D}_B Q_B^{**}] \frac{1}{T} \nabla T \quad (36)$$

with $J_B^o = -J_A^o$. Bober and Shumacher simplify (36) by defining a *process heat of transport*, which combines the reduced heats of transport in a form more convenient for evaluation from measured concentrations distributions²⁷:

$$Q_{AB}^{**} = \frac{1}{\tilde{D}_{AB}} (\bar{D}_B Q_B^{**} - \bar{D}_A Q_A^{**}) \quad (37)$$

In which case, the flux of A measured in the laboratory frame of reference would be given by:

$$J_A^o = -n\tilde{D}_{AB} \left(\nabla N_A + N_A N_B \frac{Q_{AB}^{**}}{kT^2} \nabla T \right) \quad (38)$$

If tracer diffusion coefficients are available, \tilde{D} , \bar{D}_A and \bar{D}_B may be replaced using Eqs. (24) and (25). This equation is useful in determining the redistribution of the dominant chemical species, for example uranium and plutonium in MOX as discussed in Section 2.08.4.1. In order to consider thermodiffusion of fission products, which are present generally in dilute solution at low burnup, we can treat the uranium or plutonium ions as a single metal species and then consider interdiffusion of this metal species (M) and the fission product (F). This is tantamount to considering a dilute solution of A in B, in which case Eq. (36) may be simplified greatly and expressed in terms of tracer diffusion coefficients as:

$$J_F^o = -nD_F^* \left(\nabla N_F - \frac{N_F}{kT^2} Q_{FM}^{**} \nabla T \right) \quad (39)$$

where $Q_{FM}^{**} \approx \frac{1}{D_F} (\bar{D}_M Q_M^{**} - Q_F^{**})$. This is applied to Cs in Section 2.08.4.1.

2.08.1.2.3 Single component vacancy/interstitial diffusion

There is a special and useful case remaining which differs from the above treatments by a fundamental assumption. Previously, diffusion has been considered to occur via a vacancy mechanism where the vacancies are present in local equilibrium in small numbers. In some cases it is convenient to have a considerable vacancy population and to treat them as a significant interdiffusing species. Such a case is relevant in considering thermodiffusion of oxygen excess or deficiency in hyper and hypo-to stoichiometric fuels respectively, in which case the defects are present due to a non-stoichiometry rather than being intrinsically generated. This will be discussed more in Section 2.08.4.1. Note also that this diffusion occurs on a different lattice than that hosting the cation diffusion.

We no longer consider the creation and destruction of crystal planes associated with the previous treatment of vacancy flows. In this case, the non-isothermal diffusion system, analogous to (29) is:

$$J_A = -L_{AA}\nabla_T(\mu_A - \mu_v) + L_{Aq}\frac{1}{T}\nabla T \quad (40a)$$

$$J_v = -J_A \quad (40b)$$

$$J_q = -L_{qA}\nabla_T(\mu_A - \mu_v) + L_{qq}\frac{1}{T}\nabla T \quad (40c)$$

The use of Eq. (10) is no longer possible to express the gradient of μ_v in terms of h_v^f since, as mentioned, the vacancies are not at thermodynamic equilibrium. Rather, we note that $N_A + N_v = 1$ and, through Eqs. (13) and (31) we can determine an expression for J_v :

$$J_v = -L_{vv}kT \left[\left(\frac{1}{N_A} + \frac{1}{N_v} \right) f \nabla N_v + \frac{Q_v^*}{kT^2} \nabla T \right] \quad (41)$$

$$= -nD_v \left[\nabla N_v + \frac{N_A N_V}{f} \frac{Q_v^*}{kT^2} \nabla T \right] \quad (42)$$

where $Q_v = -Q_A$ is the heat of transport of the vacancies and the vacancy diffusion coefficient, D_v has been defined:

$$D_v = \frac{L_{vv}kT}{nN_A N_V} f \quad (43)$$

Again if we can consider a dilute concentration of vacancies (although still significantly more than the thermal levels) and make approximations leading to:

$$J_v = -nD_v \left[\nabla N_v + N_v \frac{Q_v^*}{kT^2} \nabla T \right] \quad (44)$$

The case of interstitial diffusion is even simpler since the an interstitial movement need not be accompanied by a counter flow of atoms or vacancies. The mass flux is:

$$J_i = -L_{ii}\nabla_T\mu_i + L_{iq}\frac{1}{T}\nabla T \quad (45)$$

$$= -nD_i \left[\nabla N_i + \frac{N_i}{f} \frac{Q_i^*}{kT^2} \nabla T \right] \quad (46)$$

in which the interstitial diffusion coefficient has been defined as:

$$D_i = \frac{L_{ii}kT}{nN_i} f \quad (47)$$

We have now determined a set of equations for the mass flux of a system. For inter-diffusion of major constituents such as U-Pu inter-diffusion in MOX, Eq. (38) applies. For dilute solution of fission products diffusing on the same anion lattice, a simpler Eq. (39), is useful. If a single species is diffusing only, then depending on the migration mechanism, vacancy or interstitial, Eqs. (42) and (46) apply respectively. For experimental analysis, it is useful to consider the steady state given when the mass flux is equal to zero and the diffusive flux is exactly balanced by the thermodiffusion force. For Eqs. (38), (42) and (46) respectively, we obtain:

$$\nabla \ln(N_A) = \frac{N_B Q_{AB}^{**}}{f kT^2} \nabla T \quad (48a)$$

$$\nabla \ln(N_v) = \frac{1 - N_v}{f} \frac{Q_v^*}{kT^2} \nabla T \quad (48b)$$

$$\nabla \ln(N_i) = \frac{1}{f} \frac{Q_i^*}{kT^2} \nabla T \quad (48c)$$

If the heat of transport is considered to be independent of temperature, we can integrate (48c) (equivalent to the dilute limit of (48b)) to obtain the oft-quoted Aitken equation:

$$\ln(N_i) = \frac{1}{f} \frac{Q^*}{kT} + A_{Aitken} \quad (49)$$

where A_{Aitken} is a constant, and the subscript on Q^* has been dropped for convenience.

2.08.1.2.4 Origin of the heat of transport

Because of its importance to nuclear fuel restructuring and redistribution, it is worthwhile to briefly discuss some theories on the physics behind the heat of transport. A number of theories have been advanced to explain and calculate the heat of transport with varying degrees of success. In several instances, the comparison with the results have been limited to verifying the sign of the quantity and its general behavior as a function composition. In addition, understanding is hindered by confusion among the different quantities and overlapping phenomenon. The different quantities are discussed here, and calculated results specific to a particular fuel type, in particular oxygen diffusion in MOX, is left to Section 2.08.4.1.

We can carefully consider the meaning and purpose of the various quantities which characterize the phenomenon of thermomigration. It is clarified here that the heat of transport in the following discussion is rigorously defined by the TIP in (31) and occurs completely in the solid, therefore not considering any vapor phase transport. As noted below Eq. (31), Q^* is the reduced heat of transport and differentiated from the unreduced heat of transport or energy of transport, U^* by the partial specific enthalpy of the migrating atom, h_k ^{11,28}:

$$Q_k^* = U_k^* - h_k \quad (50)$$

Wirtz postulated that Q_k^* could be explained as a biased activated jump caused by the temperature gradient.^{29,30} In this conception, the activation energy associated with diffusion, H_m , is divided into three components corresponding to different positions on the migration path. Specifically, $H_m = H_i + H_s + H_f$, where H_i is the energy required by an atom to leave its initial position, H_s is the energy required by the lattice between the two sites at the saddle point in order to make a path for the migrating atom, and H_f , the energy required to make room for the atom at the final position. A temperature gradient along the migration path would imply an infinitesimal difference in the temperatures of the planes, and therefore a slight difference in the energy of atoms at the initial and final locations.

The derivation proceeds to balance the number of atoms in parallel plane which jump up and down the temperature gradient, and results in the steady state equation:

$$d \ln(N) = \frac{H_f - H_i}{kT^2} dT = - \frac{Q^*}{kT^2} dT \quad (51)$$

which is identical to Eq. (48) for dilute solutions, with the heat of transport identified as:

$$Q^* = H_i - H_f \quad (52)$$

the energy at the saddle-point having been found to cancel. The above theory also allows us to derive a relation between the activation energy for diffusion and the heat of transport:

$$|Q^*| \leq H_m \quad (53)$$

Doubt in this conclusion has however been cast by the work of Jones *et al.* whose theoretical work predicts the heat of transport to be larger than the migration enthalpy in solid argon.^{31,32} Nonetheless, Eq. (53) implies that $Q^* \approx H_m$, as is sometimes used as an approximation in calculations considering this phenomenon.^{10,33,34}

Another conclusion of (53) is that measurements of the heat of transport may provide information on how the activation energy for diffusion is divided between the initial, intermediate and final positions of the diffusing particle. If the lattice requires a relatively large amount of energy to create a path for the particle, then the heat of transport must be small. If, on the other hand, the lattice is relatively open along the migration path, then the migration enthalpy must originate in the binding energies of the atoms in initial and final sites, in which case the potential difference in energies may produce a more significant Q^* .^{35,36}

Alternate explanations suggest that the value of Q_k^* might also be explainable by the lattice energy associated with the movement of the species in the temperature gradient. This may be calculated directly for Q_k^* ,²⁸ or proposed to calculate Q_k^* based on thermodynamic functions by assuming that U^* in Eq. (50) is small in comparison to h_k .³⁷ In such a case, $Q^* \approx -h_k$.^{38,39} The partial molar enthalpy of k , h_k is then calculated from thermodynamic information on the molar heat of solution of species k in the solid, or may be related to the formation enthalpy of a Frenkel pair.^{38,39}

Another explanation for the heat of transport suggests instead of being based on lattice energies, it is influenced by the electric processes in the fuel.²⁷ The observed heat of transport would then be in fact a superposition of the true heat of transport, defined by Eq. (31) and an electric force acting on the diffusing ions.³⁶ Electrons (or holes) act as heat carriers by absorbing energy at hot regions and diffusing to cooler regions where the energy is released. Less energetic charge carriers must flow up the temperature gradient in order to maintain charge neutrality.

There are two processes in which the charge carriers may affect migration. The first is through direct interaction between energetic carriers and migrating ions, biasing their jump according to the effective charge of the ion.³⁶ (The effective charge need not be of the same magnitude or sign as the chemical valence as it contains contributions from the probability of interaction with electrons and holes, the later of which possesses a negative sign).

The second interaction is indirectly through the generation of an electrostatic potential across the temperature gradient, a phenomenon known as the *thermoelectric effect* and characterized by the *thermoelectric power*, also known as the *Seebeck coefficient* of the material. Migrating charge carriers are scattered by impurities, phonons etc. If this scattering is energy dependant, an electrostatic potential may be established in the material. The electrostatic potential may then influence the diffusion of the electrically charged ions via their valence.

Although this effect will not be written explicitly, the notion borne in mind when interpreting out-of-pile experimental data, as mentioned by Bober and Schumacher with regards to experiments involving a gas-tight rhenium capsule.⁴⁰ As will be discussed in detail in Section 2.08.4.1 this effect may be included within the TIP by considering the flux of charge carriers, and their creation and destruction as a separate diffusing species.

2.08.1.2.5 Other thermodynamic driving forces

Thus far, the thermodynamic driving forces of the type described in Eq. (5) were the temperature gradient and the gradient in chemical potential as resulting from a concentration gradient. While those are arguably the most important driving forces for nuclear fuel, there are other considerations which produce observable effects also.

2.08.1.2.5.1 Stress induced diffusion

Atoms may experience a force due to a gradient in the stress field. This may lead to a driving force for atomic movement and, similarly, for void migration.⁴¹ The flux force experienced by atoms is given by the spatial derivative of the stress gradient.¹⁴ In addition, stress induced diffusion can lead to the macroscopic phenomenon of *creep*.

2.08.1.2.5.2 Phase change

Coexistence/contact between two phases may also lead to mass redistribution if the phase change is non-congruent. The cause for this is the equilibrium between chemical potentials for species in either phase. This is the principle of Gibbs energy minimization, which is an expression of entropy production and therefore falls in line with the TIP. This effect is manifest in fuels which exhibit multiple phases, such as metallic U-Pu-Zr, where 3 phases are understood to exist at different points in the temperature gradient as discussed in Section 2.08.4.3. Redistribution by this mechanism also manifests in solid-liquid transitions for partially molten fuels, as discussed in Section 2.08.3.3.

2.08.1.2.5.3 Curvature

Atoms at the interface of a phase possess and excess *surface energy*, σ , but may also have a modified chemical potential due to the curvature of that surface. This effect originates in the slightly different number of nearest neighbors surrounding atoms on a curve. The difference in chemical potential may be described by Herring's formula which, in a simplified form results in the Gibbs-Thompson formula^{13,42}:

$$\mu_k - \mu_{k,r_1 = r_2 = \infty} = \Omega_k \sigma \left(\frac{1}{r_1} + \frac{1}{r_2} \right) \quad (54)$$

where r_1 and r_2 are the radii of curvature at the point on the surface, taken as positive for a convex surface, and $\mu_{k,r_1 = r_2 = \infty}$ is the chemical potential of species k for a flat interface, Ω_k is the specific volume of species k and σ is the surface energy.

The effect of this is motion in the solid state either by surface diffusion or vacancy diffusion through the body of the fuel in such a way that the curvature is reduced. The produced gradient in chemical potential produces a force referred to as the *sintering stress*, which is important for the 'sintering stress' in spheropac fuels Section 2.08.2.1.

2.08.1.3 Vapor Phase Transport

Apart from solid state matter transport, mass may also be transported via a gas filled void space through the so called 'evaporation-condensation' mechanism. Whenever solid fuel is adjacent to a void, it spontaneously vapourize parts of its constituents as it attempts to establish its equilibrium vapor pressure according to the local conditions. In equilibrium, the chemical potential of the

species in the solid should equal the chemical potential in the gas phase:

$$\mu_{k,vap} = \mu_{k,vap}^0 kT \ln(p_k) \quad (55)$$

where p_k is the partial pressure of species k .

Alternately, solid constituents may react with other species present in the gas phase resulting in movement via a *carrier gas* mechanism, as discussed further below. Once in the vapor phase, these species are free to diffuse in the gas phase through the void space and may reach points where the physical state of the solid is different enough that the vapor will condense. Depending on the vapor pressure and extent of the void space, this phenomenon can produce a faster matter transport mechanism than solid state diffusion.

The evaporation-condensation mechanism will produce restructuring as material is physically transported to other areas. In addition, the collection of vapor species evolved do not necessarily have the same overall chemical composition as the solid. Thus this process may separate the constituents of the solid by favorably transporting species with higher partial pressures. This is especially notable for MOX, as the vapor pressure of the *Pu* bearing species is approximately a factor of 10 greater than *U* bearing species. The enrichment of *Pu* can be seen as a result of pore migration (Section 2.08.2.3) and macroscopic gas-phase diffusion.

This section describes some of the physical conditions responsible for the evaporation-condensation mechanism, and briefly considers the associated redistribution effect.

2.08.1.3.1 Factors affecting equilibrium vapor pressure

A number of factors affect the equilibrium vapor pressure and so contribute to the evaporation-condensation mass transport mechanism. Local variation of temperature, composition and surface curvature which vary in space contribute.

2.08.1.3.1.1 Temperature

A gradient in temperature is one of the most clear sources of different vapor pressure. This is due to the exponential dependence of the vapor pressure with temperature as given by⁴²:

$$p_k = p_0 \exp(-\Delta H_{vap,k}/kT) \quad (56)$$

for vapor species k . The indication of vapor species is critical in this equation. As Breitung and Reil note in their recommendation the radii of curvature are approximately for enthalpy of vaporization of UO_2 , that since UO_2 vaporizes into a variety of species their recommendation is in fact an *effective* enthalpy of vaporization for the ensemble of species.⁴³

Due to the large temperature gradients present, this effect results in a potentially fast transport mechanism for material from the inner hot regions of the fuel to the outer cooler regions. The impact of this effect is discussed further with respect to MOX fuels and the carbides and nitrides.

2.08.1.3.1.2 Composition of the condensed phase

The relative concentrations of vapors in equilibrium with the solid may change with the chemical composition of the solid phase. If the overall fraction of one species in the vapor differs from the solid, then vapourization will alter the composition in the remaining solid. This may lead to the eventual establishment of a *congruent vaporization composition* in which the vapor has the same composition as the solid and thus will not shift the composition. Such is the case for $UO_{2\pm x}$ and multicomponent compounds such as $(U, Pu)O_{2\pm x}$ where the congruent vaporization of *U/Pu* may also depend on the state of oxidation, as discussed in Section 2.08.4.1.⁴⁴

2.08.1.3.1.3 Surface curvature

A final physical state is the curvature of the solid surface. As described in Section 2.08.1.2, the curvature of the surface affects the chemical potential of the condensed species. The equilibrium partial pressure will necessarily also be affected in the same manner via Eq. (55). Thus we arrive at the Young-Laplace equation^{42,45}:

$$\ln\left(\frac{p}{p_{k,r_1=r_2=\infty}}\right) = \frac{\Omega_k \sigma}{kT} \left(\frac{1}{r_1} + \frac{1}{r_2} \right) \quad (57)$$

The second effect concerns the equilibrium vapor pressure above curved surfaces and has two notable implications.

Similar arguments to those considered above lead to the determination of the increase in gas pressure inside a bubble which is in equilibrium with a solid:

$$P - P_{r=\infty} = \frac{2\sigma}{r} \quad (58)$$

which is useful in considering the pressure inside bubbles.

Lupis notes that this effect becomes important only when the radii of curvature are approximately 0.1 μm. He also cautions that for radii on the order of 1 nm the thermodynamic formalism begins to break down due to small numbers of participating molecules.⁴²

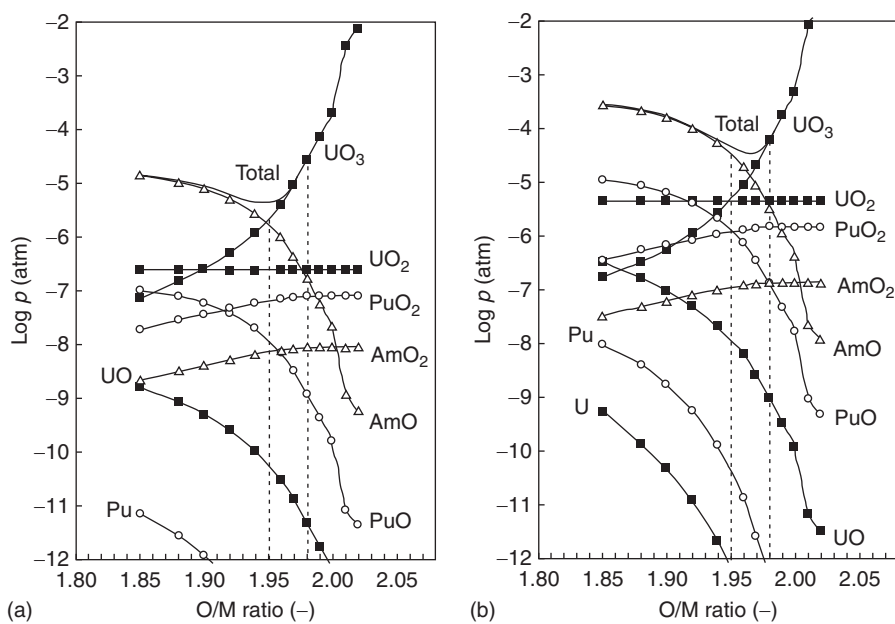


Fig. 3 Vapor pressures of actinide bearing species above Am containing MOX at (a) 2073K and (b) 2273K. Reproduced from Maeda, K., Sasaki, S., Kato, M., Kihara, Y., 2009. Radial redistribution of actinides in irradiated fr-mox fuels. J. Nucl. Mater. 389, 78–84.

2.08.1.3.2 Temperature driven vapor phase transport

Matter transport in the gas phase may be driven by a temperature gradient in one of two mechanisms. The first is simply due to a partial pressure gradient in a species, caused by Eq. (56), however this mechanism generally requires high temperatures in order to be efficient depending on the time and lengthscale of concern. Alternately, at low temperatures, components of the solid may be transported via a carrier gas.

2.08.1.3.3 Gradient in vapor pressure

At sufficiently high temperatures, evaporation of matrix material may occur. The partial pressure gradient would then drive transport of vapor species down the temperature gradient, where they would condense in regions of cooler temperature. This mechanism will generally result in restructuring as well as redistribution as the matrix itself may be transported, and vaporization may not be congruent. Fig. 3 shows the vapor pressures above a sample of 2%Am-MOX at two different temperatures, showing the change of dominant vapor species with O/M and temperature.⁴⁶ For example, this figure indicates that vaporization from a hyperstoichiometric sample will result in an enrichment of Pu at higher temperatures, and U migration down the temperature gradient by UO_3 diffusion. Likewise, O would be transported in the same way.⁴⁷ Similarly, hypostoichiometric MOX will shift the Am concentration accordingly. This mechanism is thought to be important in considering the migration of pores, as will be discussed later.

2.08.1.3.4 Carrier-gas assisted

Rand and Markin suggested that it might be possible that contamination by other elements may hasten the vapor transport of an element by acting as a carrier gas.⁴⁸ This is thought to be the case with H and C contamination of MOX, and O contamination of carbide fuels, discussed in Sections 2.08.4.1 and 2.08.4.4 respectively. The gas mixtures adjacent to the solids would then be H_2O/H_2 and CO_2/CO . As an example, even contaminations as low as 3 ppm carbon in UO_2 has a substantial effect.⁴⁹ The gases are free to react with the solid and diffuse along, for example, the length of the crack. The ratio of carrier gas species is determined by the chemical potential of oxygen (carbon) in the fuel, which varies with conditions such as temperature and oxygen (carbon) composition.

Diffusion of the carrier gas species therefore influences the distribution of the oxygen (carbon) allowing for its transport. In some cases a constant ratio of gases may be assumed in which case the resulting oxygen (carbon) redistribution results from the variation of the oxygen potential with temperature. In other cases, notably at high temperatures, the assumption of a constant ratio breaks down due to oxygen migration in the solid state or lack of interconnected void space. If the gas diffusion is considered to have reached steady state and equilibrium is assumed between the carrier gases and the solid surface, then it is possible to determine the resulting profile of the element in the solid as results from a temperature gradient. This then may be used as in Eq. (48) and an *effective heat of transport* may be derived from the chemical potentials of the gases involved.

Carrier gas assisted transport process is indirectly driven by the temperature gradient, via the dependency of the oxygen potential with temperature. It is therefore possible to derive an *effective heat of transport* to describe this effect. Aitken performed such a calculation for oxygen migration assuming a constant ratio of vapor species.³⁸ In the following derivation, the carrier gas

species will be represented as Z and ZO representing the unoxidized (H_2 , CO) and oxidized (H_2O , CO_2) species respectively. The carrier gases interchange oxygen in a reaction with the oxygen species *in the solid*:



If equilibrium is assumed, the Gibbs free energy of the reaction is zero and expressible in terms of the chemical potentials of the various species:

$$\Delta G = \mu_{Z(g)} + \frac{1}{2}\mu_{O_2(s)} - \mu_{ZO(g)} = 0 \quad (60)$$

We now expand the chemical potentials according to Eqs. (12) and (55). The mole fraction of dissolved O_2 in the solid UO_2 is replaced with the stoichiometry deviation x :

$$\frac{-\mu_{Z(g)}^0 - \frac{1}{2}\mu_{O_2(s)}^0 + \mu_{ZO(g)}^0}{kT} = \ln\left(\frac{p_{Z(g)}}{p_{ZO(g)}}\right) + \ln(\gamma x) \quad (61)$$

We now take the gradient and, exploiting the constant ratio of Z/ZO , along with Eq. (3) to obtain:

$$\frac{\left(-h_{Z(g)}^0 - \frac{1}{2}h_{O_2(s)}^0 + h_{ZO(g)}^0\right)}{k} \nabla \frac{1}{T} = f \nabla \ln(x) \quad (62)$$

where $h_{Z(g)}^0$ and $h_{ZO(g)}^0$ are the enthalpies of formation of gaseous Z and ZO respectively. Eq. (62) is comparable to (48) if we define a quantity analogous to the heat of transport, $Q_{O,vap}^*$ to be³⁸ (The definition in (62) differs from that of Bober and Schumacher in reference²⁷ who use a similar form but with the standard chemical potentials in place of specific molar enthalpies. The origin of this confusion may be the comparison of Eq. (61) with (49), however as noted in the derivation of the latter, this equation implies that Q^* is independent of T . If we take only the temperature independent component of μ^0 then we obtain h^0 and result in Eq. (63):)

$$Q_{O,vap}^* = \frac{1}{2}h_{O_2(s)}^0 + h_{Z(g)}^0 - h_{ZO(g)}^0 \quad (63)$$

It should be noted that $Q_{O,vap}^*$ is *not* the heat of transport of oxygen in the solid, nor the same in the vapor. Although it relates the transport of oxygen to the applied temperature gradient, the transport mechanism is indirect via chemical reaction and diffusion in the vapor phase and it is the gradient in this reaction potential which results in the transport. Therefore, this is not a thermodiffusion type flux, and should not be confused with the heat of transport defined in Section 2.08.1.2.

In reality, vapor transport would be accompanied by solid state thermodiffusion which Aitken suggests would result in a non-constant ratio of vapor species in (61). He continues to theorize that this would culminate in a modification to (62) which for the dilute limit is³⁸:

$$\left(-h_{Z(g)}^0 - \frac{1}{2}h_{O_2(s)}^0 + h_{ZO(g)}^0\right) \nabla \frac{1}{T} = (1 + L_s/L_g) k \nabla \ln(x) \quad (64)$$

where the mobility rates of the gaseous and solid migration, in the sense of (5) are given by L_g and L_s , respectively. While (64) recovers (62) for $L_g \gg L_s$, it does not recover (48) for $L_g \ll L_s$, a fact which Aitken attributes to the lack of considering equilibration of the solid with a gas phase when the later equations were discussed.

2.08.2 Microscopic Structures

Section 2.08.1 discussed some of the fundamental mechanisms which drive matter transport. Attention is now turned to how these phenomena leads to the development of microscopic structures and determines their evolution. In this section, we will consider sintering and grain growth before a detailed discussion of void migration.

2.08.2.1 Sintering and Grain Growth

As discussed in Section 2.08.1.2, the curvature of an interface and the minimization of interfacial area may also act as a driving force for matter transport. The interface may be the surface between the solid and a void, or the boundary between two solid crystals of different atomic structure/orientation. Both processes may be simulated using either Monte Carlo codes or multi-phase transport models such as the phase-field model.⁵⁰⁻⁵³

2.08.2.1.1 Sintering

The minimization of the surface area at an interface between solid and void leads to the sintering effect common in manufacturing processes. In this case, matter is driven to move from regions of high curvature towards areas of low curvature, in addition to reducing the overall surface area.

As a model, consider two spheres in contact. There is a sharp point near the contact area, towards which matter is driven both in the solid phase and through evaporation-condensation as described in Sections 2.08.1.2 and 2.08.1.3 respectively. The result is that the two particles *weld* together, forming a neck.¹³ If an external pressure is applied such that the spheres are pushed together, creep will also contribute to this process. Eventually, the process of curvature reduction results in the formation of spherical voids. Voids may now continue to shrink by the emission of vacancies either into the bulk solid or through diffusion along grain boundaries towards a vacancy sink.¹³

This phenomenon plays an important role in the restructuring of particle fuels as discussed for MOX fuels in Section 2.08.4.1.⁵⁴

2.08.2.1.2 Grain growth

The fuel manufacturing process produces grains of varying crystal orientation in the solid. When the temperature is favorable, i.e., during sintering and reactor operation, atoms along the curved interface between grains will experience a driving force due to the difference in curvature. Grains will therefore spontaneously grow in such a way as to reduce the total interfacial area, and so big grains will grow at the expense of smaller ones.

The process is complicated by the presence of inclusions in the solid, be they solid or gas filled voids. Inclusions prefer to reside on grain boundaries due to lower energy there than in the bulk solid. The lower energy configuration of inclusion on a grain boundary results in a *pinning* effect known as Zener pinning. In the case that the inclusion is immobile, it will effectively exert a force retarding the movement of the boundary, in which case there must be a sufficient driving force applied to the boundary in order to break free of the inclusion. Alternately, the inclusion may be mobile, as may be the case for voids. The boundary movement rate is then coupled to the migration rate of the inclusions.⁵⁵ Redistribution that occurs as the gases contained in small bubbles are moved by the boundary.

2.08.2.2 Void Migration

In reality, cracks, pores, and other vapor filled void space offer alternate modes of transport either along the solid surface or through vapor phase transport through the void. Both mechanism can result in the restructuring and redistribution of the constituents and may change the shape of the void itself. We now distinguish between microscopic voids enclosed in solid matrix such as pores and bubbles and macroscopic voids such as cracks, interconnected porosity and the space surrounding the fuel. This section will therefore discuss microscopic voids, their migration through the solid and the associated restructuring and redistribution of the solid matrix and constituents.

Voids change shape or migrate as atoms move around the surface or by the emission/absorption of vacancies from the surrounding solid. The phenomenon of void migration has been a subject of study by several authors.^{10,35,56–62} Three atomic transport mechanisms are identified: surface diffusion, volume diffusion and vapor phase transport. Vacancies and atoms on the surface are able to migrate by surface diffusion as this offers a potentially faster migration path than they experience in the solid. Alternately, vacancies may be emitted into the solid, diffuse through the solid volume and be absorbed at a different point resulting in a displacement of the void (Thus far we have been only considering vacancies however interstitials may also lead to the matter transport. However due to the relatively small concentration of interstitials compared to vacancies, the influence of this point defect may be neglected¹⁰). Finally, as the void is filled with vapor evolved from the local surface, difference in vapor pressure of matrix material may incur vapor phase transport. These mechanisms all participate in void migration but their relative magnitude vary for reasons of void geometry and material properties. These transport mechanisms are depicted schematically in Fig. 4.

In reality, these mechanisms are constantly active, with particles continuously moving around the surface, vacancies constantly being exchanged with the matrix and molecules constantly leaving and reattaching to the solid surface. For a void to remain at constant size requires that it emits voids into the solid at the same rate that it collects them. As Olander remarks, this is analogous to the dynamic equilibrium of a solid in contact with its saturated vapor, in which vaporization rate is balanced by the condensation.¹⁰ In the absence of a driving force of the type discussed in Section 2.08.1 acting on the particles, this produces random movement of the void in a manner similar to Brownian motion. If a driving force acting on the atoms (vacancies) is present, the void will migrate accordingly.

This section will focus on the migration of voids under a driving force, treating random void diffusion as a special case of zero driving force. Firstly, diffusion mechanism are discussed and modeled. Secondly, the driving forces of void migration are discussed. Finally, Following these descriptions, a comparison of the mechanisms is made and used as a basis for a division between two types of microscopic voids: bubbles and pores. As pore migration is of particular relevance to fast reactor fuel restructuring, the remainder of the article focusses on pores and pore migration.

2.08.2.2.1 Void migration mechanisms

A simple method of modeling void migration is by treating the void as a single superparticle which diffuses under a suitably modified driving force. The mobility of the superparticle is derived through consideration of particular migration mechanism, which culminates in the derivation of a void diffusion coefficient. Eq. (6) is then applicable with a suitably modified driving force, which allows for ready comparison between different driving forces. The calculation of the void diffusion coefficients also

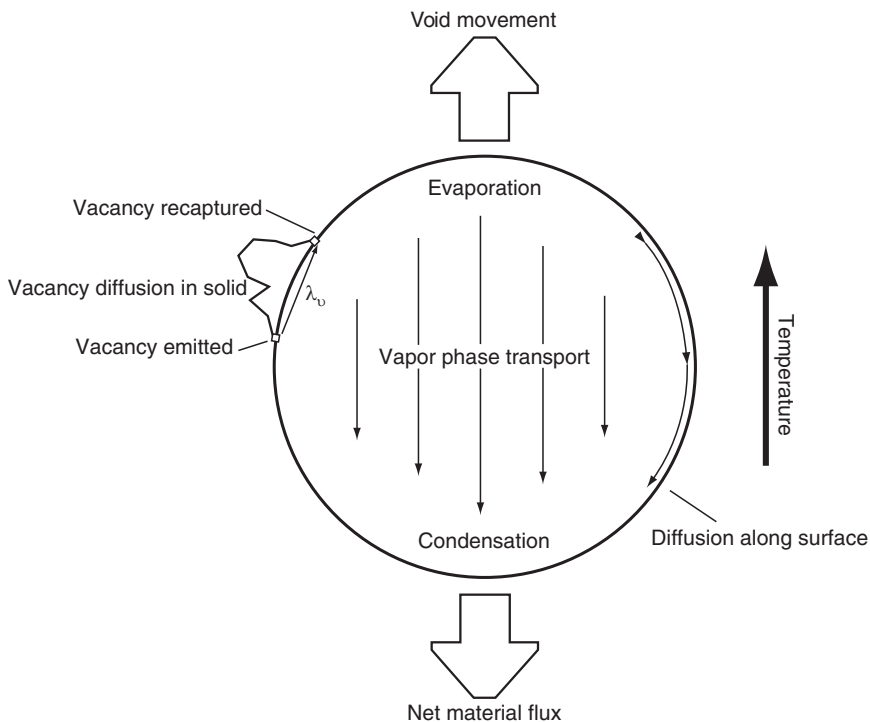


Fig. 4 Schematic description of void transport mechanisms showing vacancy surface diffusion, volume diffusion and vapor phase transport of matrix material.

naturally recovers the case of no driving force, which is important for determining how small voids move randomly and coalesce as discussed by.^{33,59} The three-dimensional mean-square distance traveled in a time Δt is calculated as $6D_{void}\Delta t$.³³

Nichols derived a set of void diffusion coefficients based on relating the jump frequency and jump distance of the superparticle to that of the rate-controlling species (U^{4+} for UO_2).^{33,59,63} The theory is based on kinetic diffusion theory which expresses the diffusion coefficient in terms of the number of potential sites, the jump frequency, Γ_{void} , and the jump distance, λ_{void} :

$$D_{void} = \frac{1}{6} \Gamma_{void} \lambda_{void}^2 \quad (65)$$

Much of the ensuing derivation assumes spherical voids, as are expected if they are in mechanical equilibrium with the matrix, however this assumption may sometimes be relaxed without affecting the primary conclusions of the analysis. The conclusions drawn may also be applied for solid inclusions in the fuel matrix but the discussion will refer to voids for the sake of convenience.

2.08.2.2.1.1 Void migration by surface diffusion

Voids may migrate due to the diffusion of molecules of the solid matrix around the surface of the void. In treating this mechanism, only the molecules on the surface are assumed to participate. Each jump of the superparticle constitutes movement of an equivalent volume of molecules. Therefore, the void jump distance, λ_{void} may be related to the jump distance of the molecules along the surface, $\lambda_{m,surf}$, by:

$$\lambda_{void} = \lambda_{m,surf} \frac{\Omega_m}{4\pi r_{void}^3 / 3} \quad (66)$$

where Ω_m is the molecular volume for the slowest moving species.

The void jump frequency may be related to that of the atomic species by similar reasoning, however since only the surface molecules participate with this mechanism, the void jump frequency is related to the molecular jump frequency by:

$$\Gamma_{void,surf} = \Gamma_{m,surf} \frac{4\pi r_{void}^2}{a_m^2} \quad (67)$$

where $a_m \approx \sqrt[3]{\Omega_m}$ is the spacing between rate-controlling species.

The atomic jump frequency along the surface, $\Gamma_{m,surf}$, is related to the volume diffusion coefficient in the same manner as (65), but with only four potential jump sites, $D_{m,surf} = \frac{1}{4} \Gamma_{m,surf} \lambda_{m,surf}$. The effective void diffusion coefficient is then be calculated from (66) and (67):

$$D_{void,surf} = D_{m,surf} \Omega_m \frac{3a_m}{2\pi r_{void}^4} \quad (68)$$

2.08.2.2.1.2 Void migration by volume diffusion

Another mechanism of void migration is the diffusion of vacancies through the solid matrix, referred to as volume diffusion. In determining the void jump distance by volume diffusion, Nichols applied the same reasoning which lead to (66) to obtain the same result.³³ Kelly's more sophisticated derivation of the jump distance differs from that of Nichols as it considers that the void does not move at the same jump distance as the vacancies in the solid, but rather considers spontaneous and continuous emission of vacancies at one point and subsequent random diffusion through the solid before they are recaptured at a different position.⁶⁴ The characteristic distance involved in this process is then the root-mean-square distance between the point of emission and that of recapture, as illustrated in Fig. 4. For the limiting case of $r_{void} \gg a_m$, this distance is (corrected for a factor of two as noted by Nichols)⁶⁰:

$$\overline{\lambda_v^2} = 2r_{void}a_m \quad (69)$$

the square root of which is then used in (66) for the vacancy jump distance. The result coincides with that of Nichols but is placed on a sounder physical basis.

$$\lambda_{void} = \lambda_{v,vol} \frac{\Omega_m}{4\pi r_{void}^3/3} \quad (70)$$

The void jump frequency was evaluated by Olander by considering the void to be a perfectly absorbing sphere surrounded by a concentration of vacancies in the solid.¹⁰ The resulting formula for a void in equilibrium is:

$$\Gamma_{void,vol} = \Gamma_{v,vol} \frac{4\pi r_{void}^3/3}{\Omega_m} \quad (71)$$

which is the same as proposed by Nichols using the logic which lead to (67) but again with a firmer physical basis. The resulting diffusion coefficient is then:

$$D_{void,vol} = D_{v,vol} \Omega_m \frac{3}{4\pi r^3} \quad (72)$$

Void migration by volume diffusion must be treated cautiously since it involves vacancy diffusion through the solid. Similar to the treatment of the Kirkendall effect in Section 2.08.1.2, the surrounding solid matrix itself is moving with respect to the solid far from the void. An example of this treatment is given below when calculating the void velocity in a thermal gradient in Section 2.08.2.2.

2.08.2.2.1.3 Void migration by vapor phase transport

A third mechanism of void migration is through vapor phase transport. The solid surrounding the void spontaneously develops vapor in an attempt to establish its equilibrium vapor pressure. If the equilibrium pressure varies along the surface, due to a temperature difference for example, the concentration gradient of matrix species will incur diffusion through the gas filling the void, leading to matter transport and void migration. The magnitude of this effect depends on the magnitude of the equilibrium vapor pressure and its gradient within the void, e.g.,: the temperature and the temperature gradient. The concentrations of the individual vapor species vary with temperature and the composition of the condensed phase and will not necessarily exist with the same composition as the condensed phase. In effect, preferential evaporation of one species over the others may shift the composition of the remaining solid, in addition to acting as a redistribution mechanism for the chemical species which is independent, and potentially contrary to solid state diffusion.

The most accurate method to predict void migration from vapor phase transport is by solving the diffusion of the vapor species across the void. This implies solving the mass balance equation which, for a steady state concentration profile is:

$$\nabla \cdot J_{vap} = 0 \quad (73)$$

the mass flux may be calculated through the fill gas using the TIP. The case is simple as we have only one vapor component diffusing through a fill gas:

$$J_{vap} = -L_{vap,vap} \nabla_T \mu_{vap} + L_{vap,q} \frac{1}{T} \nabla T \quad (74a)$$

$$J_q = -L_{q,vap} \nabla_T \mu_{vap} + L_{qq} \frac{1}{T} \nabla T \quad (74b)$$

Using similar arguments as used to develop solid state mass flux in a temperature gradient in Section 2.08.1.2 but with Eq. (55) to relate the chemical potential of the vapor to its partial pressure, ρ_{vap} , we obtain:

$$J_{vap} = -\frac{D_{vap}}{kT} \left(\nabla \rho_{vap} + Q_{vap}^* \frac{1}{T} \nabla T \right) \quad (75)$$

Through an analysis of kinetic theory, Sens asserts that $Q_{vap}^* = 0$ with a caveat that this is only valid for diffusion without restriction and therefore is not necessarily valid in the presence of a barrier, such as a porous membrane.⁶¹ Therefore the mass flux of vapor is simply:

$$J_{vap} = -\frac{D_{vap}}{kT} \nabla \rho_{vap} \quad (76)$$

and the balance equation for the steady state is:

$$\nabla \cdot \left(\frac{D_{vap}}{kT} \nabla p_{vap} \right) = 0 \quad (77)$$

The boundary condition of Eq. (77) is the partial pressure of the vapor species at the surface. The solution of this equation may become complicated if we consider that the vapor pressure need not be at the thermodynamically equilibrium value. Additionally, we can consider that the surface of the void moves at a rate $J_{vap}\Omega_m$. Finally, if thermodiffusion is considered to be the driving force, then a complete treatment must include solving for the temperature profile surrounding the void. This is discussed for a simple case in the next section and in more details when considering pores in Section 2.08.2.3.

It is however possible to treat the problem in a simplified manner as a spherical superparticle. While this simplification neglects several important phenomena, it is useful for ready comparison between void migration mechanisms. In this case, the equations are similar to volume diffusion but include the density difference between solid and gas. The jump distance is derived as was equation (66). The jump frequency is similar to his derivation of (71) but includes the concentration of vapor calculated from the equilibrium partial pressure of the rate controlling species and the departure from that equilibrium, $\alpha \leq 1$. Nichol's diffusion coefficient is then³³:

$$D_{void,vap} = \frac{3D_{vap}\Omega^2}{4\pi r_{void}^3} \frac{\alpha p_v}{kT} \quad (78)$$

The diffusion coefficient of vapor through the gas in the void may be calculated from kinetic gas theory.^{10,61} Typically, the magnitude of the diffusion coefficient depends on the total gas pressure in the void. For a void in equilibrium with the surrounding solid, the pressure varies with the radius as described in (58). Thus the dependence of Eq. (78), and the migration speed of the void is dependant on the behavior of the coefficient of vapor diffusion through the void fill gas, which may be linearly dependant on the radius of the bubble or independence on the radius if D is only proportional to T .

2.08.2.2.2 Void migration forces

Having discussed the mechanisms of void migration, we can now consider how driving forces of stress and temperature may influence void migration. Eq. (6) is the basic form of this relation but the driving force of the void superparticle, F_{void} , must be related to the molecular driving force F_m by noting that the energy of moving the void forward must be equivalent to moving an equal amount of atoms:

$$F_{void} = n_m \frac{4\pi r_{void}^3}{3} F_m \quad (79)$$

2.08.2.2.2.1 Migration driven by thermodiffusion

When considering thermodiffusion, the applicable temperature gradient must be considered as the presence of the void perturbs the macroscopic gradient, ∇T . The temperature gradient in the void, $(\nabla T)_{void}$ is applicable for surface diffusion and vapor diffusion whereas the gradient in the solid immediate surrounding the void, $(\nabla T)_{sur}$ is applicable for volume diffusion. The temperature gradient in and around the void may be derived in terms of the thermal conductivity of the void and the surrounding solid, K_{void} and K_{sur} respectively, may be derived from a classical solution to yield⁶⁰:

$$(\nabla T)_{void} = \frac{3K_{sur}}{2K_{void} + K_{sur}} \nabla T \quad (80a)$$

$$(\nabla T)_{sur} = \frac{1 - 2(K_{sur} - K_{void})}{2K_{void} + K_{sur}} \nabla T \quad (80b)$$

The void velocity in a macroscopic thermal gradient, ∇T is therefore:

$$v_{void,surf} = D_{v,surf} \Omega \frac{2a}{r_{void}} \frac{1}{kT} \frac{3K_{sur}}{2K_{void} + K_{sur}} \frac{Q_{surf}^*}{T} \nabla T \quad (81a)$$

$$v_{void,vap} = D_{v,vap} \Omega \alpha p_v \frac{1}{kT} \frac{3K_{sur}}{2K_{void} + K_{sur}} \frac{\Delta H}{kT} \nabla T \quad (81b)$$

Shewmon warns that the heats of transport for surface and volume migration need not be equal, and therefore any value calculated from experiments must then be attributed to either surface or volume according to the dominant mechanism.

As pointed out by Biebsack and Diez, the velocity of void migration due to vacancy diffusion in the solid must be treated as a special case since it involves vacancy diffusion in the solid.⁵⁷ As was the case in considering the Kirkendall velocity in (18), we must therefore account for the movement of the surrounding lattice also. The surrounding lattice moves as the vacancies diffuse and are annihilated/created in the macroscopic temperature gradient:

$$v_{lattice} = D_v \frac{Q_v^*}{kT^2} \nabla T \quad (82)$$

which implies that the void velocity with respect to the bulk material is:

$$v_{void,vol} = D_{v,vol} \frac{1}{kT} \frac{Q_v^* 2(K_{sur} - K_{void})}{T} \frac{2K_{void} + K_{sur}}{2K_{void} + K_{sur}} \nabla T \quad (83)$$

An interesting feature in (83) is that, unlike migration due to surface diffusion or vapor transport, the *direction* of void migration depends on the relative conductivities of void and surrounds. Although typically the void conductivity is much less than the surroundings, this may not be the case in the treatment of migrating solid inclusions, for which the treatment of surface and volume diffusion applies. Therefore even the sign of the heat of transport in (83) must be considered carefully.

The impact of the stress field surrounding a void has also been addressed.^{10,33,34,41} The analysis considers the work done by compressing the gas inside the void, changing the surface area and the change in energy of the surrounding solid. This driving force may be compared to that of thermal diffusion and ranges, depending on the chosen parameters, on the order of 1%–4%.^{10,34} A more sophisticated approach investigated the effect of stress driven migration and geometry evolution for voids located on grain boundaries.⁴¹ It was suggested that stress driven migration may become comparable to thermodiffusion along the surface for the case of oblate pores with the polar axis perpendicular to the grain boundary.^{34,41}

2.08.2.2.2.2 Pinning

As mentioned in the discussion of grain growth, when a small void migrates to a grain boundary, the reduction in surface energy can pin it. The typical migration length of small voids may therefore be limited by the size of the grain.^{55,65} They do not therefore provide a large contribution to fuel restructuring, although they do significantly affect the macroscopic behavior of the fuel. If sufficient bubbles exist at the grain boundaries, they can interlink, creating macroscopic voids which span large distances in the fuel solid. These voids enable the evaporation-condensation on the macroscopic scale. The pinning of bubbles to grain boundaries and dislocations is the subject of several papers, notably a statistics based grain/bubble growth algorithm,⁵⁰ however the details of this process are not elaborated on here.

2.08.2.2.3 Comparison of void migration behavior and experimental applications

By comparing the dependence of the void mobility to the void radius, it is possible to gain insight into which of the surface, volume or vapor diffusion mechanisms is dominant. Through examination of Eqs. (81a and b) and (83) it is apparent that only the surface diffusion mechanism is dependant inversely on the void radius. This conclusion was first proposed by Shewmon,³⁵ who used this theory to analyse the results of Barnes and Mazey's experiments in which He-filled bubbles, approximately 10^{-2} μm in radius, were implanted into copper foil and a temperature gradient applied which drove the bubbles to migrate due to thermodiffusion.⁶⁶ When the migration pattern was examined, it was determined that the rate of migration was proportional to the inverse of the bubble radius, in accordance with the predictions of Shewmon and Nichols. The conclusion of size dependence is also supported by molecular dynamics simulations and a phase-field model considering vacancy diffusion through the solid bulk.^{34,67,68}

The three mechanism need not operate independently but can occur cooperatively, as is the postulated explanation of void migration in $(U, Pu)C$. In this fuel, the equilibrium vapor contains very little carbon, and so it is thought that while U and Pu transport across the void via vapor transport, rapid solid state carbon diffusion moves carbon to balance the molecule.⁶⁹ The migration rate of the void is then determined by the smaller of the two rates which, in this case, is the vapor transport of the metal. This is discussed more thoroughly in the carbide fuel section, Section 2.08.4.2.

Nichols reminds us that while the rate of a mass transport process such as void migration is limited by the speed of diffusion, there are other factors that may be relevant in reducing the speed of the process.³³ Such a rate-controlling step may be the transfer of material across the void-solid interface. As Nichols discusses, local equilibrium at the surface may be considered quite generally except for interfaces which are atomically smooth and crystallographically low-indexed.⁷⁰ At such a surface, deposition of diffusing atoms may involve the nucleation of new atomic layers, a difficult and therefore slow process. This limitation may however be overcome by a strong force driving the interface movement such as that of a thermal gradient in excess of 1000 K/cm, in which case the situation returns to diffusion control.⁷¹ Therefore, it may be that interface control may only be important in the case of little or no driving force. Shewmon also considers the interface reaction control and concludes that for a spherical void, the migration speed should increase with r_{pore}^n , an important conclusion as it ensures the deduction of the surface diffusion mechanism from the inverse radius behavior remains a valid conclusion. The surface reaction rate will initially determine the migration behavior until a radius is reached where the faster of surface or volume diffusion will determine the speed of migration. In support of this supposition, Shewmon cites the work of Wernick⁷² who conducted experiments with molten aluminum wires in germanium, under a temperature gradient. The migration rate displayed exponential behavior for small wire radii before becoming radius independent, which may be explained by interface control leading to volume diffusion.

A distinction may now be made between two types of voids, bubbles and pores, based on their migration behavior as determined by size, shape, and gas pressure. Bubbles are considerably smaller, typically contain fission gases at a high pressure comparable to the Laplace pressure given by (58), and are typically in a shape determined by the balance of interfacial energies; spherical for intragranular bubbles and lenticular for intergranular bubbles. Pores are larger, contain gas at low pressure and are typically not in shapes determined by interfacial energetics. Therefore much of the preceding theory may be directly applied to bubble migration, whereas pore migration must be dealt with in greater detail in the following section. A summary of these differences is given in Table 2.

Table 1 Enthalpies of formation of carrier gas species

	CO_2	CO	H_2O	H_2
$\Delta H^\circ [kJ/mol]$	-393	-109	-234	0

Note: Aitken, E.A., 1969. Thermal diffusion in closed oxide fuel systems. J. Nucl. Mater. 30, 62–73.

Table 2 Comparison of some characteristics between bubbles and voids observed in MOX fuels

	Bubbles	Voids
Size	<1 μm diameter	>1 μm in smallest dimension
Pressure	~300 atm	~3 atm
Shape	Spherical/lenticular	Lenticular
Contents	Gaseous fission products	Predominately cover gas
Origin	Fission yield	Initial porosity and cracks

Bubbles nucleate by fission gas, mostly Xenon, precipitating from the solid matrix. The gas originates as fission products which diffuses to the bubble from the surround solid. Their migration, coalescence and interlinkage is of particular importance for fuel swelling. The dominant migration mechanism is significantly affected by the bubble radius. High internal gas pressure is required to balance the isostatic stress of the surrounding matrix and the effect of the interfacial energy as calculated by Eq. (58). However, experiments have demonstrated that low temperature bubbles may be overpressurized as compared to (58) possibly due to a lack of vacancy availability.⁷³ The large pressure suppresses vapor phase diffusion, while the surface diffusion mechanism becomes more important due to small bubble radii.

This analysis of bubble migration has been applied to nuclear fuels by several authors. Cornell and Williamson observed the migration of Krypton bubbles in UO_2 and verified that their migration also adheres to the $1/r_{void}$ relationship.⁷⁴ In another case, Michels *et al.* observed fission-gas filled bubbles in an irradiated mixed oxide element at a temperature range 1933–2153K and gradient 4900 to 3900 K/cm. The voids had radii of 1–5 μm and migrated between 0.65 and 12.9 $\text{\AA}/\text{s}$ with no apparent relation between the migration speed and the void size, indicating that the dominant diffusion mechanism was most likely not surface diffusion but vapor phase transport.⁷⁵ They also credit a large spread in migration velocities to the effect of dislocations and grain boundaries. Speight summarizes the comparison of the vapor and surface diffusion mechanisms for UO_2 and, for a rough calculation with several assumed values, calculates that the critical radius for the change between surface and vapor diffusion mechanisms at 2000K is approximately 1 μm , a conclusion later supported by extrapolation of molecular dynamics simulation results.^{34,56}

The treatments of surface and vacancy diffusion above are in fact not restricted to gas filled voids, but also apply to solid inclusions in the fuel matrix. Michels *et al.*, also examined the migration of solid inclusions in MOX up the temperature gradient.⁷⁵ Inclusions were of radius of 0.5–3.25 μm , in a temperature range of 1973–2143K and a temperature gradient of 4900 to 3900K/cm. Migration speeds averaged 0.2–9.2 $\text{\AA}/\text{s}$ and were found to be inversely proportional to the radius of the inclusion, in conformation to the surface diffusion mechanism.

2.08.2.3 Pore Migration

The characteristics and behavior of pores differs quite significantly from that of bubbles. Bubbles are typically observed in either a spherical or lenticular shapes for intra-and intergranular bubbles respectively, which optimize their total interfacial energies. In comparison, pores are typically observed to exist in the shape of a lens with the minor axis aligned with the temperature gradient, and a relatively flat trailing edge as shown in Fig. 5. Such an irregular shape implies that the shape of the void is not being determined by interfacial energy.

Pores are typically filled with gasses used in fuel manufacturing, such as He or Ar , at low pressure. As burn-up increases, Fission products, notably Xenon and Krypton may also be found as they diffuse into the pore or are swept up during pore migration. When they merge with a large fissure or the central void, the accumulated gaseous inventory is released. Fission products which are not volatile and are insoluble in the fuel matrix form precipitates and these too may be captured in migrating pores and deposited in the central region. Such is the case with Ru , which precipitates into a metal phase in the fuel but was nonetheless found in the central cavity following irradiation.³

Due to the low gas pressure found in voids and their irregular shape, it is thought that the evaporation-condensation mechanism is the dominant material transport mechanism. This implies a quite complex system as the equilibrium partial pressure depends on the surface temperature and the solid composition, both of which are perturbed and altered by the presence of the pore. The temperature gradient in the region of the pore is perturbed due to the lower thermal conductivity within the low pressure gas-filled pores. The composition is altered due to preferential evaporation which redistributes the constituents as the pore moves.

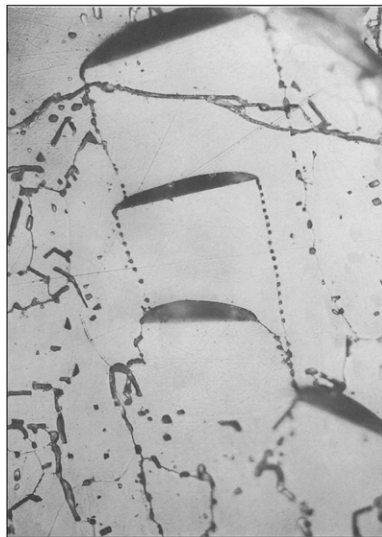


Fig. 5 Lenticular pores migrating up the temperature gradient (upper edge is at higher temperature). © European Communities, reproduced with permission.

Pores also differ from bubbles in that they are very mobile in the fuel, migrating up the temperature gradient until it reaches a macroscopic void. This transient existence may explain why the spherical shape or lenticular along a grain boundary, corresponding to an interfacial energy optimum, is never achieved. In contrast to bubbles, they are too large to be pinned to grain boundaries and in fact consume grains to form new columnar grains in their wake. In accordance with the supposition of a vapor transport migration mechanism, it was also found that pores migrate at approximately the same speed, regardless of size. Considering that they do not get pinned to grain boundaries, this implies that they are unlikely to coalesce with each other before reaching the highest temperature solid region where they do meet and form one of the most pronounced features of fast reactor fuels, the central void. The effect of pore migration on the microstructure of the fuel is thus significant and so will be dealt in greater detail in the following section.

The following section discusses some theories behind the shape and migration speeds of pores in greater detail.

2.08.2.3.1 The origin of pores

Pores are initially present in the sample as part of the fabrication process. The density of modern fuels following the manufacturing process is less than the maximum, theoretical density in order to leave space to accommodate fission products. The empty volume is distributed approximately homogeneously throughout the matrix as pores. As will be discussed later, the migration speed is fast, and can completely remove the initial porosity within a matter of hours. However, as indicated in Fig. 6, pores continue to be created from cracks, and so the effect of their migration continues as burnup increase. Ronchi and Sari suggested that the formation of pores from the fabrication porosity was dependant on the pressure of He in the fuel matrix and that large He pressure could prevent the pores from forming lenticular shapes.⁷⁶ Lewis *et al.* showed that high density fuels did not, in general, exhibit pores and columnar grain growth.^{63,77}

2.08.2.3.2 The shape of migrating pores

During pore migration, the pore may change its shape depending on the condensation rate at various points on the surface and eventually morph into the lenticular pores seen in (5). Studies showed the appearance of lenticular voids at the head of radially-oriented columnar grains, with small spheres between the grains, spaced roughly regularly at intervals approximately equal to the width of the pore. The radially oriented pores do not appear to be mobile⁶¹ however do appear to be related to the pore migration/shape. Explaining the shape of the migrating pores has been a subject of much examination and debate. Hypotheses to account for the shape of the pores and the origin of the trailing bubbles include arguments based on vapor transport dependence on the geometry of the pores, the attachment kinetics of vapor molecules to the trailing edge and the presence of volatile impurities.

As discussed in Section 2.08.2.2, proper treatment of the evaporation-condensation mechanism involves modeling both temperature and mass transport in and around the pore. The effect of pore geometry on heat and mass transport was investigated by Sens for pores which were initially spherical, tubular or disk-shaped solving the equations for vapor transport and heat transport numerically, although surface energy was neglected.⁶¹ The simulation showed that the initially spherical pores tended to elongate as the leading edge moved faster than the trailing edge. The tubular pores showed the same behavior and also a slower overall pore migration speed. The elongation of spherical pores to cigar shape was also predicted by Nichols.^{60,63} The disk shaped pores showed leading and trailing edges moving at the same rate, and a pore velocity greater than either the sphere or the tube.

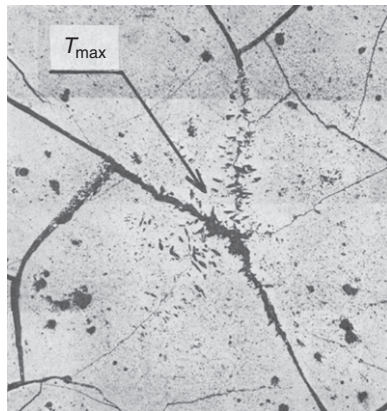


Fig. 6 Evidence of cracks acting as a source of pores. Also visible is the congregation of pores at the maximum temperature, which will lead to a central void formation. Reproduced from Sens, P.F., 1972. The kinetics of pore movement in UO₂ fuel rods. J. Nucl. Mater. 43, 293–307.

More modern treatments of pore-migration using phase-field models also show the evolution of initially spherical voids into the lenticular pore shape.⁷⁸

Because of their observed role in fuel restructuring, disk-shaped pores were investigated in more detail. Sens' simulations showed that during the course of migration, the disk-shaped pores evolved towards the lenticular pores observed experimentally. Initially, the disk bends as a whole, until the curvature at the trailing periphery is speculated to pinch off to form spherical voids, which serves to flatten the trailing edge.⁶¹

Oldfield and Markworth performed a similar analysis of pore migration based on thermodynamic argument for determining the driving force for solid growth.⁵⁸ Two effects are discussed which may affect the shape of the pore. Firstly, the kinetics of vapor molecules attaching to the surface is considered. A model was employed where vapor molecules impinging on the surface temporarily attach and may diffuse along the surface until they meet a suitable low energy site where they may attach permanently. Such a site includes ledges or pits in the crystal lattice, effectively providing nearest neighbors. Attachment may thus proceed as a series of moving ledges, as illustrated in Fig. 7. The resulting evolution of the pore shape is towards a disk shape.

The second factor considered by Oldfield and Markworth was the effect of the impurities in the pore. As the pore migrates, it will encounter fission products dissolved in the solid matrix, caused by burnup. Volatile fission products will be transported across the pore, whereas non-volatile products will accumulate on the leading edge. The impurities at the trailing edge impede the rate of condensation and eventually destabilize the advancing solid front. The front, now undergoing cellular growth, forms steep sided grooves into which impurities are trapped when the grooves pinch off. The grooves then form a string of regularly spaced bubbles which have been postulated to stretch over the grain boundary as they relax mechanically.⁴¹ The combined effect of these two factors may yield the lenticular pores as observed, with a string of fission products filled bubbles in its wake as shown in Fig. 8.

2.08.2.3.3 Pore migration speed

The speed of pore migration is important for understanding how the behavior of the fuel evolves over time. Pores migrate rapidly enough such that when the fuel is brought up to power, the pores present from the initial porosity complete their journey to the highest temperature within a matter of minutes to hours.^{27,40} As the pore migration results in restructuring, the speed and extent of the migration is of considerable interest. Several authors have developed theories of pore migration, however they all amount to the same expression of mass flux via a partial pressure gradient across the pore.^{10,61,63,79,80}

In the general case, the movement of the void is given by the matter flux of the slowest moving species, given by Eq. (76) multiplied by the specific volume of the molecule in the solid. A common model is to assume a large disk as shown in Fig. 9 which migrates undeformed, with the migration speed given by: $v_{pore} = -J_{vap}\Omega_m$. Expressing the mass flux in terms of the temperature gradient via (56):

$$v_{pore} = \Omega_m \frac{D_{vap}(T, P)}{kT} \frac{\Delta H_{vap}}{kT^2} e^{-\frac{\Delta H_{vap}}{kT}} (\nabla T)_{pore} \quad (84)$$

where $D_{vap}(T, P)$ is the diffusion coefficient of the matrix vapor species (or slowest moving component) through the gas in the pore. An interesting feature of Eq. (84) is that the velocity of the pores approaches zero as the pore reaches the centreline due to the diminishing temperature gradient. Meyer suggests that the final process which drives the pore to coalesce with the central void is in fact a sintering process.⁸¹

The diffusion coefficient $D_{vap}(T, P_{fill})$ is often estimated by kinetic gas theory, of which a variety are available of varying complexity and sophistication.^{10,33,61,80} Typically, kinetic treatments require the total gas pressure within the pore which may vary with the local temperature, or as a result of dynamic processes. In general, the various theories may be expressed in the form:

$$v_{pore} = A_{vap} \frac{1}{P_{fill} T^{3/2}} e^{-\frac{\Delta H_{vap}}{kT}} (\nabla T)_{pore} \quad (85)$$

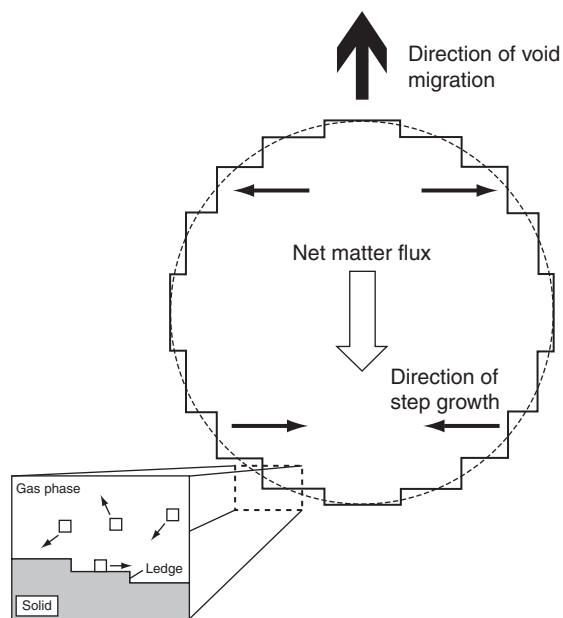


Fig. 7 Schematic of how pore shape may evolve due to attachment kinetics at the trailing edge. Growth direction indicated by arrows. Based on Olander, D.R., 1976. Fundamental Aspects of Nuclear Reactor Fuel Elements. Technical Information Center, Office of Public Affairs. Oldfield, W., Markworth, A.J., 1969. The theory of bubble migration applied to irradiated materials. Mater. Sci. Eng. 4, 353–366.

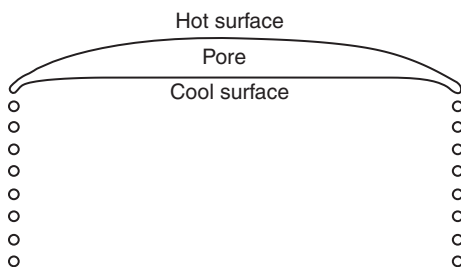


Fig. 8 Resulting pore shape from vaporization arguments. Reproduced from Oldfield, W., Markworth, A.J., 1969. The theory of bubble migration applied to irradiated materials. Mater. Sci. Eng. 4, 353–366.

where A_{vap} is a collection of constants which combines the enthalpy of vaporization with terms depending on the choice of kinetic theory employed.⁷⁶ Note that according to the Oldfield model, the term in the exponential will not be ΔH_{vap} but a larger factor which accounts for attachment kinetics and the effects of impurities.⁵⁸

During pore migration, pinching off of trailing bubbles may result in the loss of volume and/or gas or similarly the pore may gain volume and/or gas by digestion of other voids or dissolved fission gas in its path. The gas content of the pore may also change by processes common with fission gas bubbles, loss by resolution or diffusion-controlled absorption from the solid matrix. In the case that the pressure is only affected by the local temperature, Olander points out that, if the pores were sealed off during sintering at temperature T_{sint} , the pressure in the pore would actually be given by $P_{fill} = T/T_{sint}$.¹⁰ Guarro and Olander predict an increase in the diffusion coefficient (assumed equal for U and Pu species) by a factor of 6.7 which, via Eq. (84) results in an increase in migration speed by the same factor.⁸²

Eq. (84) implies some specific behavior about pore migration. Firstly, the velocity of the pore is not dependant on the size (insofar as the temperature gradient is not further perturbed), which implies that pores move at the same rate, an experimentally verified feature. Secondly, if the fill gas pressure is assumed to behave ideally with temperature, and not be dependant on the pore size, then the velocity varies as $T^{-5/2}$, which was confirmed by Ronchi and Sari.⁷⁶ Finally, Ronchi and Sari also observed that the migration speed roughly describes an Arrhenius plot with an activation energy of 5 ± 0.5 eV/molecule, comparable to their reported evaporation enthalpy of UO_2 , 5.8 ± 0.1 eV/molecule which indicates that the energetic effects proposed by Oldfield and Markworth are not rate determining.

Clement pointed out a discrepancy between the velocity predictions of Nichols and the experimental results of Ronchi and Sari by as much as a factor of 400,^{33,76,80} which can be rectified by considering the sample as even slightly hyperstoichiometric due to the large increase in UO_3 vapor pressure resulting from such a shift.

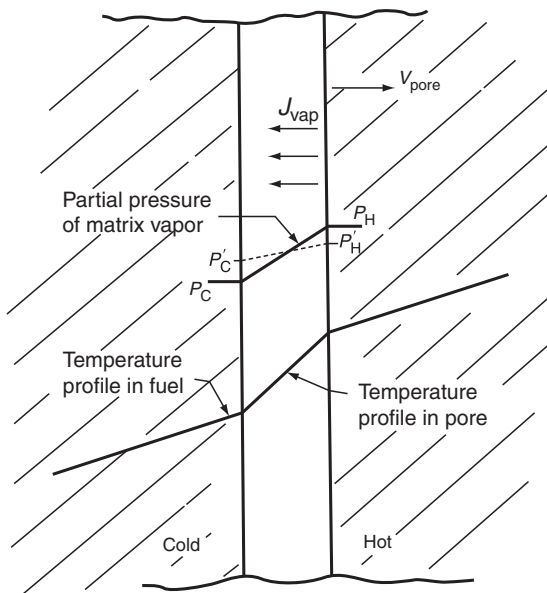


Fig. 9 Model migrating pore as an infinite slab, showing the partial pressure and perturbed temperature profiles across the pore. Partial pressures indicated at the hot (H) and cold (C) side of the pore are P^o and P' representing the ideal value and the change resulting from impurity accumulation and attachment kinetics respectively. Modified from Olander, D.R., 1976. Fundamental Aspects of Nuclear Reactor Fuel Elements. Technical Information Center, Office of Public Affairs.

Similar to the discussion in Section 2.08.2.2 for the general case of a void in the solid matrix, the presence of the pore perturbs the local temperature field in such a way that the temperature gradient across the pore may be significantly larger than in the surrounding matrix. In his treatment, Nichols calculated as $(\nabla T)_{pore} = \frac{3}{2}(\nabla T)_{matrix}$ assuming an insulating sphere. This calculation was followed by a numerical calculation by Sens on the same simulation as used to determine the pore shape described previously. His prediction is $(\nabla T)_{pore} = 4(\nabla T)_{matrix}$.

Sens briefly considers the contribution of radiation to the heat transport in the pore. For his disk-shaped pore of width 20 μm , he reports that the radiative contribution is below 10% of the total heat flux at 2000K. He further states that the radiative contribution becomes comparable in magnitude to the conductive flux at temperatures approaching 10,000K.

Another modification to (84) comes from the reduction of the driving force, the difference in partial pressure, resulting from the combined effects of impurity accumulation at the leading edge, and attachment kinetics at the trailing edge.^{10,58} The presence of impurities dissolved in the solid matrix, as caused by burnup, lowers the equilibrium partial pressure of the matrix material in accordance with Raoult's law. If the impurities are volatile, they will be transported across the pore, but if they are non-volatile, they will accumulate at the leading edge and progressively decrease the matrix partial pressure. In addition, the attachment kinetics discussed above may also affect the rate of condensation on the trailing edge. This concept arises from the theory that molecules in vapor attach most easily to ledges in the solid matrix. The relatively flat trailing edge implies a retardation of this effect and so an excess in partial pressure in the vapor may develop in order to overcome this kinetic effect. The results of these two effects on the equilibrium vapor pressure are shown schematically in Fig. 9, where the vapor pressures at the hot and cold side, p_H and p_C respectively, move towards p'_H and p'_C . Olander performed a calculation of these combined effects assuming the pore is infinite in transverse dimension and determined that the rate of migration may significantly decrease as a consequence.¹⁰ Specifically, for an soluble impurity mole fraction at the leading edge of 0.01, a condensation coefficient (the fraction of impinging molecules which adhere to the solid) of 0.9, and a pore width of 10 μm results in a decrease in the migration velocity of 41%. If the pore width is increased to 20 μm , then the reduction is 59%.¹⁰ The calculations thus suggest a large impact of soluble fission products and attachment kinetics on the pore migration velocity, the magnitude of which depends on the width of the pore. Smaller pores may then be immobilized, whereas larger pores may continue unimpeded.

2.08.2.3.4 Redistribution of matrix material

As discussed in Section 2.08.1.3, the different vapor pressures of species in the condensed phase may lead to unmixing as pores migrate. The magnitude of this redistribution mechanism has been investigated by numerous authors but remains somewhat unclear especially in comparison to redistribution by vapor phase through cracks.^{2,27,81–86}

Guarro and Olander performed a sophisticated analysis considering the actinides transported across the pores but also the distribution of those actinides in the solid phase ahead and behind migrating pores.⁸² A schematic of the pore migration and concurrent redistribution is shown in Fig. 10 for a pore modeled as an infinite slab, with the U/Pu ratio represented by q . The figure describes an initial startup spike of Pu depletion followed by a quasi-steady state migration of the pore lead by a Pu rich bow wave.

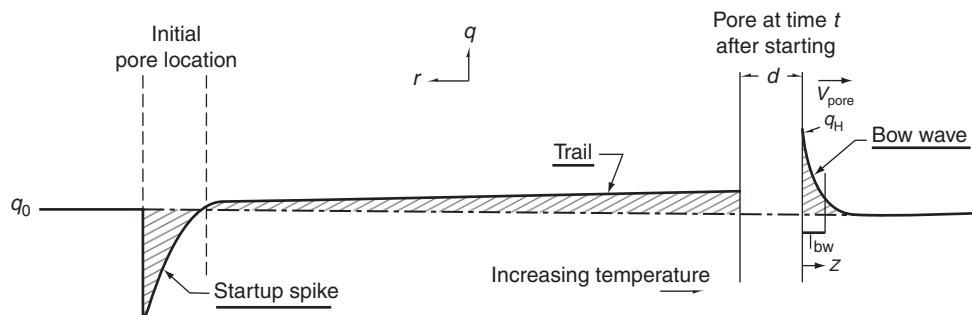


Fig. 10 Schematic of *Pu* redistribution as a result of pore migration. Modified from Guarro, S., Olander, D.R., 1975. Actinide redistribution due to pore migration in hyperstoichiometric mixed-oxide fuel pins. *J. Nucl. Mater.* 57, 136–144.

Initially, the hot and cold side of the pore are at the initial composition, q_0 . Preferential evaporation of *U* bearing species from the hot side leaves It *Pu* rich and the cold side *Pu* depleted while advancing the pore slightly. The total vapor composition evolved from the hot surface becomes slightly more *Pu* rich due to the increased mole fraction of *Pu* in the solid, resulting in more *Pu* being transported across the pore and deposited on the cold side. This process continues until the original composition is reached on the cold side, leaving the start up spike depicted in Fig. 10.

Once the initial startup spike is generated, the pore migrates in a quasi-steady state manner where the hot surface is preceded by bow wave of *Pu* caused by diffusion of *Pu* into the solid ahead of the pore. The bow wave follows an exponentially decaying *Pu* concentration with a characteristic depth depending on the speed of *Pu* diffusion in the solid, D_{U-Pu} , compared to the pore velocity, v_p ⁸⁵:

$$l_{bw} = \frac{D_{U-Pu}}{v_p} \quad (86)$$

which, for example is calculated to be $\approx 1 \mu\text{m}$ at 2000K ⁸² for MOX. This parameter is temperature dependant in both D_{U-Pu} and v_p , but with increasing temperature the pore velocity increases faster implying a shrinkage of the *Pu* enrichment wave. The *Pu* lost from the wave in front of the pore is deposited on the cold surface as the pore migrates, leading to a gradual increasing concentration of *Pu* in the tail of the pore.⁸⁵

The issue of solid state diffusion around the pore, and thus the validity of the infinite slab model, may be examined by considering the depth of the *Pu* wave compared to the width of the pore. Guarro and Olander noted that for actinides, the width is large enough to justify this assumption, however note that the oxygen can migrate around the pore in this manner.⁸² Therefore the model is justified for consideration of actinide separation, and the bulk stoichiometry is considered to be quickly restored by this mechanism despite the UO_3 vaporization from the hot surface.

The conclusion of the study by Olander and Guarro and Olander is that pore migration will not significantly contribute to actinide redistribution considering the current models of pore migration velocity.^{82,85} Olander also considered *Pu* migration by the accumulation of *Pu* rich vapor in the pore volume, a process analogous to zone refinement but found that this effect was too small to be significant.⁸⁵ This conclusion is in disagreement with the model of Meyer.^{81,87} The model used by Clement and Finnis supports the claim by Olander that pore migration cannot contribute to *Pu* redistribution.⁸⁸ They conclude that the pore migration velocity must be reduced in order for greater redistribution to occur, which may happen during operation as previously discussed.

2.08.3 Bulk Phenomena

We have now discussed mass transport occurring in nuclear fuels on an atomic and microscopic level. During the course of operation, macroscopic structures and characteristics will develop. In particular, this section addresses cracks, porosity evolution and the consequence of melting.

2.08.3.1 Cracks

Cracks in the fuel pellet develop very quickly due to thermal stresses. During operation they may also be generated during power cycles, either in heating up or cooling down. As mentioned in Section 2.08.2.3, cracks may form a source of migrating pores. These pores then remove some of the empty volume of the crack, leading to its healing.

Cracks may be present in radial or circumferential directions. Radial cracks in particular play a role in redistribution as they offer long channels of void space, appropriate for mechanisms such as carrier-gas based redistribution discussed in Section 2.08.1.3.



Fig. 11 Lenticular pores migrating with trailing bubbles. © European Communities, reproduced with permission.

2.08.3.2 Porosity Evolution

Restructuring of the solid affects the local porosity, an important consideration for understanding fuel behavior as heat and mass transport both depend largely on the local porosity and the degree of interconnectedness in that porosity. Both solid state and vapor transport are capable of altering the solid structure, either by vacancy diffusion or by evaporation-condensation. However, in order for the solid matrix to move, and not simply change composition, all chemical constituents must move. Therefore, the solid state effect is rate limited to the slowest diffusing species, which in the case of MOX, is the (U , Pu) cations.

The model for vapor transport driven porosity evolution was developed as a result of pore migration.² As discussed with regards to the equation for pore velocity, (84), the migration velocity is independent of pore size and so coalescence is not expected. We may then consider conservation of the number of pores, n_p as a divergence of their flux:

$$\frac{\partial n_{pore}}{\partial t} = -\nabla v_{pore} n_{pore} \quad (87)$$

If we assume constant pore volume, then this equation may also be written in terms of the fractional porosity:

$$\frac{\partial \text{Porosity}}{\partial t} = -\nabla v_{pore} \text{Porosity} \quad (88)$$

subject to the initial porosity and, the assumption can be made, a Dirichlet condition equating the porosity at the outer periphery to the initial porosity. Eq. (88) should be solved simultaneously with an equation for the temperature gradient considering the effects of porosity redistribution and the effects of the temperature profile on the pore velocity as given by Eq. (84).

Although derived for migrating pores, the same model may be applied to porosity evolution by evaporation-condensation through large interconnected void space such as is spherepac fuels. This is because the pore migration velocity is calculated on the assumption that vapor pressure is always at equilibrium. Furthermore, what is actually calculated is the matter flux in the free volume, from which the pore migration speed is assumed to be the negative (an assumption implying fast attachment kinetics). Therefore there is no difference between considering this model for migrating pores and for large interconnected porosity.

2.08.3.2.1 Columnar grain growth

As discussed in Section 2.08.2.3, pores will spontaneously migrate up the temperature gradient in nuclear fuels, towards the centreline via the evaporation-condensation mechanism. When the fuel material condenses on the cool side of the pore, it does so in a single-crystal configuration. Therefore, pore migration acts as a mechanism for restructuring the polycrystalline material ahead of the pore, to a single crystal behind it. Due to the disk-like cross-section of the pore, the deposited material grows in a column and is often referred to as a columnar grain.

In addition to removing the initial porosity, pore migration also serves to heal cracks, producing a dense area in their wake. In this region, macroscopic voids are not present to act as channels for vapor transport of redistributing species and so subsequent redistribution in this region may be considered to occur primarily due to solid state mechanisms, i.e., thermodiffusion.

2.08.3.2.2 Central void

The central void is considered to be created as the result of materials movement down the temperature gradient although local sintering may also impact its formation.⁸¹ This may be the result of closed pores migrating as indicated in Fig. 11, or vaporization of hot material at the center and migration through connected voids to the cooler periphery.

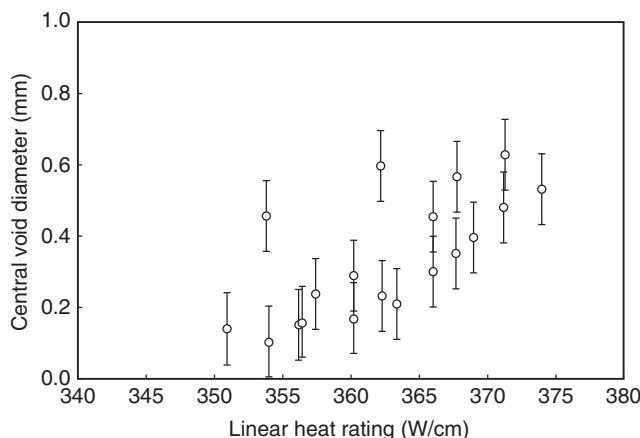


Fig. 12 Measured central void diameter vs. linear power for a fast reactor. Reproduced from Katsuyama, K., Nagamine, T., Matsumoto, S.-I., Ito, M., 2002. Measurement of central void diameter in fbr mox fuel by x-ray computer tomography. *J. Nucl. Sci. Tech.* 39, 804–806.

The creation of the central void via relocation of the fuel to the periphery of the element serves to lower the maximum temperature of the fuel. Measurements of the diameter of the central void has also been conducted using a non-destructive technique.^{89–91} The results show an increasing diameter with linear power and irradiation time, as expected. The void forms rapidly, in as little as 10 min⁹¹ (Fig. 12).

2.08.3.3 Melting

The formation of molten fuel may significantly produce restructuring and redistribution. Restructuring clearly occurs when the liquid is able to flow into available voids. This is of course a significant hazard to the structural integrity of the clad as the molten fuel is extremely hot. However, upon flowing away from the hot centreline, the liquid may solidify, filling in the open porosity it encounters. Halas and Horn discuss several examples where centreline melting was speculated to have occurred.⁷⁹ In particular they speculate that for upon heating the central core may melt due to poor thermal conductivity in the outer regions. Restructuring would then occur, leading to a rise in the conductivity and lowering of the inner temperature with consequent solidification of the melt. The melt would then solidify into a region of columnar grains (resultant from the advancing solidification front) but would become porous along the grain boundaries due to pulling apart by volume shrinkage on solidification.

If the solid-liquid phase change is non-congruent then the development of molten fuel will also largely redistribute the chemical species in accordance with the phase diagram. For example, Christiansen found enrichment of O in previously melted region of UO_{2+x} samples.^{47,92} As noted by Lackey, this phenomenon will dominate over other redistribution effects in the case of center-melted fuels, which adds complexity to experimental analysis.² Welland *et al.* conducted a theoretical study on the behavior of melting UO_{2+x} and showed the effects of oxygen redistribution upon melting served to limit the melting process due to a shift of the remaining solid's melting temperature towards higher temperature.^{93,94} As an example, Fig. 13 shows a simulation result for the temperature and oxygen profile in a sample with overall O/U = 2.05, heated to different linear powers, showing the large solubility gap between solid and liquid.

2.08.4 Fuels

At this point, the theoretical background relating to the evolution of nuclear fuel has been laid down in detail. The thermodynamic origin of the driving forces of fuel evolution has been set. The TIP has been used to describe the formation of microscopic structures, with particular emphasis on pores and their migration. The macroscopic effects of the microscopic phenomena were then discussed as they may apply to all fuel types. This section makes use of the preceding theory to discuss a selection of modern fuel types and related experiments, predictions and where relevant, models pertaining to each.

Four types of fuel are discussed. The first and most detailed section is dedicated to MOX as this is the most thoroughly researched and widely used fuel type in fast, and thermal reactors. The second section discusses carbide and nitride fuels, followed by U-Pu-Zr in the third section. Finally, TRISO particles are described with particular reference to a particular migration phenomenon they exhibit.

2.08.4.1 Mixed Oxide Fuels

Mixed oxide fuels are mixtures of urania and plutonia which may have an excess or deficiency of oxygen. MOX fuels typically contain 15–30 at% Pu in substitutional solution with the U. Most power-generating reactors are fueled with UO_2 , which is transmuted to plutonium as irradiation proceeds. Thus it is sensible to discuss $UO_{2\pm x}$ as a special case of $(U, Pu)O_{2\pm x}$.

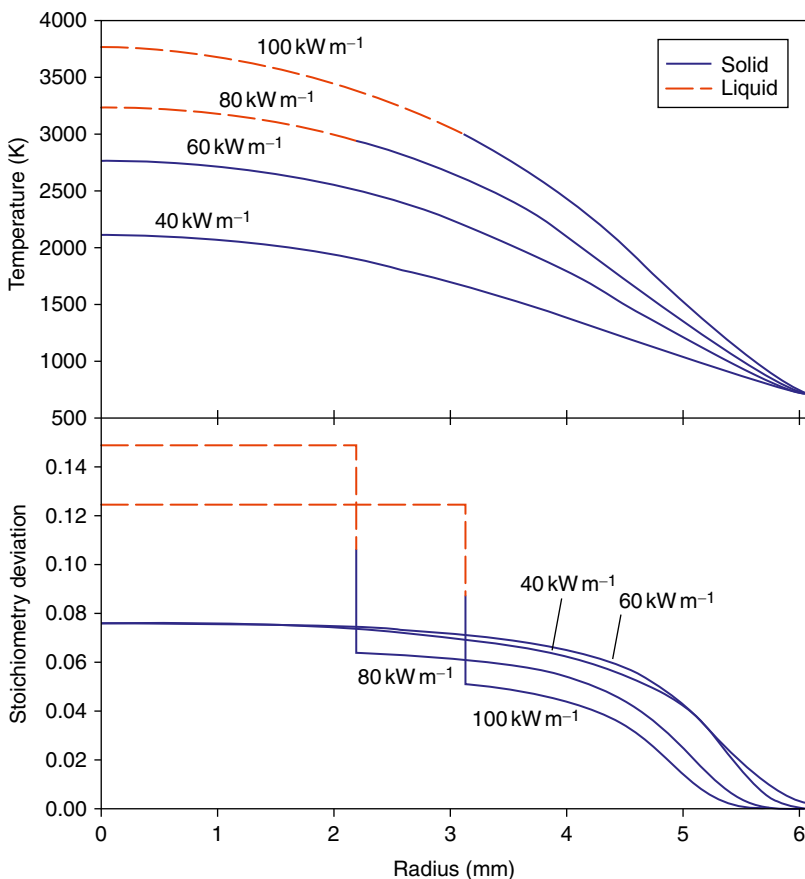


Fig. 13 Simulation of temperature and oxygen profiles in a centreline melted sample of $UO_{2.05}$ for a sequence of four linear powers. Solid phase thermomigration is shown, and the non-congruent separation of oxygen across the phase boundary is shown. Reproduced from Welland, M.J., 2009. Simulation of Melting Uranium Dioxide Nuclear Fuel (PhD Thesis). Royal Military College of Canada. Welland, M.J., Lewis, B.J., Thompson, W.T., 2011. Review of high temperature thermochemical properties and application in phase-field modelling of incipient melting in defective fuel. J. Nucl. Mater. 412, 342–349.

The fuel element may be produced in a variety of forms: pelletized, spheropac or vipac. The difference lies in how the fuel is processed before insertion in the sheath/cladding. With the exception of large amount of porosity in particle fuels these fuels forms generally behave in a similar manner.^{2.95}

The low thermal conductivity of MOX fuels implies the possibility of high temperatures and large temperature gradients. Large thermally driven mass transport effects are therefore expected and observed. The ensuing section summarizes some of the experience with MOX fuels considering first the restructuring behavior, followed by the redistribution of the constituent elements with reference to the mechanisms previously discussed.

2.08.4.1.1 MOX restructuring

MOX fuel is often divided into regions defined by their restructured state. Proceeding outward from the centreline they are:

- (1) Central void
- (2) Columnar grain region
- (3) Equiaxed grain growth
- (4) As fabricated microstructure
- (5) High burnup structure

As the name implies, the High Burnup Structure, is observed at high burnup and is notably found at cooler temperatures such as the fuel periphery.⁷ The behavior of this region is complex and not discussed in depth in this article.

Knowledge of the dimensions of each region is important as it affects the thermal conductivity and the heat generation. In addition, the microstructure has influence on the material properties of the fuel such as diffusion of fission gases etc.

A schematic of the evolution of the MOX microstructure is given in Fig. 14 in which burnup increases clockwise. Of note is the fast appearance of the columnar grains as discussed in Section 2.08.2.3. An experimental micrograph is shown in Fig. 15 which

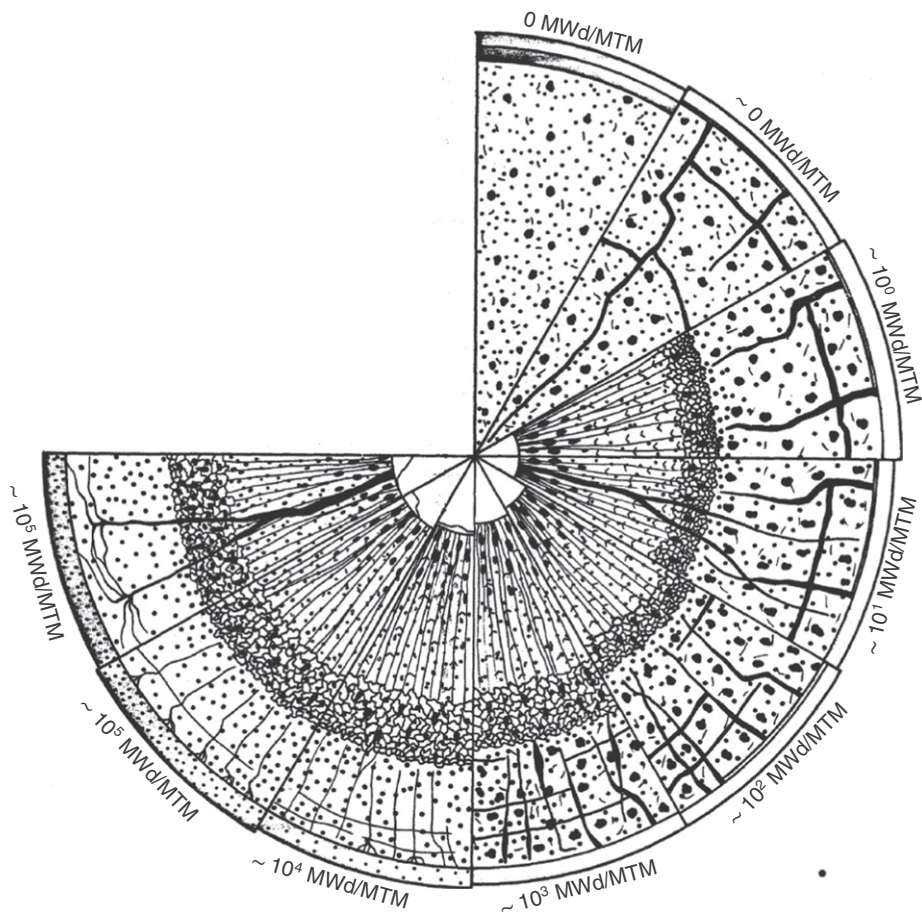


Fig. 14 Expected evolution of microstructure in MOX fuel, operating at 42.3 kW/m shown at a sequence of increasing burnups. Reproduced from Christensen, J.A., 1970. Technical Report WHAN-SA-79. WADCO Corporation.



Fig. 15 Slice of a pelletized MOX fast reactor fuel sample showing as fabricated region, equiaxed grain growth and columnar grain growth leading towards the central void. © European Communities, reproduced with permission.

also shows the evolved structure. The presence of cracks is visible in the micrograph, and the healing process is depicted in the schematic evolution.

We can use the analytical expressions of pore migration given in Eq. (84) to model the extent of columnar grain growth. In examination of irradiated fuel elements, the extent of the columnar grain growth is usually clearly determinable due to their high sensitivity to temperature and temperature gradient. This allows a fairly accurate prediction of the radial extent of the columnar grains and the temperature at that location. Calculations of this kind have been preformed by Nichols and Olander and experimental results have been presented by Christensen.^{10,63,96} The results of Olander's calculations are shown in Fig. 16, and show the variation of the radial extent of the columnar grains for a series of centreline temperatures, along with the temperature at the outer region.¹⁰

The results show that the temperature at the columnar grain boundary is roughly independent of the centreline temperature, T_C . The radius however is dependant on the centreline temperature. Olander notes that these predictions give a larger radius and a lower temperature than those of Nichols,⁶³ and that Christiansen observed the temperature at the boundary to be lower by approximately 200K.⁹⁶ However, this calculation does not include the variation of temperature profile with the evolving microstructure and this effect would lower the rate of the boundary's movement.

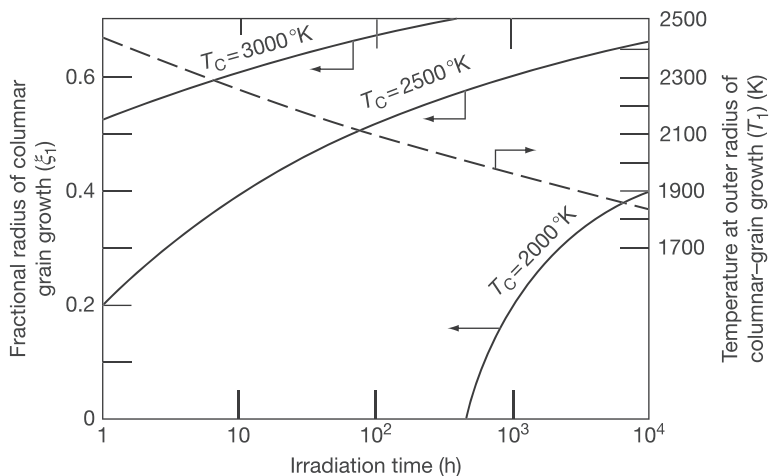


Fig. 16 The outer radius and temperature of the columnar grain region as a function of irradiation time and centreline temperature T_c , calculated for UO_2 . Reproduced from Olander, D.R., 1976. Fundamental Aspects of Nuclear Reactor Fuel Elements. Technical Information Center, Office of Public Affairs.

The coupling of porosity evolution and heat transport implies a changing pore migration velocity with the changing temperature profile as described in Section 2.08.2.3. Sens performed a calculation considering this coupled effect on pelletized UO_2 calculating the pore velocity, porosity and temperature profile as a function of radius, at a series of operation times.⁶¹ He presents the results of his simulation of a 0.5 cm radius pin of UO_2 in a water cooled thermal reactor operated at linear power of 600 W/cm in Fig. 17. This theory was later shown to reasonably describe observed migration rates of lenticular voids.^{76,97}

It is possible to apply the results presented in (17) to hyper/hypostoichiometric MOX by considering the changes in vapor pressures above the solid phases. In hyperstoichiometric $(\text{U}_{0.8}\text{Pu}_{0.2})\text{O}_{2+x}$, Olander predicted the increased vapor pressure of UO_3 associated with hyperstoichiometric urania, as shown in Fig. 3, would overcome the reduction in urania concentration (only 80% compared to UO_2) and result in an increase in the migration speed by a factor of ≈ 3.5 .⁸⁵ In contrast, the reduction of UO_2 concentration in hypostoichiometric MOX was predicted to lower the migration speed by a factor of $\approx 5/7$ by Guarro and Olander.⁸² Maeda *et al.* compared short term irradiation tests on 30% Pu MOX with other minor actinides in the range O/M = 1.95–2.00 and found that the extent of restructuring decreased significantly with lower O/M. The most notable drop was between O/M = 2.00 and 1.98, which they attribute to the strong drop in UO_3 partial pressure in the same range.^{98,99}

Ronchi and Sari performed experiments to determine the rate of columnar grain growth in samples of $(\text{U}_{0.85}, \text{Pu}_{0.15})\text{O}_2$. In this experiment, they used "old" samples of MOX in which they speculated the decay of Pu with time would build up a pressure of He in the sample. They found that only pores which appeared to come from cracks formed the expected lenticular shape, whereas the fabrication porosity appeared to coalesce into immobile pores either small and spherical or elongated cigar-shaped pore aligned with the radial temperature gradient, in accordance with the predictions of Nichols and Sens as discussed in Section 2.08.2.3.^{61,63} Interestingly, columnar grains were observed to grow *without* lenticular pores at their head, and at virtually the same rate as that predicted by pore migration, as shown in Fig. 18. Maeda *et al.* reported similar observations in 93% dense $(\text{Am}_{0.02}, \text{Pu}_{0.29}, \text{Np}_{0.02}, \text{U}_{0.67})\text{O}_{1.98}$ irradiated at high power for 10 min. Columnar grains were present with a number of spherical and tubular pores inside, however lenticular pores were only observed from the fuel cracks.⁴⁶

Ronchi and Sari theorized that the growth of columnar grains without lenticular voids indicated the importance of cation diffusion in columnar grain growth and that vapor-phase transport was not required.⁷⁶ Further, they cite experiments by Potter and Elyard who concluded that additions of 0.5 w% Ir or 1 – 5 w% Y_2O_3 , the latter of which also retards sintering speeds, suppressed columnar grain growth.¹⁰⁰ In the same investigation, it was noted that additions of 0.05–0.5 w% Pt, Ru and W did not prevent columnar grains, nor did additions of ≤ 1.0 w% CaO , Ga_2O_3 or CeO_2 , although Nd_2O_3 did have some retarding effect at 1.0 w%. Recent simulation results also show pore migration by temperature driven vacancy diffusion.¹⁰¹ The appearance of lenticular pores would then be affected by the nucleation of such pores, which may be hindered by high He pressure in the experiments of Ronchi and Sari.⁷⁶

Lackey *et al.* performed a numerical simulation to study the porosity evolution for sphercap fuels in thermal and fast neutron spectra fluxes.² They compare a sample of a low burnup thermal reactor fuel element to their simulation results, with the results shown in Fig. 19. Also reported in the figure is the calculated plutonium redistribution as will be discussed in the following section. In commenting about this calculation Lackey *et al.* suggested that axial transport of vapor may have occurred but did not make a quantified measurement of this which may account for the discrepancy in the observed vs. predicted central void size. Similar results were obtained for medium burn-up elements for thermal and fast reactors as reproduced in Fig. 20 which shows their measured values for the thermal reactor pin, and a micrograph of the fast reactor pin. A reassuring observance was that the redistribution did not appear to vary between thermal and fast spectra, which is to be expected since the restructuring process is understood to be thermally driven and not dependant on the energy spectrum of the neutron flux. The results of the experiment

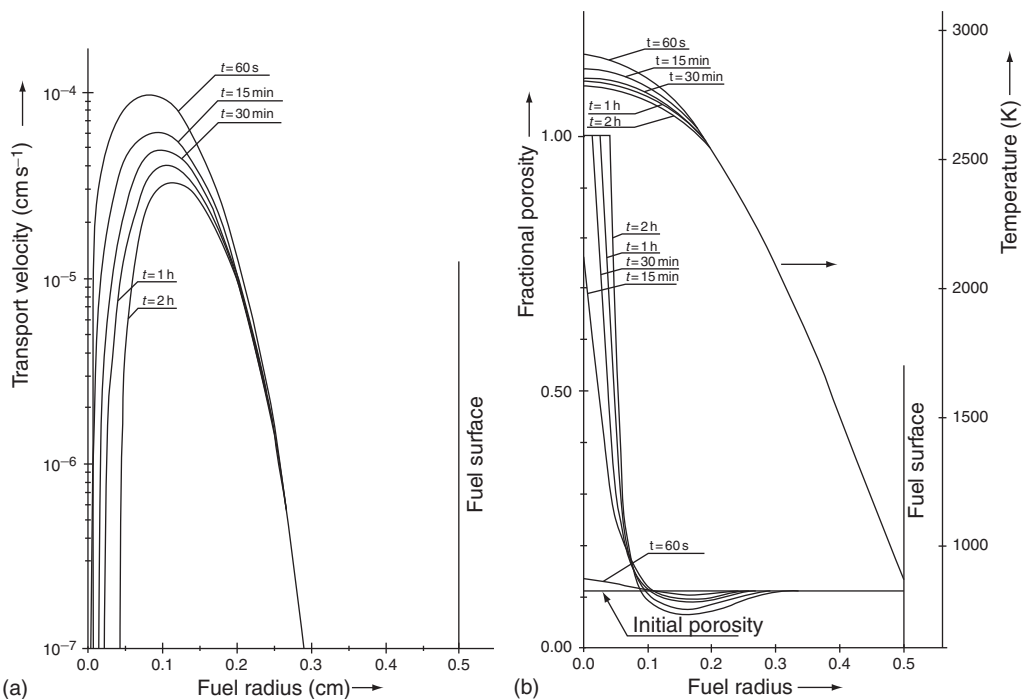


Fig. 17 Simulation results using the PREMOVSKI code for a fuel sample is a 1 cm diameter pin, initially at 89% TD, surface temperature of 873K, linear power 600 W/cm in a thermal reactor showing (a) pore migration velocities and (b) corresponding porosity and temperature evolution. Reproduced from Sens, P.F., 1972. The kinetics of pore movement in UO₂ fuel rods. J. Nucl. Mater. 43, 293–307.

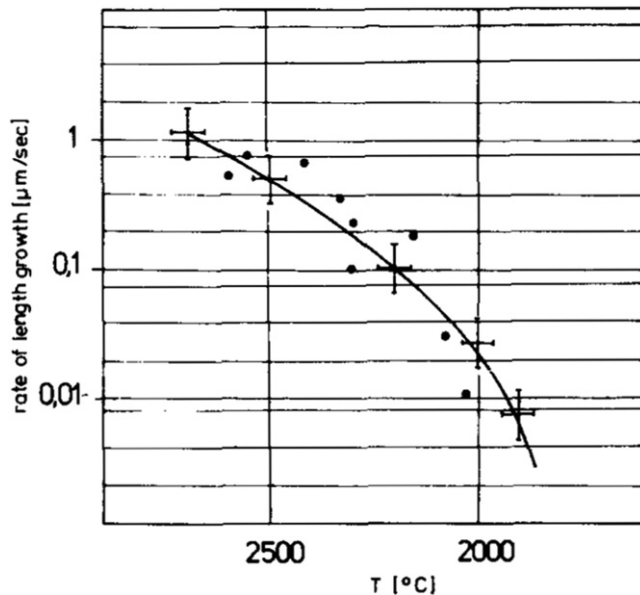


Fig. 18 The growth rates of columnar grains in aged ($U_{0.85}, Pu_{0.15}$)O₂ in which He pressure in the sample was speculated to immobilize pores created from fabrication porosity (+) but could still occur via cracks (•). Reproduced from Ronchi, C., Sari, C., 1974. Properties of lenticular pores in UO₂, (U, Pu)O₂ and PuO₂. J. Nucl. Mater. 50, 91–97.

The model Lackey *et al.* used predicted regions of columnar grain formation arising from vapor transport, and negligible vapor transport towards the fuel periphery as labeled in (19a).² The porosity measurements support the prediction of the columnar grain development, and the lack of vapor deposition may be corroborated qualitatively. In the medium burnup element, Lackey *et al.* noted the deposition of vapor on the inner surface of the cladding, having apparently traversed the region of negligible vapor transport at fractional radius ~ 0.9 in Fig. 20. Such a deposition would lead to an increase in the gap conductance as the gap is filled with solid material.²

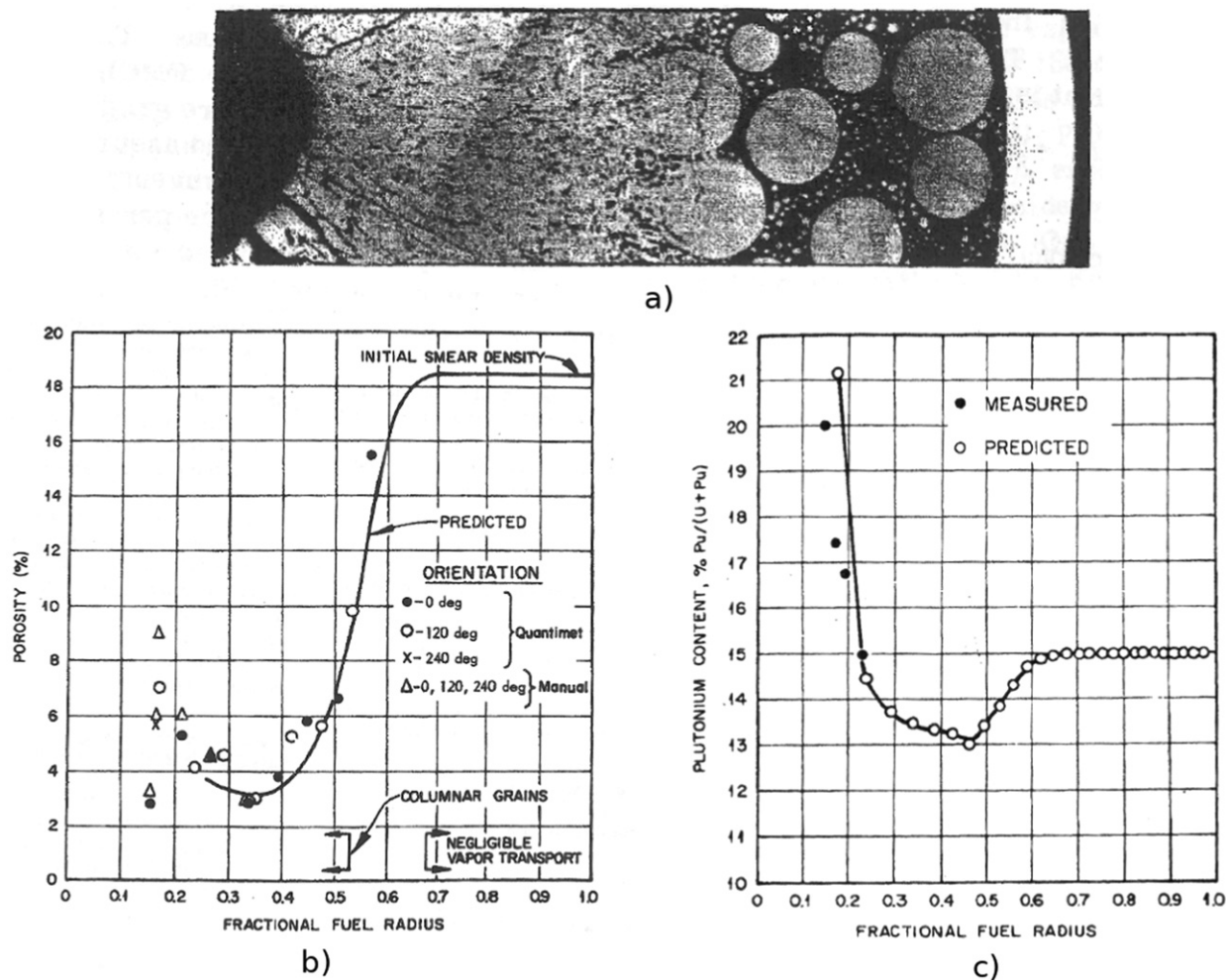


Fig. 19 Sample rod section (unetched), spherepac element, initially 81.4% smear density, $U_{0.85}Pu_{0.15}O_{2.00}$, irradiated in a thermal reactor at 44.6 kW/m to 0.7% FIMA. (a) micrograph of fuel section. (b) porosity measurements compared to model predictions, scatter near central void is due to actual variation of porosity in this area. (c) Measured and calculated Pu/M ratio. Reproduced from Lackey, W.J., Homan, F.J., Olsen, A.R., 1972. Porosity and actinide redistribution during irradiation of $(U, Pu)O_2$. Nucl. Technol. 16, 120–142.

2.08.4.1.2 $U - Pu$ redistribution

The redistribution of uranium and plutonium affects several properties of nuclear fuel. In particular to nuclear reactors is the neutronic effects and the change in heat generation which, as mentioned in the introduction to this article, may culminate in a penalty of the maximum linear heat rating by as much as 8.2 kW/m, 15% for a liquid metal fast breeder reactor MOX fuel element compared to the restructured case without plutonium redistribution¹ although, as noted by Lackey *et al.*,² this conclusion is incomplete as it misses the effects of relocation of oxygen to the outer radii and the lowering of the melting point by local Pu content. Naturally, the fission process will also affect the Pu distribution, both from fission and transmutation processes, and this fact must be borne in mind.¹⁰²

Uranium and plutonium may redistribute as a result of several overlapping mechanisms. Vapor transport may result in redistribution from either macroscopic interconnected voids or via migrating closed porosity although the latter has previously been discussed not to contribute largely to redistribution in Section 2.08.2.3. Segregation by vapor transport relies on non-congruent evaporation of U and Pu bearing vapor species. The ratio of U/Pu in the vapor turns out to be dependant on the O/M in the solid, and there is a particular composition where $U/Pu = 1$. This was investigated by Bober *et al.* by experiments on cylindrical samples of $(U_{85}, Pu_{15})O_{2-x}$ with a hole bored out in the middle.¹⁰³ The samples were subjected to an axial temperature gradient of maximum temperature 2673K. Within the borehole, redistribution was able to occur predominately by preferential evaporation from the surface of the sample into the empty space. The α -autoradiographs were then examined and, based on alpha activity, the composition of U and Pu was observed. With the maximum temperature at 2673K, experiments with $O/M \geq 1.97$ were seen to preferentially evaporate uranium oxides, whereas plutonium oxides preferentially evaporated for $O/M \leq 1.96$.

Lackey *et al.* calculated actinide redistribution through the use of their restructuring model with the results shown in Fig. 19.² Redistribution was included by considering the ratio of Pu/M in the vapor phase depending on the temperature and local O/M

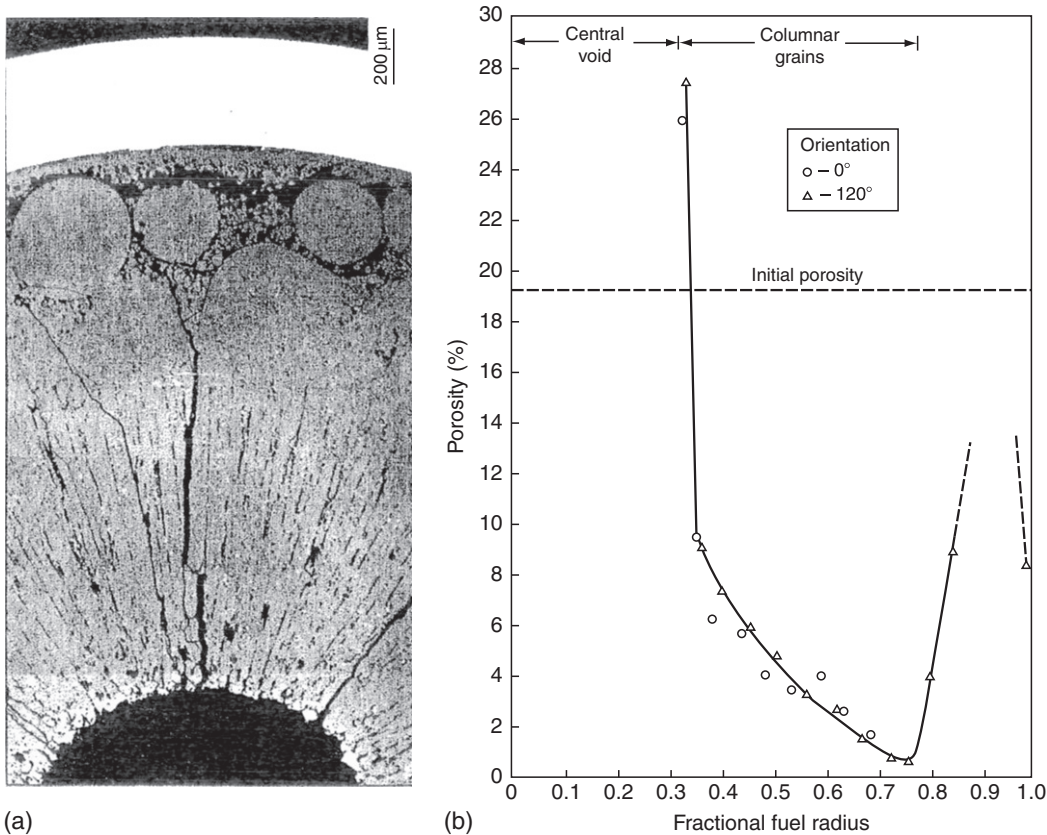


Fig. 20 Micrograph and measured porosity for pins irradiated to medium burnup showing deposition of material onto inner surface of cladding. (a) Micrograph of $(U_{0.8}Pu_{0.2})O_{1.99}$ irradiated in fast neutron flux at 44.3 kW/m to 5.7% FIMA (unetched). (b): Measured porosity distribution for $(U_{0.85}Pu_{0.15})O_{2.00}$ irradiated at thermal flux, 44.0 kW/m to 4.2% FIMA. Reproduced from Lackey, W.J., Homan, F.J., Olsen, A.R., 1972. Porosity and actinide redistribution during irradiation of $(U, Pu)_O_2$. Nucl. Technol. 16, 120–142.

ratio as determined by the thermodynamic model of Rand and Markin.⁴⁸ Although the model employed by Lackey *et al.* is in fact based on pore migration, which has been postulated not to result in much redistribution (ref Section 2.08.2.3), the results may still be considered valid as it is derived from a vapor-phase equilibrium that is applicable to macroscopic porosity as previously discussed. Ishii and Asaga modeled U - Pu redistribution and report good results using a fit parameter to determine U - Pu separation as the pore migrates, and the pore migration rate of Clement and Finnis.^{88,104}

Clear evidence of the vapourization mechanism acting on the macroscale was also observed by Lackey *et al.* through comparison of a photomicrograph and an α -autoradiograph investigation of the spherepac element described in Fig. 20(b). Comparison of the results show that the space between the spheres near the periphery appears to have been filled with a material of much lower Pu concentration, as is visible on the α -autoradiograph. Thus the appearance of the Pu islands remain from the original microstructure. This, along with a notable enrichment of Pu as the surface of the central void indicates that U bearing species preferentially evaporated from the inner region and condensed in the free space between the outer spheres (Fig. 21).

The effects of sintering on closing vapor transport pathways was addressed by Meyers, who emphasizes the importance of this phenomenon.⁸¹ The model includes vapor transport and sintering although discounts thermodiffusion, citing a much lower driving force compared to vapor transport. He does acknowledge the buildup of Pu in front of a migrating pore but, in contrast to Olander's treatment, he assumes that this will dissipate rapidly and so not require the treatment discussed in Section 2.08.2.3.⁸⁵ The results of his computer model reproduce the features of the observed behavior well, and leads him to consider sintering to be of high importance in modeling restructuring and redistribution.

The appearance of a dense region in which segregation may no longer proceed via vapor transport and pore migration implies that solid state thermodiffusion would be responsible for any further redistribution. To investigate the thermomigration of U - Pu , a series of out-of-pile experiments were performed by Bober, Sari and Schumacher.^{3,27,40,105} The apparatus employed a gas-tight capsule in order to prevent evaporation of fuel material, or oxygen exchange with the environment. A linear temperature gradient was applied with a quoted maximum temperature of approximately 2800K, with an approximately linear gradient of up to 1500 K/cm in the sample. Experiments were performed with this apparatus on MOX samples with $Pu/M = 15\%$ and differing stoichiometry and the resulting Pu distributions measured by alpha counting. Two experimental results are shown in Fig. 22 and

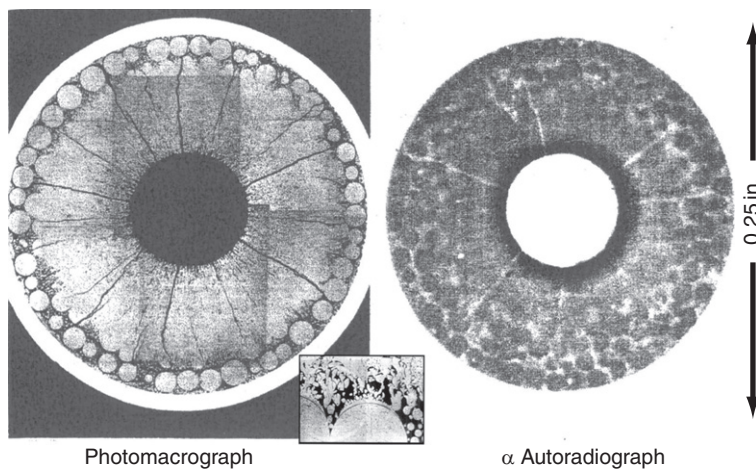


Fig. 21 Composite photomicrograph and matching autoradiograph of a spheropac fuel element. Photomicrograph (left) shows extent of restructuring in filling in the gaps between spheres. Autoradiograph (right) reveals Pu islands, and enrichment of Pu at central void periphery, indicating preferential vaporization of U . Inset shows fuel deposited from the vapor as dendrites on the hot side of the spheres at the region between columnar and equiaxed grains. Lackey, W.J., Homan, F.J., Olsen, A.R., 1972. Porosity and actinide redistribution during irradiation of $(U, Pu)O_2$. Nucl. Technol. 16, 120–142.

exhibit different profile characteristics corresponding to different dominant redistribution mechanisms for the experimental time and stoichiometry.

The first sample shown with a dashed line in Fig. 22 was heated for two hours and had $O/M = 2$ and so is expected to vaporize urania preferentially. Pore migration, which was also seen in microstructural analysis, was postulated to move Pu up the temperature gradient but only extend to the outermost radius of the columnar grain growth region at the 2173K isotherm resulting in a sharp discontinuity. In addition, preferential evaporation also occurred at the hot surface into the space between the sample and the sample holder, resulting in an additional Pu enrichment.

The second sample was heated for 48 h with $O/M = 1.98$. The stoichiometry was closer to the congruent vaporization composition and therefore preferential evaporation should not have had a large effect. The lack of vaporization shift and the longer heating time allowed thermodiffusion to act in the densified (columnar grain region), which gradually moved Pu up the temperature gradient, producing a smooth minimum before the rise. Pu could not have been shifted from the periphery as the temperature was too low to produce significant diffusion on this time scale. This minimum before the rise is a characteristic of thermodiffusion and allowed the experimenters to determine the process heat of transport using Eq. (38) assuming $f = 1$, citing a constant activity coefficient found in hyperstoichiometric MOX fuel with $(U_{0.6}Pu_{0.4})O_2$ ^{40,104–106}:

$$Q_{UPu}^{**} = -146.4 \text{ kJ/mol} \quad (89)$$

They further note that if the diffusion coefficients of the two actinides are equal then $D_U \approx D_{Pu} = \bar{D}_{U-Pu}$ and that the process heat of transport becomes the difference between the individual heats of transport $Q_{U-Pu}^{**} \approx Q_{Pu}^* - Q_U^*$. In general, the experimenters note that Q_{UPu}^{**} in addition to \bar{D}_{U-Pu} may depend on both temperature and the O/M ratio of the fuel.

2.08.4.1.3 Oxygen redistribution

The diffusion coefficient of oxygen anions in the MOX fluorite structure is several orders of magnitude greater than that of the cations.²⁴ This permits modeling the system as a perfect cation lattice of uranium and plutonium, with an excess of oxygen interstitials for hyperstoichiometric case, and oxygen vacancies for the hypostoichiometric case. Oxygen ions (vacancies) may then redistribute in MOX due to the superposition of several factors related to vapor-phase transport and thermomigration. A schematic outline of the various mechanism is shown in Fig. 23.⁴⁷

Vapor phase may play a large role in the redistribution of oxygen in MOX fuels through either non-congruent vaporization of matrix material, or via carrier gas. This transport mechanism has been investigated by a number of authors^{38,47,49,108–111} and some theories have evolved based on thermodynamic arguments as described in Section 2.08.1.3. As discussed, the carrier gas transport mechanism may result from contamination of the fuel by elements such as C or H. Adamson attempted to eliminate C contamination as far as possible from his experiments but was unsuccessful and instead reported that even 3 ppm C is significant enough to produce the carrier gas migration mechanism.⁴⁹

If a constant ratio of carrier gas concentrations is assumed then the Aitken model for the effective heat of transport of oxygen in MOX is applicable. Aitken calculated these quantities, the results of which are reproduced in Table 3 using the information listed in Table 1.³⁸ Carrier gas transport is a likely explanation for the conclusions of Fryxell and Aitken who cite that Q_O^* is independent of the oxygen content in UO_{2+x} .^{38,109} In their experiment, Aitken theorized that initial hydrogen ingress into the crucible produced enough vapor transport to have an effective heat of transport as 209 kJ/mol. As oxygen migrated out of the crucible, this value dropped until a stable value of 96 kJ/mol was reached, which Aitken attributes to a flow of matrix vapors.

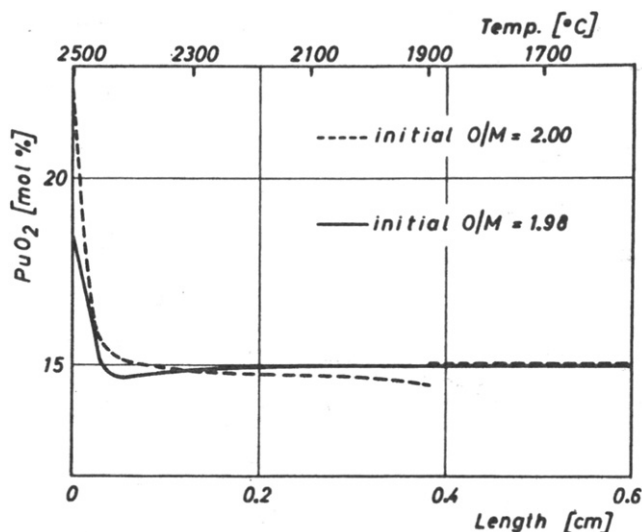


Fig. 22 Redistribution of uranium and plutonium through pore migration, preferential evaporation from the surface and solid state thermodiffusion. Reproduced from Bober, M., Sari, C., Schumacher, G., 1971. Redistribution of plutonium and uranium in mixed (U, Pu) oxide fuel materials in a thermal gradient. J. Nucl. Mater. 39, 265–284.

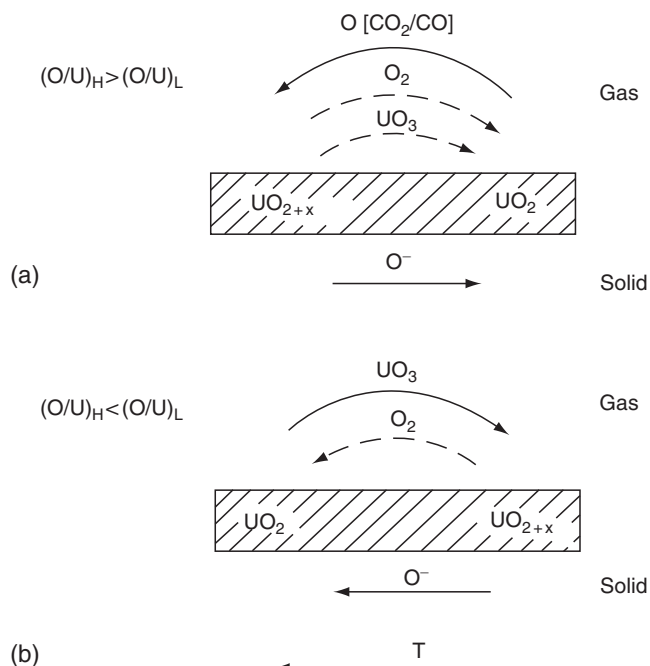


Fig. 23 Schematic of overlapping oxygen transport mechanisms of vapor transport, carbon based carrier-gas transport and solid state thermomigration. Reproduced from Adamson, M.G., Carney, R.F.A., 1974. Mechanistic study of oxygen thermal diffusion in hyperstoichiometric urania and urania-plutonia solid solutions. J. Nucl. Mater. 54, 121–137.

Aitken applied Eq. (64) to the experiments of Evans *et al.* on $(Pu_{0.8}U_{0.2})O_{2-x}$ ^{38,107} where, due to low H_2O pressures, he comments that a constant ratio of partial pressures can not be considered and assumes $L_s/L_g = 3$ in order to reconcile the experimental results of –30 to 50 kJ/mol with the model values given in Table 3. There was however a sharp increase in the magnitude of the effective heat of transport to 418 kJ/mol upon reaching $O/Pu = 1.98$, which Aitken suggests is due to the sudden increase in H_2O partial pressure, although the model still under predicts the experimental results quite significantly.³⁸

The claim of constant ratio of carrier gases is questionable and in general cannot be considered for all cases. Lackey *et al.* note that a constant carrier gas ratio is inconsistent with their observations and their thermodynamic model. In particular, for their oxygen profile observed post-irradiation, the corresponding ratio of actinide containing vapors would lead to uranium enrichment in the central hot regions, contrary to the Pu enrichment at the central region shown in (21).²

Table 3 Table of calculated $Q_{O,vap}^*$ from thermodynamic data in MOX. Quantities are in kJ/mol

Oxide	\bar{h}_{O_2}	$Q_{O,vap}^*[CO/CO_2]$	$Q_{O,vap}^*[H_2/H_2O]$
UO_{2+x}	-272	-151	105
UO_{2-x}	-837 to -1172	-134 to -301	-180 to -347
$(U_{0.8}Pu_{0.2})O_{2-x}$ for O/Pu			
1.98	-1008	-222	-268
1.90	-920	-176	-221
1.80	-808	-121	-167
1.70	-736	-84	-130
$(U_{1-y}Pu_y)O_{2+x}$ (For $x = 0.01 \sim 0.06$, $y = .1 \sim .3$)	-272	-151	-105

Note: Aitken, E.A., 1969. Thermal diffusion in closed oxide fuel systems. J. Nucl. Mater. 30, 62–73. Adamson, M.G., Carney, R.F.A., 1974. Mechanistic study of oxygen thermal diffusion in hyperstoichiometric uranium and urania-plutonia solid solutions. J. Nucl. Mater. 54, 121–137.

The mechanistic code of Lewis *et al.* which considers fuel oxidation in the operation of defective fuel, yields a similar conclusion. This work considers the presence of steam in contact with fuel resulting from a breach in the fuel sheath and resulting contact with the coolant in a CANDU reactor. The model considers steam (Actually gaseous D_2O due to the use of heavy water in CANDU reactors, however deuterium is assumed to behave in a chemically identical fashion to hydrogen) diffusion in the radial cracks, reaction with the solid fuel and thermodiffusion along with the evolving temperature profile. The simulation results show that H_2/H_2O (D_2/D_2O) ratio along the cracks is not constant in the region of applicability.^{112–114}

Olander preformed a theoretical investigation on the idea of a constant ratio CO_2/CO and determined that this assumption is valid for regions of lower temperature but smoothly diminishes at higher temperatures.¹¹¹ Adamson proposed the limit for dominance of carrier gas via the $CO - CO_2$ transport be set to 1873K in UO_{2+x} , above which UO_3 vapor pressure is high enough to dominate oxygen redistribution.⁴⁷ The exact effect of UO_3 diffusion is difficult to calculate due to sluggish reaction kinetics with solid fuel implying that the vapor and the solid may not be in equilibrium, a requisite for the treatment of the type described in Section 2.08.1.3. However, the effect may be seen as a departure from linearity compared to Eq. (48) although this may also be attributed to a varying carrier gas ratio.⁴⁷

At higher temperatures, the mobility of oxygen ions increases and so solid state thermomigration is thought to play an increasingly important role. Sari and Schumacher conducted a set of experiments designed to determine the degree of oxygen redistribution in MOX as a function of stoichiometry and U/Pu , and compared it with other experimental results.¹¹⁵ This required the minimization of carrier-gas assisted oxygen diffusion which was done by coating the hypostoichiometric samples with Mo , and tightly fitting the hyperstoichiometric samples in W or Mo containers. The authors of the work acknowledge that while the decision to use tight metallic capsules minimizes vapor phase transport, the metallic sample containers may affect the electric potential which the sample generates by the thermoelectric effect, which should be considered part of the heat of transport as discussed in Section 2.08.1.2. Experiments were conducted with both a radial and axial heating apparatus.

The point defects are considered to be in dilute solution in the fuel matrix, and so Eqs. (42) and (46) may be considered to apply. With this treatment of the system, we can relate the mole fraction of vacancies/interstitials to the stoichiometry deviation by $N_v = -x/2$ and $N_i = x$ in the dilute limit. The mass flux equations are thus given by:

$$J_i = -nD_i \left[\nabla N_i + \frac{N_i}{f_i} \frac{Q_i^*}{kT^2} \nabla T \right] \quad (90a)$$

$$J_v = -nD_v \left[\nabla N_v + \frac{(1 - N_v)N_v}{f_v} \frac{Q_v^*}{kT^2} \nabla T \right] \quad (90b)$$

in which n represents the total local concentration of oxygen ions. For the steady state this gives a form analogous to (48):

$$\nabla x = -\frac{x(1 - x/2)}{1 + 2(\partial \ln \gamma / \partial \ln x)} \frac{Q_v^*}{RT^2} \nabla T \quad (91)$$

for hypostoichiometric $(U, Pu)O_{2-x}$ and

$$\nabla x = -\frac{x}{1 + (\partial \ln \gamma / \partial \ln x)} \frac{Q_i^*}{RT^2} \nabla T \quad (92)$$

for hyperstoichiometric $(U, Pu)O_{2+x}$.

The results are presented in Fig. 24 and compared against other measurements,^{11,108,116,117} and fit to curves given in (93).

$$Q_v^* = -9.45 \cdot 10^5 + 5.66 \cdot 10^5 V_{Pu} - 8.5 \cdot 10^4 V_{Pu}^2 \quad (93a)$$

$$Q_i^* = -8.3 \cdot 10^{33} \exp(17V_U) \quad (93b)$$

As can be seen from Fig. 24, the heat of transport does not appear to be influenced by the U/Pu ratio in either the hyper- or hypostoichiometric case, rather only the U/Pu valence. Scatter increases approaching the stoichiometric state as a result of uncertainty in the measurement of oxygen concentration as O/M approaches 2. The valence of U and Pu is a useful parameter

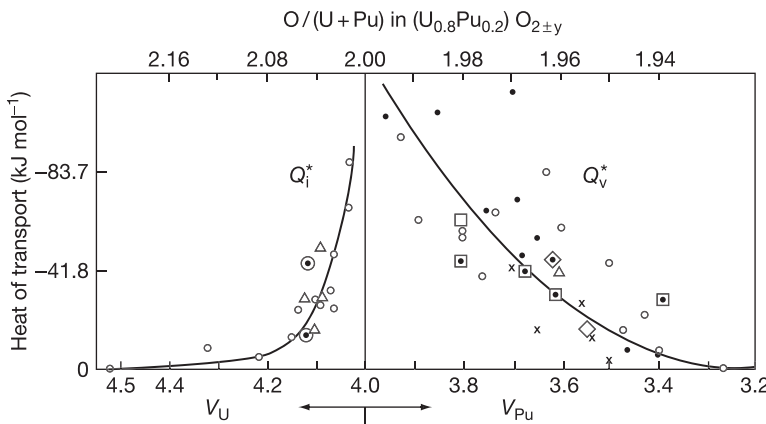


Fig. 24 The heat of transport of oxygen vacancies/interstitials in MOX showing results from Sari, C., Schumacher, G., 1976. Oxygen redistribution in fast reactor oxide fuel. *J. Nucl. Mater.* 61, 192–202, with \circ – 15, Δ – 20, $+$ – 30, x – 40, \blacksquare – 50, \diamond – 85, \cdot – 100 mol% PuO_2 . Other data includes \odot – Adamson, M.G., Aitken, E.A., Evans, S.K., Davies, J.H., 1975. Thermodynamics of nuclear materials. In: Proceedings of the Symposium on International Atomic Energy Agency, vol. 1, p. 59. Vienna: IAEA, \square – Evans, S.K., Aitken, E.A., Craig, C.N., 1967. Effect of a temperature gradient on the stoichiometry of urania-plutonia fuel. *J. Nucl. Mater.* 30, 57–61, and \diamondsuit – De Groot, S.R., Mazur, P., 1984. Non-Equilibrium Thermodynamics. General Publishing Company Ltd.

which occurs since a deficit or excess oxygen may preferentially associate with plutonia or urania respectively.⁴⁸ Thus, hypostoichiometric fuel may be considered as a solid solution of UO_2 and PuO_{2-x} , whereas hyperstoichiometric fuel would be a solid solution of UO_{2+x} and PuO_2 .²⁷ It may be related to the deviation from stoichiometry quite readily¹¹⁸:

$$V_U = 4 + \frac{2(O/M - 2)}{1 - q} \quad (94a)$$

$$V_U = 4 + \frac{2(O/M - 2)}{q} \quad (94b)$$

where $q = Pu/M$.

There has been some theoretical work on calculating the heat of transport of oxygen in MOX, however these efforts have met with little success. As discussed in Section 2.08.1.2, Q_v^* or Q_i^* can be calculated from either a thermodynamic or electrochemical standpoint. Proponents of the thermodynamic contribution tend to cite a change in sign of the thermoelectric power at approximately 1373–1573K.²⁸ Later, Ruello *et al.* determined that the sign of the Seebeck coefficient changes sign depending on oxygen potential above 1200K.¹¹⁹ Aitken first proposed that the heat of transport be expressed in terms of the partial molar enthalpy of oxygen in the solid phase and determined $Q^* = \mp \frac{1}{2}\bar{h}_{O_2}$ corresponding to hyper and hypostoichiometric fuel respectively.³⁸ However, since \bar{h}_{O_2} is always negative for MOX, which implies oxygen always migrates down the temperature gradient in contrast to observations of Sari and Schumacher who eliminated vapor-phase transport and observed oxygen accumulating at low and high temperatures for hypo- and hyperstoichiometric fuels respectively.^{28,115} Norris realized this and proposed that in fact the partial molar enthalpy of interest should be half the enthalpy of formation of an oxygen Frenkel pair, implying $Q^* = -\frac{1}{2}\Delta h_F$ which, since Δh_F is always positive, assures the correct sign of Q^* , although the magnitude was still incorrect.³⁹ Finally, Sugisaki performed a similar calculation for Q^* directly, via a computer simulation technique to calculate the excess energy associated with a defect movement, however while again predicting the correct sign, this did not reproduce the experimental results well.²⁸

A greater degree of success seems to be obtained by considering the thermoelectric effect. The justification for this is that since UO_2 is a mixed ionic and electronic conductor which may negate the previous argument regarding the change of sign in the Seebeck coefficient.¹²⁰ Theoretical treatments are developed from the TIP and Eq. (5) but including also a charge current. The results of Kamata and Esaka are in reasonably good agreement with the experimental data of Sari and Schumacher, indicating that indeed the electrochemical contribution from the thermoelectric effect may play an important, if not dominant role in the perceived thermomigration. Janek and Timm however criticized the work of Kamata and Esaka citing an unreasonable behavior near stoichiometry and report their own calculations, which are summarized in Fig. 25 and show quite good agreement.

Once one considers that the thermoelectric effect may enter into the experimental determination, one must consider that encapsulating the sample in a metallic container may short-circuit the field generated by the sample and so perturb the measurement of, for example the experiment of Sari and Schumacher. Millot and Gerdanian treated the system *including the surrounding container* in order to consider the effects of short circuiting the thermoelectric field via interaction with tight-fitting metallic containers.¹²¹ They determined that not only did electrotransport contribute to the observed heat of transport, but it is of the same sign and is of comparable magnitude for $UO_{2.03}$.

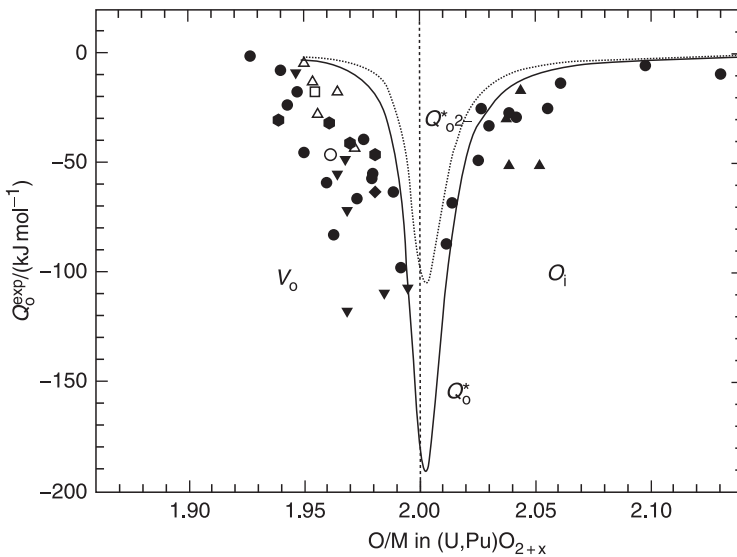


Fig. 25 Investigation on the actual heat of transport of oxygen in MOX. (a) The true heat of transport Q_o^* and ionic heat of transport heat of transport $Q_{o^2-}^*$ by Janek and Timm compared to experimental Q_o^{exp} from Fig. 24. Figure modified from Janek, J., Timm, H., 1998. Thermal diffusion and soret effect in $(U, Me)O_{2+\delta}$: The heat of transport of oxygen. *J. Nucl. Mater.* 255, 116–127.

2.08.4.1.4 Fission product redistribution

The creation of fission products change the fuel from its original composition into a multicomponent system. Fission products may be present in the fuel either in the form of solid precipitates, gas bubbles or in solid solution with the fuel matrix. All three forms are affected by thermodiffusion, but the application differs. Tracking the migration of all species would require a very large system of equations in the form of Eq. (1), but such a complete treatment is impractical due to computational requirement and lack of knowledge of the cross diffusion coefficient. Moreover, it is not required since often the dilute limit is applicable.

We first consider fission products in solid solution in the fuel matrix, which comprise approximately 2.5 at% of the fuel after 5% FIMA burnup. These species are subject to solid state thermodiffusion similar to uranium and plutonium. If the flows are considered to be in dilute solution, we may assume the fluxes are independent, and so proceed with calculation of the flux of fission products using Eq. (39). For FPs which diffuse more easily than U or Pu , $D_F^* \gg D_U, D_{Pu}$ and Q_{FP}^* becomes approximately equal to Q_o^* , however this is not necessarily the case.

In order to investigate the redistribution of cerium, experiments were conducted on samples of uranium-cerium mixed oxides.¹²² The case is analogous to that of $(U, Pu)O_2$ as cerium oxide forms a homogeneous solid solution with UO_2 , however the mobility of Ce is higher and so lower temperatures are required to observe appreciable effects. In particular, a case of $(U_{0.8}Ce_{0.2})O_2$ subjected to a linear thermal gradient of about 1273K with a maximum temperature of 2393K showed a concentration distribution shown in (26). The concentration profile demonstrates the result of thermodiffusion and void migration resulting acting in opposite directions. Specifically, the minimum is attributed to thermomigration acting to drive Ce up the gradient, in opposition to the void migration, which preferentially moves Ce preferentially down the gradient, producing a maximum nearer to the top of the sample. It is also noted that some preferential Ce evaporation from the surface has occurred, resulting in a decrease of the average Ce/M ratio. The process heat of transport was calculated using Eq. (39) as:

$$Q_{U-Ce}^* = -100.4 \text{ kJ/mol} \quad (95)$$

by consideration of the minimum concentration, with a caveat that the value is influenced by the migrating voids and would be larger for pure thermodiffusion (Fig. 26).

The transport of cesium, tellurium and iodine in $U-Pu$ fuels were measured in stainless steel capsules for 100 h.⁴ Volatile fission products were found to migrate down the temperature gradient via vapor transport. This was influenced by the O/M ratio, with a notable effect on Cs in hyperstoichiometric fuel due to the formation of the less volatile cesium oxide.

The redistribution of americium has been observed and shows an increasing concentration near the central void. MOX pellets with $O/M = 1.98$ and 3 and 5% Am were irradiated for 10 minutes and 24 h.^{90,91,123} Visual investigation determined pore migration and central void formation had already occurred, and chemical characterization showed an increase in Pu and Am fractions near the central void as shown in Fig. 27. Furthermore, it was noted that the increase in Pu and Am appeared correlated to the size of the central void.⁹¹ Maeda *et al.* measured Am concentrations on samples with O/M of 1.98 and 1.95 and modeled the phenomena assuming pore migration and thermodiffusion.⁴⁶ Pore migration showed good agreement with the observed Am profiles whereas thermodiffusion was reported to occur too slowly to contribute during the 24 h irradiation time. They also reported more Am enrichment for the 1.98 sample, in line with the larger UO_3 vapor pressure at this O/M . Later, this trend of

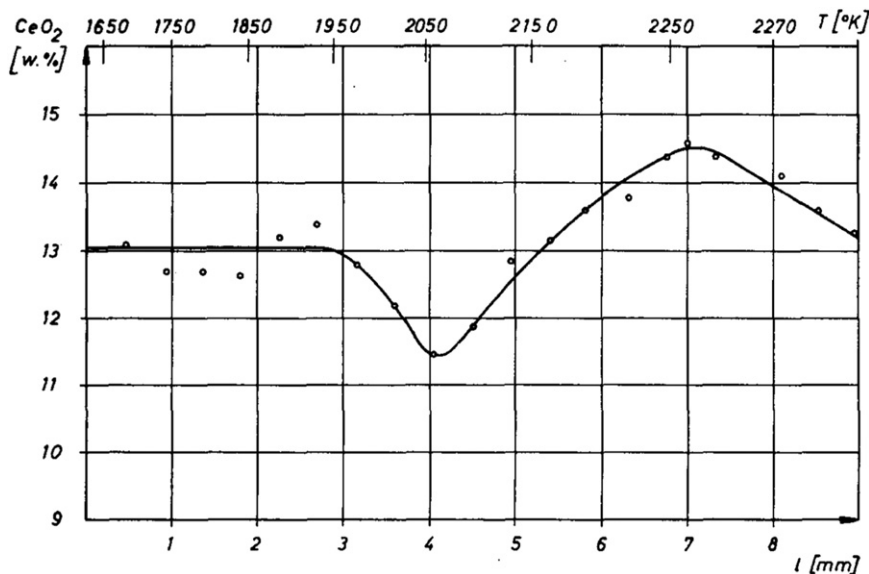


Fig. 26 Redistribution in the $(U, \text{Ce})\text{O}_2$ system showing thermodiffusion of Ce up the temperature gradient superimposed on preferential CeO_2 vaporization down the gradient. Reproduced from Bober, M., Schumacher, G., 1973. Material Transport in the Temperature Gradient of Fast Reactor Fuels, vol. 7. Academic Press New York, p. 121 and Beisswenger, H., Bober, M., Shumacher, G., 1967. Thermodiffusion in system UO_2-CeO_2 . J. Nucl. Mater. 21, 38–52.

increasing Am enrichment with higher O/M was observed from $\text{O/M} = 1.96\text{--}2.00$.⁹⁸ The authors correlated this with increased restructuring due to pore migration.

Neptunium was also measured by Maeda *et al.* in irradiation tests of 10 min to 24 h on $(\text{Am}_{0.02}, \text{Pu}_{0.29}, \text{Np}_{0.02}, \text{U}_{0.67})\text{O}_{2-x}$ with O/M of 1.95 and 1.98. Despite significant columnar grain growth and redistribution of Pu and Am, Np did not notably redistribute.

2.08.4.2 U-Pu-C-N

Carbide and nitride fuels are an attractive alternative to oxide fuels as they possess higher thermal conductivities and density of fissile elements and high melting temperatures. The higher conductivity reduces the potential for high centreline temperatures, unless the linear power is scaled accordingly, which tends to produce less thermally induced restructuring and redistribution.²⁷ A typical centreline temperature is $\sim 1500\text{K}$.¹²⁴ More detail is available on the behavior of carbides over nitrides and so this section focuses more on carbide behavior.

The diffusion rate of carbon in uranium-carbides is known to be greater than that of the metal actinides. Therefore Gulden, as well as Bober and Shumacher suggest that carbon diffusing through carbides may be treated as occurring through vacancies and interstitials through an immobile metal lattice.^{27,125} The mass flux may be represented by Eq. (46), and the steady state distribution by Eqs. (48c and b).

The heat of transport of carbon has been measured experimentally. Wallace *et al.* concluded that the heat of transport of carbon in $\beta - \text{UC}_{1.83}$ is 1.5 kJ/mol, however Gulden comments that this analysis neglects the thermodynamic factor, which is large for UC_2 .^{125,126} Gulden conducted an experiment to measure the heat of transport of carbon in UC_2 via the migration rate of a UC_2 disk through Pyrolytic carbon, leaving graphite in its wake.¹²⁵:

$$Q_C^* = 386 \pm 113 \text{ kJ/mol} \quad (96)$$

He also verified that another potential thermodynamic driving force, the chemical potential between the pyrolytic carbon and the rejected carbon, was negligible.

Bubbles of fission gas also are produced in carbide fuels. In analysing the mobility of spherical bubbles compared to their radius as discussed in Section 2.08.2.2, Weeks *et al.* determined that volume diffusion of carbon is important in bubble migration in UC .¹²⁷ This conclusion was later challenged by Matzke who proposed that while carbon may diffuse rapidly in the solid state, uranium bulk diffusion is slow. He also noted that the equilibrium vapor in contact with $(\text{U}, \text{Pu})\text{C}$ is predominantly U and Pu , with very little C .^{128,129} Therefore he proposed a transport mechanism which relied on vapor phase transport of (U, Pu) across the void supported by fast carbon diffusion.⁶⁹ The resulting graph of migration speed vs. bubble size is shown in Fig. 28, including an experiment datum from a fast flux irradiation experiment.¹³⁰ The activation energy for void migration is thus the slower of the steps required to move a complete molecule and so the activation energy of the pore migration is ~ 5 eV, the heat of vaporization of U from UC .

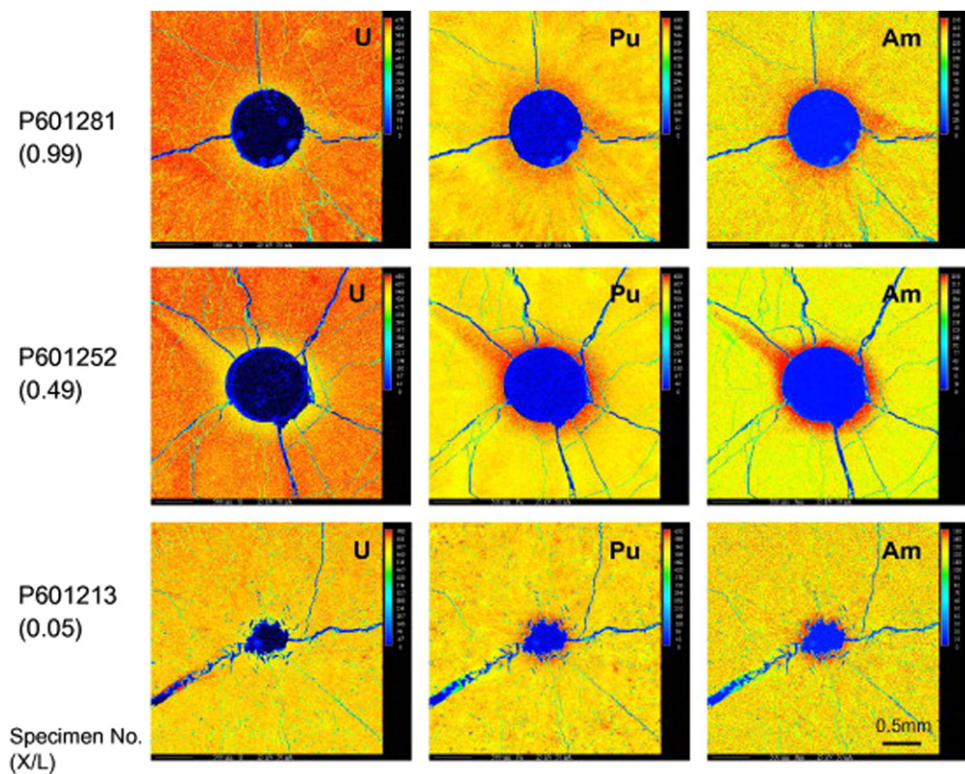


Fig. 27 Electron Probe Microanalysis of *U*, *Pu*, and *Am* in *Am* doped 29 wt% *Pu* MOX fuel with O/M = 1.95 irradiated for 24 h at 45 kW/m. Rows correspond to slices at relative rod lengths and P601281 3 wt% *Am*, P601252 5 wt% *Am*, P601213 3 wt% *Am*. Reproduced from Tanaka, K., Miwa, S., Sekine, S., et al., 2013. Restructuring and redistribution of actinides in *Am*-MOX fuel during the first 24h of irradiation. J. Nucl. Mater. 440 (1), 480–488. Copyright (2013) with permission from Elsevier.

It was also noted that the vapor pressure above uranium carbide contains a much greater amount of *Pu* than *U*.^{69,129} This of course has implication on vapor transport which may occur in this fuel type. As void migration is considered to occur by vapor transport of the actinide species, this then implies redistribution of actinides as the void migrates in such a way that uranium is moved up the temperature gradient. As Matzke points out, this results in increased heat generation on the cold side due to *Pu* enrichment which may decrease the temperature gradient across the void and slow its migration.⁶⁹

Post irradiation analysis of samples showed a central porous zone surrounded by a dense zone, although a band of increased density is also noted at the outer circumference of the inner region. Examples of carbide and nitride fuels are given in Fig. 29. It is also interesting to note the appearance of a central void in the nitride sample. An analysis of the *Pu/M* ratio for a sample of $U_{0.8}Pu_{0.2}C_{0.8}N_{0.2}$ irradiated to 3.9% FIMA in a fast flux at approximately 125 kW/m is shown in Fig. 30. The ratio shows significant variation depending on fuel morphology. In particular, spikes are noted at cracks, which is consistent with the notion that *Pu* rich vapor has evaporated from the hot central region and condensed on the surface of cracks in the fuel.¹²⁴

Void migration was examined by color etching technique to reveal slight changes in crystal orientation and composition. The results of examination on C rich carbonitride fuels are shown in Fig. 31, which shows migration of voids up a temperature gradient with a trail behind them. These pores are either spherical ($r_{void} = 5 - 15 \mu\text{m}$) or ovoidal with the major axis of 20–25 μm . They appear to have migrated $\sim 50 \mu\text{m}$, but only in a specific band, corresponding to the densified zone, and seem to be unaffected by grain boundaries. No pore migration was reported for experiments with nitrogen rich fuels.

2.08.4.3 U-Pu-Zr

U-Pu-Zr fuel in reactors redistribute in such a way as to show three concentric microstructure zones with differing ratios of *U* and *Zr* as shown in Fig. 32.¹³¹ The defining characteristic of these regions is the phase of the solid, which is determined by the temperature during operation and the local chemical composition. Redistribution is then driven by equilibrium compositions in these phases in addition to thermomigration.^{131–135} Interdiffusing species are primarily *U* and *Zr*, while *Pu* did not appear to largely redistribute between the phases. Nonetheless, *Pu* may have enhanced the speed of *U* and *Zr* migration, potentially due to increased gas bubble swelling.¹³⁶

The innermost region is reportedly in the bcc γ phase and exists between 923 and 1023K.¹³⁶ The phase is enriched in *Zr*, showing an increase from the initial 23–42 at% with a corresponding loss of *U* from 61 to 38 at%.¹³¹ The second region contains a mix of γ and ζ phases from 873 to 923K.¹³¹ This phase is enriched in *U* and depleted in *Zr* and does not exhibit a gradient in

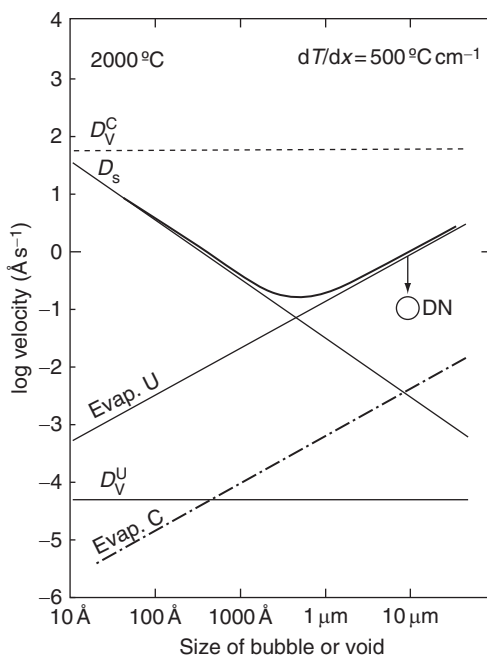


Fig. 28 Schematic plot of diffusion coefficients for surface, bulk and vapor phase migration of *U* and *C*. The overall speed of *UC* migration is given by the slowest moving component, and is shown with a thick line. Reproduced from Matzke, H.J., 1975. On mass transport in nuclear carbides by evaporation-condensation. *J. Nucl. Mater.* 57, 180–186.

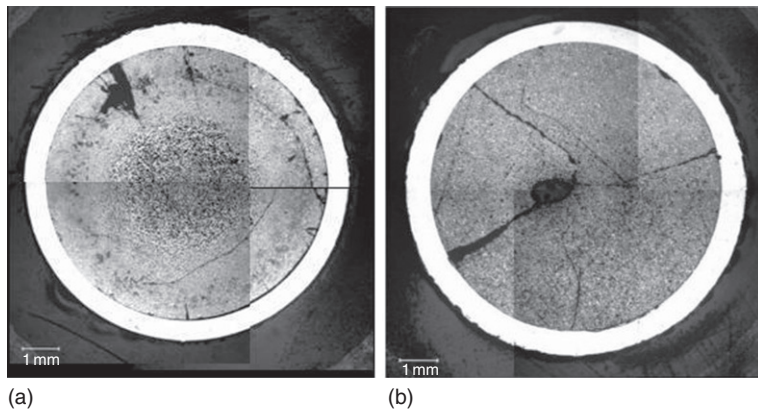


Fig. 29 Fuel samples irradiated to (7% FIMA) in the Phenix fast reactor showing (a) (*U*, *Pu*)*C* fuel with porous inner region and (b) (*U*, *Pu*)*N* fuel with porous interior and formation of a non-centered central void. © European Communities, reproduced with permission.

concentration. It is also the densest and contains fine bubbles.¹³⁷ The third, lowest temperature region contains a mixture of δ and ζ phases below 873K.¹³¹ This phase is slightly enriched in Zr and contains irregular voids originating from grain boundary tearing due to anisotropic growth of *U* grains.

Kim *et al.* conducted experiments in order to determine ternary diffusion coefficients, heats of transport and enthalpies of solution for this system.^{131,134} Minor actinides, *Am* and *Np* were also added to the *U-Pu-Zr* fuel and their migration studied. Tests indicated the presence of the actinides (1.2–1.3 wt%) did not greatly affect the migration of *U*, *Pu* or *Zr*. The results suggested that *Am* behaves similarly to *Zr* by increasing in the central zone and slightly in the outer periphery. *Am* was also found in regions of large porosity, with a notable reduction in the intermediate, dense zone. *Np* was not observed to significantly redistribute.¹³¹ Later, the migration of some lanthanides (*La*, *Ce*, *Nd*, *Pr*) were also studied and compared to *Am* in *U-Zr* and *U-Pu-Zr* fuels. The results of irradiation experiments suggest that they migrate by interdiffusion in the matrix and precipitation in pores.¹³⁵

More recently, Ohta *et al.* examined the addition of minor actinides *Np*, *Am*, and *Cm*, along with rare earths *Y*, *Nd*, *Ce*, *Gd* and determined that the addition of ≤ 5 wt% minor actinides and ≤ 5 wt% rare earths didn't significantly affect the morphology of the

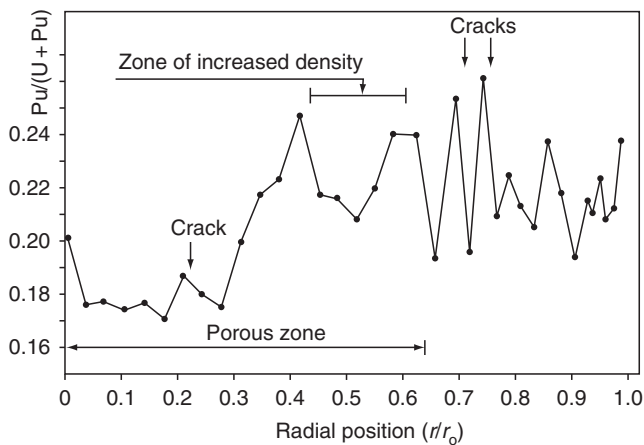


Fig. 30 Pu/M graph measurements in a sample of $U_{0.8}Pu_{0.2}C_{0.8}N_{0.2}$ irradiated to 3.9% FIMA in a fast flux at 125 kW/m. Reproduced with permission from Benedict, U., Saunders, R.A., Schmidt, H.E., Whitlow, W.H., 1977. Programme Progress Report: Plutonium Fuels and Actinide Research. Technical Report 3438. European Institute for Transuranium Elements. © European Communities.

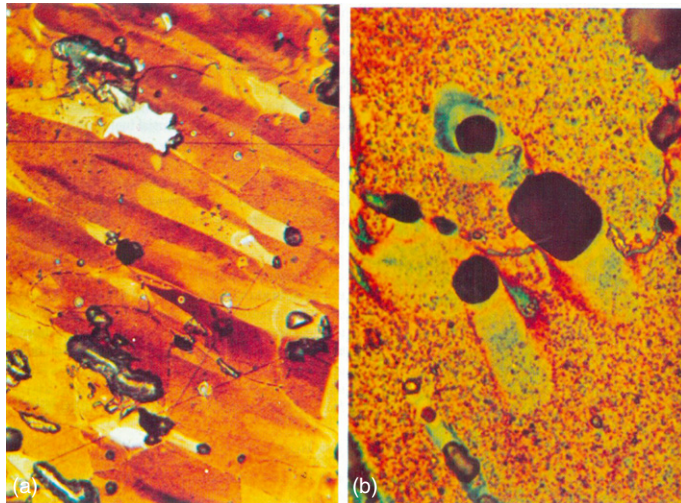


Fig. 31 Pictures of void migration in C rich carbonitride fuels as revealed by a color etching technique. Trails are clearly visible indicating variations of composition and structure trailing migrating voids. Reproduced with permission from Benedict, U., Saunders, R.A., Schmidt, H.E., Whitlow, W.H., 1977. Programme Progress Report: Plutonium Fuels and Actinide Research. Technical Report 3438. European Institute for Transuranium Elements. © European Communities.

matrix phases. However, they did observe some precipitation of the additions as large deposits in pores in the hot region, and along grain boundaries in the intermediate temperature zones.^{138–140}

2.08.4.4 TRISO Particles

TRISO particles are of interest for use in High Temperature Gas-cooled Reactors as they can permit high coolant temperatures and fuel burn-up. TRISO particles consist of a fuel kernel, which contains a fissionable element (uranium, plutonium, thorium or another transuranic element) in an oxide, carbide or oxycarbide form. Surrounding the kernel is a porous carbon buffer which catches recoil fission fragments, accommodates internal gas buildup and dimensional change. Continuing outwards are an inner pyrolytic carbon layer, a silicon carbide layer and an outer pyrolytic carbon layer.¹⁴¹

The dimensions of TRISO particles depends on the intended design but are typically hundreds of micrometers in radius. Thousands of particles are collected into pebbles or compacts. As the coolant passes around the surface of these compacts, a temperature gradient develops across the compact and constituent particles. The temperature gradient may induce kernel migration, also known as the *Ameba effect*, an image of which is shown in **Fig. 33**. The effect has been observed in all TRISO

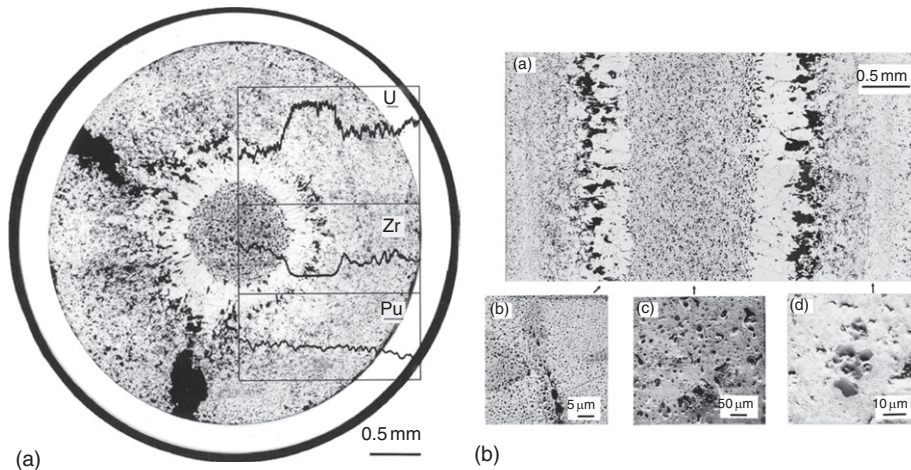


Fig. 32 Postirradiation analysis of U-Pu-Zr fuel with weight percents 71/19/10 at 1.9% FIMA burnup, 42 kW/m linear heat rate, with maximum calculated temperature of approx 943K. Side A results from optical metallography with an overlay of constituent concentration from X-ray intensities to reveal 3 zone microstructure. Side B: from optical and SEM enlargements of various zones showing (a) axial section, (b) intermediate zone, (c) central zone and (d) outer zone. Modified from Kim, Y.S., Hofman, G.L., Hayes, S.L., Sohn, Y.H., 2004. Constituent redistribution in U-Pu-Zr fuel during irradiation. J. Nucl. Mater. 327, 27–36.

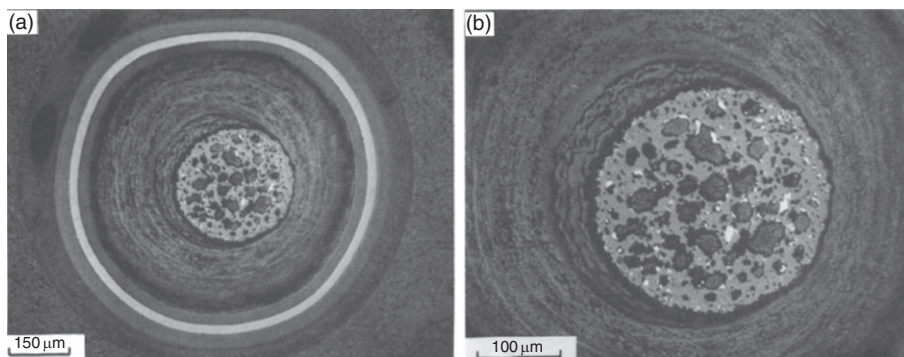


Fig. 33 Migration of a UO_2 kernel through the porous graphite buffer showing (a) full cross-section and (b) enlargement of kernel. Crescent layers are visible behind the kernel movement, indicating a possible C transport mechanism. Also of note is the filling of voids inside the kernel by carbon. Reproduced from Bullock, R.E., Kaae, J.L., 1983. Performance of coated UO_2 particles gettered with ZrC. J. Nucl. Mater. 115, 69–83.

particles with a UO_2 kernel and also thoria based fertile kernels, $(Th, U)O_2$, ThO_2 , $(Th, U)C_2$, ThC_2 .^{143,144} If kernel migration proceeds far enough, it may result in a breach of the structural coating layer, causing fuel coating failure.

The kernel migration speed is often described by the *Kernel Migration Coefficient*, KMC :

$$KMC = K_{KMC} \exp(-\Delta H_{m,kernel}/kT) \quad (97)$$

in which K_{KMC} is a coefficient which depends on the mechanism by which the kernel moves, and $\Delta H_{m,kernel}$ is an effective activation energy. For UCO and UC₂ kernels, carbon is thought to migrate down the temperature gradient via solid state thermodiffusion as discussed in Section 2.08.4.2.^{125,145,146} In this case, the KMC would depend on Q_C^* . In UO_2 based kernels however, thermodiffusion of C is not considered to be rate controlling, and instead a more elaborate vapor-based concept, reliant the presence of oxygen from contamination or liberated from UO_2 is generally considered.¹⁴⁶ This hypothesis of oxygen playing a key role in kernel migration is supported by observations that the presence of an oxygen 'getter' such as ZrC eliminates this phenomenon. Similarly, using a $UO_2 - UC_2$ mixed kernel lowers the CO and CO₂ pressures, reducing the kernel migration rate.¹⁴²

Potential mechanisms for kernel migration via vapor phase transport of carbon is shown in Fig. 34.¹⁴⁶ In this conception, carbon is transported down the temperature gradient by a carrier based vapor transport mechanism made possible by the presence of O liberated from the kernel or present by contamination. The vapor may diffuse down the temperature gradient through the porous buffer and reduce to deposit the carbon on the cold side, thereby *pushing* the kernel up the temperature gradient. Evidence of this mechanism is the appearance of crescent layers behind the kernel shown in Fig. 33. Oxygen must then be returned to the hot side of the kernel in order for the process to continue, although the mechanism for this return is not clear. The first mechanism is

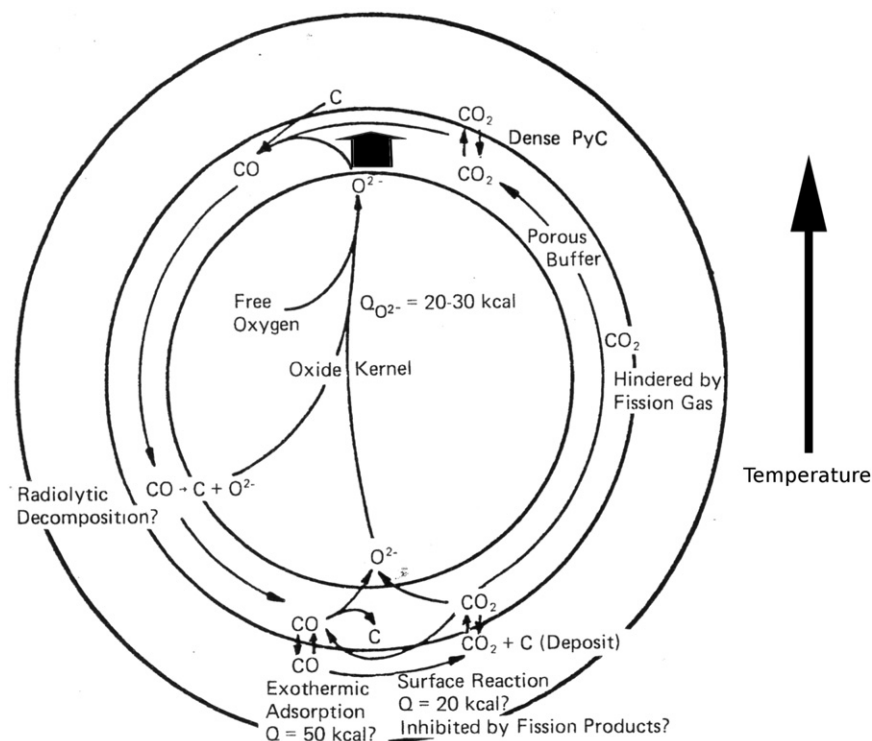


Fig. 34 Schematic of potential mechanisms for UO_2 kernel migration in coated particle fuels. Modified from Wagner-Löffler, M., 1977. Amoeba behaviour of UO_2 coated particle fuel. Nucl. Tech. 35, 392–402.

by a counter-current flow of CO_2 gas flowing in the opposite direction. The second is the uptake of the oxygen by the kernel and solid state diffusion driven by either differing oxygen partial pressure at the front and rear surface, or via thermomigration of the oxygen ions as described in Section 2.08.4.1. [141,145](#)

2.08.5 Summary

In summary, the causes and effects of some major matter transport phenomena in nuclear fuel has been reviewed. Fundamental thermodynamic driving forces of matter transport were considered, and their mathematical expressions derived. The emergence and behavior of microscopic structures was then discussed, and their effect on restructuring and redistribution determined. The bulk, macroscopic effects of matter transport demonstrated the results of restructuring on scales comparable to the dimensions of the fuel itself. Finally specific cases of different fuel types were given and described using the framework set forth by the other sections.

It is the goal of the author that this work help in clarifying concepts and physical quantities associated with matter transport, and how the variety of matter transport phenomena in different fuel types is in fact manifestation of the same fundamental mechanisms. In looking forward it seems apparent that future discussions must account for radiation induced restructuring and redistribution. Of particular note is the mentioned rim structure, JOG and white phase. Additionally, the importance of the thermoelectric effect on matter transport in MOX may also be further investigated.

See also: 5.01 Metal Fuel. 5.13 Modeling of Sphere-Pac Fuel. 7.02 Actinide Alloy Phase Diagram. 7.03 Thermodynamic and Thermophysical Properties of the Actinide Oxides

References

1. Sha, W.T., Huebotter, P.R., Lo, R.K., 1971. The effect of plutonium migration on allowable power rating and doppler broadening. Trans. Am. Nucl. Soc. 14, 183–184.
2. Lackey, W.J., Homan, F.J., Olsen, A.R., 1972. Porosity and actinide redistribution during irradiation of $(\text{U}, \text{Pu})\text{O}_2$. Nucl. Technol. 16, 120–142.
3. Bober, M., Schumacher, G., 1973. Transport Phenomena in Mixed Oxide Fuel Pins. Technical Report KFK 1887. Institute für Neutronenphysik und Reaktortechnik.
4. Aitken, E.A., Evans, S.K., Rosenbaum, H.S., Rubin, B.F., 1971. Transport and reaction of fission products with stainless-steel cladding out-of-pile thermal gradient testing. Trans. Am. Nucl. Soc. 14, 176.

5. Tourasse, M., Boidron, M., Pasque, B., 1992. Fission product behaviour in phenix fuel pins at high burnup. *J. Nucl. Mater.* 188, 49–57.
6. Tanaka, K., Maeda, K., Sasaki, S., Iskusawa, Y., Abe, T., 2006. Fuel-cladding chemical interaction in mox fuel rods irradiated to high burnup in an advanced thermal reactor. *J. Nucl. Mater.* 357, 58–68.
7. Noirot, J., Desgranges, L., Lamontagne, J., 2008. Detailed characterisations of high burn-up structures in oxide fuels. *J. Nucl. Mater.* 372 (2), 318–339.
8. Maeda, K., 2005. Distribution of volatile fission products in or near the fuel-cladding gap of the fbr mox fuel pins irradiated to high burn-up. *J. Nucl. Mater.* 344, 274–280.
9. Rondinella, V.V., Wiss, T., 2010. The high burn-up structure in nuclear fuel. *Mater. Today* 13 (12), 24–32.
10. Olander, D.R., 1976. Fundamental Aspects of Nuclear Reactor Fuel Elements. Technical Information Center, Office of Public Affairs.
11. De Groot, S.R., Mazur, P., 1984. Non-Equilibrium Thermodynamics. General Publishing Company Ltd.
12. Fitts, D.D., 1962. Non-Equilibrium Thermodynamics. New York: McGraw-Hill.
13. Philibert, J., 1991. Atom Movements: Diffusion and Mass Transport in Solids. Les Éditions de Physique.
14. Allnatt, A.R., Lidiard, A.B., 1993. Atomic Transport in Solids. Cambridge: University Press.
15. Kreuzer, H.J., 1983. Nonequilibrium Thermodynamics and its Statical Foundations. Oxford University Press.
16. Bi, Z., Sekerka, R.F., 1998. Phase-field model of solidification of a binary alloy. *Phys. A* 261, 95–106.
17. Soret, C., 1881. Sur l'état d'équilibre qui prend, au point de vue de sa concentration, une dissolution saline primitivement homogène dont deux parties sont portées à des températures différentes. *Ann. Chim. Phys.* 22, 293.
18. Dufour, L., 1873. Diffusion, mobility and their interrelation through free energy in binary metallic systems. *Pogg. Ann.* 148, 490.
19. Hartley, G.S., 1946. Diffusion and swelling of high polymers. Part I—The swelling and solution of a high polymer solid considered as a diffusion process. *Trans. Faraday Soc.* 42, 6.
20. Smigelskas, A.D., Kirkendall, E.O., 1947. Zinc diffusion in alpha brass. *Trans. AIME* 171, 130.
21. Manning, J.R., 1968. Diffusion Kinetics for Atoms in Crystals. Princeton: Van Nostrand.
22. Darken, L.S., 1948. Diffusion, mobility and their interrelation through free energy in binary metallic systems. *Trans. Met. Soc. AIME* 175, 184–187.
23. Darken, L.S., Gurry, R.W., 1953. Physical Chemistry of Metals. New York: McGraw-Hill Book Company, Inc.
24. Matzke, H.J., 1987. Atomic transport properties in UO_2 and mixed oxides $(U, Pu)O_2$. *J. Chem. Soc. Faraday Trans. 2*, 1121–1142.
25. Lay, K.W., 1970. Oxygen chemical diffusion coefficient of uranium dioxide. *J. Am. Ceram. Soc.* 53, 369–373.
26. Breitung, W., 1978. Oxygen self and chemical diffusion coefficients in $UO_{2\pm x}$. *J. Nucl. Mater.* 74, 10–18.
27. Bober, M., Schumacher, G., 1973. Material Transport in the Temperature Gradient of Fast Reactor Fuels. vol. 7. New York: Academic Press, p. 121.
28. Sugisaki, M., Sato, S., Furuya, H., 1981. Solid phase thermal diffusion as a mechanism for oxygen redistribution in $UO_{2\pm x}$ and $(U, Pu)O_{2\pm x}$. *J. Nucl. Mater.* 97, 79–87.
29. Wirtz, K., 1939. Zur kinetik der thermodiffusion in flüssigkeiten. *Annalen der Physik* 428 (3–4), 295302.
30. Wirtz K., 1943. Zur kinetischen theorie der thermodiffusion im kristallgitter. *Phys. Z* 44, 221.
31. Jones, C., Grout, P.H., Lidiard, A.B., 1997. The heat of transport of solute atoms in solid argon. *Ber. Bunsenges. Phys. Chem.* 101, 1232.
32. Janek, J., Timm, H., 1998. Thermal diffusion and soret effect in $(U, Me)O_{2+\delta}$: The heat of transport of oxygen. *J. Nucl. Mater.* 255, 116–127.
33. Nichols, F.A., 1969. Kinetics of diffusional motion of pores in solids. *J. Nucl. Mater.* 30, 143–165.
34. Desai, T.G., Millett, P., Tonks, M., Wolf, D., 2010. Atomistic simulations of void migration under thermal gradient in UO_2 . *Acta Mat.* 58, 330–339.
35. Shewmon, P.G., 1964. The movement of small inclusions in solids by a temperature gradient. *Trans. Met. Soc. AIME* 230, 1134–1137.
36. Shewmon, P.G., 1989. Diffusion in Solids, second ed. McGraw-Hill Book Company, Inc.
37. Raleigh, D.O., Sommer, A.W., 1962. Thermodynamic significance of heat of transport in interstitial solid solutions. *J. Phys. Chem.* 36, 381.
38. Atiken, E.A., 1969. Thermal diffusion in closed oxide fuel systems. *J. Nucl. Mater.* 30, 62–73.
39. Norris, D.I.R., 1979. Solid state transport as a mechanism of oxygen thermomigration in $(U, Pu)O_{2\pm x}$. *J. Nucl. Mater.* 79, 118–127.
40. Bober, M., Sari, C., Schumacher, G., 1971. Redistribution of plutonium and uranium in mixed (U, Pu) oxide fuel materials in a thermal gradient. *J. Nucl. Mater.* 39, 265–284.
41. Gill, S.P.A., 2009. Pore migration under high temperature and stress gradients. *Int. J. Heat Mass Transf.* 52, 1123–1131.
42. Lupis, C.H.P., 1983. Chemical Thermodynamics of Materials. Elsevier Science Publishing Co., Inc.
43. Breitung, W., Reil, K.O., 1989. Vapor pressure measurements on liquid uranium oxide and (U, Pu) mixed oxide. *Nucl. Sci. Eng.* 101, 26.
44. Biachi, M., Chatillon, C., Ducros, G., Forment, K., 2006. Thermodynamics of the o-u system: lii-critical assessment of phase diagram data in the $U-UO_{2+x}$ composition range. *J. Nucl. Mater.* 349, 57–82.
45. Stolen, S., Grande, T., 2003. Chemical Thermodynamics of Materials. John Wiley & Sons, Ltd.
46. Maeda, K., Sasaki, S., Kato, M., Kihara, Y., 2009. Radial redistribution of actinides in irradiated fr-mox fuels. *J. Nucl. Mater.* 389, 78–84.
47. Adamson, M.G., Carney, R.F.A., 1974. Mechanistic study of oxygen thermal diffusion in hyperstoichiometric urania and urania-plutonia solid solutions. *J. Nucl. Mater.* 54, 121–137.
48. Rand, M.H., Markin, T.L., 1967. Some thermodynamic aspects of $(U, Pu)O_2$ solid solutions and their use as nuclear fuels. In Thermodynamics of Nuclear Materials. International Atomic Energy Agency. pp. 637–650.
49. Adamson, M.G., 1971. Letters to the editors: Thermal diffusion of oxygen in hyperstoichiometric urania with very low carbon content. *J. Nucl. Mater.* 38, 213–216.
50. Tikare, V., Holm, E., 1998. Simulation of grain growth and pore migration in a thermal gradient. *J. Am. Ceram. Soc.* 81, 480.
51. Miodownik, M., Martin, J.W., Cerezo, A., 1999. Mesoscale simulations of particle pinning. *Philos. Mag. A* 79, 203.
52. Chen, L.-Q., 2002. Phase-field models for microstructure evolution. *Annu. Rev. Mater. Res.* 32 (1), 113–140.
53. Hu, S., Henager Jr., C.H., Heinisch, H.L., et al., 2009. Phase-field modeling of gas bubbles and thermal conductivity evolution in nuclear fuels. *J. Nucl. Mater.* 392, 292–300. (Nuclear Fuels and Structural Materials 2, Proceedings of the Second Symposium on Nuclear Fuels and Structural Materials for Next Generation Nuclear Reactors).
54. Matthews, J.R., 1979. The initial stages of sintering and hot-pressing in vibro-compacted fuels. *J. Nucl. Mater.* 87, 356–366.
55. Veshchunov, M.S., 2009. Modelling of grain growth kinetics in porous ceramic materials under normal and irradiation conditions. *Materials* 2, 1252–1287.
56. Speight, M.V., 1964. The migration of gas bubbles in material subject to a temperature gradient. *J. Nucl. Mater.* 13, 207–209.
57. Biebsack, J., Diez, W., 1968. Motion of markers and bubbles in solids by self-diffusion in a temperature gradient. *Phys. Stat. Sol.* 27, 139–144.
58. Oldfield, W., Markworth, A.J., 1969. The theory of bubble migration applied to irradiated materials. *Mater. Sci. Eng.* 4, 353–366.
59. Greenwood, G.W., Speight, M.V., 1963. An analysis of the diffusion of fission gas bubbles and its effect on the behaviour of reactor fuels. *J. Nucl. Mater.* 10, 140–144.
60. Nichols, F.A., 1968. Pore migration in ceramic fuel elements. *J. Nucl. Mater.* 27, 137–146.
61. Sens, P.F., 1972. The kinetics of pore movement in UO_2 fuel rods. *J. Nucl. Mater.* 43, 293–307.
62. Gruber, E.E., 1967. Calculated size distribution for gas bubble migration and coalescence in solids. *J. Appl. Phys.* 38, 243–250.
63. Nichols, F.A., 1967. Theory of columnar grain growth and central void formation in oxide fuel rods. *J. Nucl. Mater.* 22, 214–222.
64. Kelly, R., 1967. Bubble diffusion and the motion of point defects near surfaces. *Phys. Status Solidi* 21, 451.
65. Bourgeois, L., Dehaut, P.H., Lemaignan, C., Fredric, J.P., 2001. Pore migration in UO_2 and grain growth kinetics. *J. Nucl. Mater.* 295, 73–82.
66. Barnes, R.S., Mazey, D.J., 1963. The migration and coalescence of inert gas bubbles in metals. *Proc. R. Soc. (Lond.), Ser. A* 275, 47–57.
67. Hu, S.Y., Henager Jr., C.H., 2010. Phase-field simulation of void migration in a temperature gradient. *Acta Mater.* 58, 3230–3237.

68. Li, Y., Hu, S., Sun, X., *et al.*, 2010. Phase-field modeling of void migration and growth kinetics in materials under irradiation and temperature fields. *J. Nucl. Mater.* 407, 119–125.
69. Matzke, H.J., 1975. On mass transport in nuclear carbides by evaporation-condensation. *J. Nucl. Mater.* 57, 180–186.
70. Herring, C., 1953. *Page 5*. University of Chicago Press.
71. Cahn, J.W., 1960. Theory of crystal growth and interface motion in crystalline materials. *Acta. Met.* 8, 554–562.
72. Wernick, J.H., 1957. Effects of crystal orientation, temperature, and molten zone thickness in temperature-gradient zone-melting. *AIME Trans.* 209, 1169.
73. Une, K., Kashibe, S., Takagi, A., 2006. Fission gas release behavior from high burnup UO₂ fuels under rapid heating conditions. *J. Nucl. Sci. Tech.* 43 (9), 1161–1171.
74. Cornell, R.M., Williamson, G.K., 1965. The behaviour of fission product gases in uranium dioxide. *J. Nucl. Mater.* 17, 200.
75. Michels, L.C., Poepel, R.B., Niemark, L.A., 1970. The movement of fission gas bubbles and inclusions in mixed-oxide fuel. *Trans. Am. Nucl. Soc.* 13, 601.
76. Ronchi, C., Sari, C., 1974. Properties of lenticular pores in UO₂, (U, Pu)O₂ and PuO₂. *J. Nucl. Mater.* 50, 91–97.
77. Lewis, W.B., MacEwan, J.R., Stevens, W.H., Hart, R.G., 1964. Technical Report AECL-2019. Chalk River Nuclear Laboratories.
78. Vance, I.W., Millett, P.C., 2017. Phase-field simulations of pore migration and morphology change in thermal gradients. *J. Nucl. Mater.* 490, 299–304.
79. Hales, D.R., Horn, G.R., 1963. Evolution of uranium dioxide structure during irradiation of fuel rods. *J. Nucl. Mater.* 8, 207–220.
80. Clement, C.F., 1977. The movement of lenticular pores in UO₂ nuclear fuel elements. *J. Nucl. Mater.* 68, 63–68.
81. Meyer, R.O., 1974. Comments on papers by olander regarding actinide redistribution in mixed oxide fuels. *J. Nucl. Mater.* 52, 326–328.
82. Guarro, S., Olander, D.R., 1975. Actinide redistribution due to pore migration in hyperstoichiometric mixed-oxide fuel pins. *J. Nucl. Mater.* 57, 136–144.
83. Olander, D.R., 1973. The conservation equations governing porosity and actinide redistribution in mixed-oxide fuels. *J. Nucl. Mater.* 47, 251–254.
84. Olander, D.R., 1973. The kinetics of actinide redistribution by vapour migration in mixed oxide fuels (i): By cracks. *J. Nucl. Mater.* 49, 21–34.
85. Olander, D.R., 1973. The kinetics of actinide redistribution by vapour migration in mixed oxide fuels (ii): By pores. *J. Nucl. Mater.* 49, 35–44.
86. Olander, D.R., 1974. Reply to “comments on papers by olander regarding actinide redistribution in mixed oxide fuels” by R. O. Meyer. *J. Nucl. Mater.* 52, 329–330.
87. Bramman, J.I., Powell, H.J., 1975. Redistribution of fuel and fission products in irradiation oxide fuel pins. *J. Br. Nucl. Energy. Soc.* 14, 63.
88. Clement, C.F., Finnis, M.W., 1978. Plutonium redistribution in mixed oxide (U, Pu)O₂ nuclear fuel elements. *J. Nucl. Mater.* 75, 193–200.
89. Katsuyama, K., Nagamine, T., Matsumoto, S.-I., Ito, M., 2002. Measurement of central void diameter in fbr mox fuel by x-ray computer tomography. *J. Nucl. Sci. Tech.* 39, 804–806.
90. Maeda, K., Katsuyama, K., Ikusawa, Y., Maeda, S., 2011. Short-term irradiation behavior of low-density americium-doped uranium plutonium mixed oxide fuels irradiated in a fast reactor. *J. Nucl. Mater.* 416 (1), 158–165.
91. Tanaka, K., Miwa, S., Sekine, S., *et al.*, 2013. Restructuring and redistribution of actinides in Am-MOX fuel during the first 24h of irradiation. *J. Nucl. Mater.* 440 (1), 480–488.
92. Christensen, J.A., 1967. Technical Report BNWL-536. Battelle Northwest.
93. Welland, M.J., 2009. Simulation of Melting Uranium Dioxide Nuclear Fuel (PhD Thesis). Royal Military College of Canada.
94. Welland, M.J., Lewis, B.J., Thompson, W.T., 2011. Review of high temperature thermochemical properties and application in phase-field modelling of incipient melting in defective fuel. *J. Nucl. Mater.* 412, 342–349.
95. Hellwig, C.H., Bakker, K., Ozawa, T., *et al.*, 2006. FUJI: A comparative irradiation test with pellet, sphere-pac, and vipac fuels. *Nucl. Sci. Eng.* 153, 233.
96. Christensen, J.A., 1972. Columnar grain growth in oxide fuels. *Trans. Am. Nucl. Soc.* 15, 214.
97. Kawamata, H., Kaneko, H., Furuya, H., Koizumi, M., 1977. Migration rate of lenticular voids in UO₂ under the influence of temperature gradient. *J. Nucl. Mater.* 68, 48–53.
98. Maeda, K., Sasaki, S., Kato, M., Kihara, Y., 2009. Short-term irradiation behavior of minor actinide doped uranium plutonium mixed oxide fuels irradiated in an experimental fast reactor. *J. Nucl. Mater.* 385 (2), 413–418.
99. Maeda, K., Katsuyama, K., Ikusawa, Y., Maeda, S., 2011. Short-term irradiation behavior of low-density americium-doped uraniumplutonium mixed oxide fuels irradiated in a fast reactor. *J. Nucl. Mater.* 416 (1–2), 158–165.
100. Potter, T.J., Elyard, C.A., 1967. Columnar grain growth in uranium dioxide. *Proc. Br. Ceram. Soc.* 7, 273.
101. Zhang, L., Tonks, M.R., Millett, P.C., *et al.*, 2012. Phase-field modeling of temperature gradient driven pore migration coupling with thermal conduction. *Comp. Mater. Sci.* 56, 161–165.
102. Zwicky, H.U., Aerne, E.T., Hermann, A., Thomi, H.A., Lippens, M., 1993. Radial plutonium and fission product isotope profiles in mixed oxide fuel pins evaluated by secondary ion mass spectrometry. *J. Nucl. Mater.* 202, 65–69.
103. Bober, M., Sari, C., Schumacher, G., 1971. Redistribution of uranium and plutonium during evaporation processes in mixed oxide fuel. *J. Nucl. Mater.* 40, 341–345.
104. Ishii, T., Asaga, T., 2001. An investigation of the pu migration phenomena during irradiation in fast reactor. *J. Nucl. Mater.* 294, 13–17.
105. Bober, M., Sari, C., Schumacher, G., 1969. Plutonium migration in a thermal gradient in mixed (U, Pu) oxide fuels. *Trans. Am. Nucl. Soc.* 12, 603.
106. Aitken, E.A., Evans, S.K., Adamson, M.G., 1971. A Thermodynamic Data Program Involving Plutonia and Urania at High Temperatures. Technical Report.
107. Bober, M., Schumacher, G., Geithoff, D., 1973. Plutonium redistribution in fast reactor mixed oxide fuel pins. *J. Nucl. Mater.* 47, 187–197.
108. Evans, S.K., Aitken, E.A., Craig, C.N., 1967. Effect of a temperature gradient on the stoichiometry of urania-plutonia fuel. *J. Nucl. Mater.* 30, 57–61.
109. Fryxell, R.E., Aitken, E.A., 1969. High temperature studies of urania in a thermal gradient. *J. Nucl. Mater.* 30, 50–56.
110. Perron, P.O., 1968. Oxygen redistribution in uranium dioxide fuels. *J. Nucl. Mater.* 27, 237–238.
111. Olander, D.R., 1971. Oxygen redistribution in UO_{2+x}. *J. Nucl. Mater.* 44, 116.
112. Lewis, B.J., Thompson, W.T., Akbari, F., *et al.*, 2004. Thermodynamic and kinetic modelling of fuel oxidation behaviour in operating defective fuel. *J. Nucl. Mater.* 328, 180–196.
113. Higgs, J.D., Lewis, B.J., Thompson, W.T., He, Z., 2007. A conceptual model for the fuel oxidation of defective fuel. *J. Nucl. Mater.* 366, 99–128.
114. Shaheen, K., Lewis, B.J., 2009. Platform-Based Modelling of Intact and Defective Fuel Behaviour. SFEN. pp. 654–667.
115. Sari, C., Schumacher, G., 1976. Oxygen redistribution in fast reactor oxide fuel. *J. Nucl. Mater.* 61, 192–202.
116. Adamson, M.G., Aitken, E.A., Evans, S.K., Davies, J.H., 1975. Thermodynamics of nuclear materials. In: Proceedings of the Symposium on International Atomic Energy Agency, vol. 1, p. 59. Vienna: IAEA.
117. Bober, M., Schumacher, G., 1973. Considerations on the oxygen distribution in hypostoichiometric mixed oxide fuel pins. *J. Nucl. Mater.* 49, 322–324.
118. Lassman, K., 1987. The oxired model for redistribution of oxygen in nonstoichiometric uranium-plutonium oxides. *J. Nucl. Mater.* 150, 10–16.
119. Ruello, P., Petot-Ervas, G., Petot, C., Desgranges, L., 2005. Electrical conductivity and thermoelectric power of uranium dioxide. *J. Am. Ceram. Soc.* 88, 604–611.
120. Kamata, M., Esaka, T., 1994. Thermodynamic descriptions of oxygen redistribution in a nuclear fuel pellet: Heat of transport of oxygen in mixed conductors. *J. Appl. Electrochem.* 24, 390.
121. Millot, F., Gerdanian, P., 1980. The measurement of thermo- and electrotransport in fluorite oxides. *J. Nucl. Mater.* 92, 257–261.
122. Beisswenger, H., Bober, M., Shumacher, G., 1967. Thermodiffusion in system UO₂–CeO₂. *J. Nucl. Mater.* 21, 38–52.
123. Tanaka, K., Miwa, S., Sato, I., *et al.*, 2009. Microstructure and elemental distribution of americium-containing uranium plutonium mixed oxide fuel under a short-term irradiation test in a fast reactor. *J. Nucl. Mater.* 385, 407–412.
124. Benedict, U., Saunders, R.A., Schmidt, H.E., Whitlow, W.H., 1977. Programme Progress Report: Plutonium Fuels and Actinide Research. Technical Report 3438. European Institute for Transuranium Elements.
125. Gulden, T.D., 1972. Carbon thermal diffusion in the UC₂–C system. *J. Am. Ceram. Soc.* 55, 14–18.

126. Wallace, T.C., Witterman, W.G., Radosevich, C.L., Bowman, M.G., 1968. Carbon Diffusion in the Carbides of Uranium. Technical Report LA-DC-8840. Los Alamos National Laboratory.
127. Weeks, R.W., Scattergood, R.O., Pati, S.R., 1970. Migration velocities of bubble-defect configurations in nuclear fuel. *J. Nucl. Mater.* 36, 223–229.
128. Storms, E.K., 1967. The Refractory Carbides. Academic Press.
129. Mardon, P.G., Potter, P.E., 1970. Uranium-Plutonium-Carbon phase diagram, part II: The freezing of the alloys and calculation of some equilibria. *Nucl. Metall.* 17, 842.
130. Richter, K., Coquerelle, M., Gabolde, J., Werner, P., 1974. Fuel and Fuel Elements for Fast Reactors. vol. 1. IAEA. p. 71.
131. Kim, Y.S., Hofman, G.L., Hayes, S.L., Sohn, Y.H., 2004. Constituent redistribution in U-Pu-Zr fuel during irradiation. *J. Nucl. Mater.* 327, 27–36.
132. Ishida, M., Ogata, T., Kinoshita, M., 1993. Constituent migration model for U-Pu-Zr metallic fast reactor fuel. *Nucl. Technol.* 104 (1), 37–51.
133. Hofman, G.L., Hayes, S.L., Petri, M.C., 1996. Temperature gradient driven constituent redistribution in uzn alloys. *J. Nucl. Mater.* 227 (3), 277–286.
134. Kim, Y.S., Hayes, S.L., Hofman, G.L., Yacout, A.M., 2006. Modeling of constituent redistribution in uzn metallic fuel. *J. Nucl. Mater.* 359 (1–2), 17–28.
135. Kim, Y.S., Hofman, G.L., Yacout, A.M., 2009. Migration of minor actinides and lanthanides in fast reactor metallic fuel. *J. Nucl. Mater.* 392, 164–170.
136. Porter, D.L., Lahm, C.E., Pahl, R.G., 1990. Fuel constituent redistribution during the early stages of U-Pu-Zr irradiation. *Metall. Trans. A* 21A, 1871.
137. Hofman, G.L., Pahl, R.G., Lahm, C.E., Porter, D.L., 1990. Swelling behavior of U-Pu-Zr fuel. *Metall. Trans. A* 21, 517.
138. Ohta, H., Ogata, T., Papaioannou, D., et al., 2011. Development of fast reactor metal fuels containing minor actinides. *J. Nucl. Sci. Tech.* 48 (4), 654–661.
139. Ohta, H., Ogata, T., Papaioannou, D., et al., 2015. Irradiation of minor actinide bearing uranium-plutonium-zirconium alloys up to 2.5 at%, 7 at%, and 10 at% burnups. *Nucl. Technol.* 190 (1), 36–51.
140. Ohta, H., Ogata, T., Van Winckel, S., Papaioannou, D., Rondinella, V.V., 2016. Minor actinide transmutation in fast reactor metal fuels irradiated for 120 and 360 equivalent full-power days. *J. Nucl. Sci. Technol.* 53 (7), 968–980.
141. Powers, J.J., Wirth, B.D., 2010. A review of triso fuel performance models. *J. Nucl. Mater.* 405, 74–82.
142. Bullock, R.E., Kaae, J.L., 1983. Performance of coated UO_2 particles gettered with ZrC. *J. Nucl. Mater.* 115, 69–83.
143. Maki, J.T., Pettit, D.A., Knudson, D.L., Miller, G.K., 2007. The challenges associated with high burnup, high temperature and accelerated irradiation for triso-coated particle fuel. *J. Nucl. Mater.* 371, 270–280.
144. Smith, C.L., 1977. Migration of ThO_2 kernels under the influence of a temperature gradient. *Nucl. Tech.* 35, 403–412.
145. Lee, J.K., Choi, Y., 2006. An analytical model for the amoeba effect in UO_2 fuel pellets. *J. Nucl. Mater.* 357, 213–220.
146. Wagner-Löffler, M., 1977. Amoeba behaviour of UO_2 coated particle fuel. *Nucl. Tech.* 35, 392–402.